UNIVERSITÉ DU QUÉBEC À CHICOUTIMI

MÉMOIRE PRÉSENTÉ À
L' UNIVERSITÉ DU QUÉBEC À CHICOUTIMI
COMME EXIGENCE PARTIELLE DE LA MAITRISE
EN INGÉNIERIE

PAR
ATEF LABIB

L'EFFET DES NIVEAUX DE REFROIDISSEMENT (TEMPÉRATURE DE DU MOULE) ET DES TRAITEMENTS THERMIQUES SUR LES PROPRIÉTÉS MÉCANIQUES ET SUR LA MICROSTRUCTURE DES DEUX ALLIAGES COMPOSITES Al-Si-Mg/SiC/10_p.

NOVEMBRE 1993

Bibliothèque
Paul-Émile-Boulet

UQAC
Université du Québec
à Chicoutimi

Mise en garde/Advice

Afin de rendre accessible au plus grand nombre le résultat des travaux de recherche menés par ses étudiants gradués et dans l'esprit des règles qui régissent le dépôt et la diffusion des mémoires et thèses produits dans cette Institution, **l'Université du Québec à Chicoutimi (UQAC)** est fière de rendre accessible une version complète et gratuite de cette œuvre.

Motivated by a desire to make the results of its graduate students' research accessible to all, and in accordance with the rules governing the acceptation and diffusion of dissertations and theses in this Institution, the **Université du Québec à Chicoutimi (UQAC)** is proud to make a complete version of this work available at no cost to the reader.

L'auteur conserve néanmoins la propriété du droit d'auteur qui protège ce mémoire ou cette thèse. Ni le mémoire ou la thèse ni des extraits substantiels de ceux-ci ne peuvent être imprimés ou autrement reproduits sans son autorisation.

The author retains ownership of the copyright of this dissertation or thesis. Neither the dissertation or thesis, nor substantial extracts from it, may be printed or otherwise reproduced without the author's permission.

RÉSUMÉ

Les composites à matrice métallique (CMM) et particules de SiC offrent potentiel de résistance, de module de Young et de tenue à l'usure supérieurs à ceux obtenus couramment par les alliages conventionnels. Le mélange de particules de carbure de silicium au métal liquide est considéré, en principe, pour être la manière la plus directe et la plus économique de production des CMM où le matériau composite peut être transformé directement en pièce moulée.

Dans le présent travail, certains facteurs importants influençant la microstructure et les propriétés finales des composites contenant 10% (volumique) de particules de SiC sont particulièrement étudiés. Ces facteurs comprennent la quantité de silicium de l' alliage de la matrice (7 et 10% en masse), la vitesse de refroidissement qui influencent la distribution des particules et l'effet de renforcement.

L'effet du traitement thermique de mise en solution (T4) sur les deux alliages F3A.10S et F3S.10S sont étudiés. La mise en solution est effectuée à une température de 540°C, le temps de mise en solution étant de 4, 8, 12 et 24 heures. Les températures et le temps de vieillissement varient respectivement de 155 à 160°C et de 5 à 24 heures. Les paramètres étudiés sont la limite élastique, la limite ultime, l'allongement à la rupture. L'examen métallographique montre un développement graduel de la structure de l' eutectique, suite au traitement de mise en solution. Le traitement de mise en solution optimal se situe autour de 540°C pour des temps de l'ordre de 8 à 12 heures.

Pendant le traitement de mise en solution, nous observons un phénomène de sphéroïdisations du silicium (forme, aspect ratio et taille en μm^2) et une mise en solution du magnésium avec une stabilisation des propriétés mécaniques (résistance à la traction). Durant le traitement de vieillissement, il y a précipitation de composé Mg_2Si qui influence les propriétés mécaniques finales.

REMERCIEMENT

Je remercie Professeur F.H. Samuel, le Dr. H. Liu et le Dr. A.M. Samuel, pour l'appui et les judicieux conseils prodigués durant toute la durée de ce travail.

Je remercie le Dr.A.Sh.Rezk, Monsieur Gilles Lemire et Monsieur Régis Boucher pour leur aide technique lors de la réalisation des expériences.

Je remercie la Société d'Électrolyse et de Chimie Alcan Limitée, le Conseil de Recherches en Sciences Naturelles et en Génie du Canada, et la Fondation de l'Université du Québec à Chicoutimi.

Je tiens à remercier particulièrement ma famille et mes amis, ainsi que le personnel de l'Université du Québec à Chicoutimi, qui ont contribué à l'avancement de ce travail de recherche.

TABLE OF CONTENTS

List of Symbols

V_{cr} = theoretical critical velocity

n = positive number near 4 or 5

L = the latent heat of fusion per unit volume

a = the atomic diameter of the liquid.

D = the diffusivity of the liquid.

R = the radius of irregularties on the particle surface.

KT = boltzman constant and temperature.

η = The liquid viscosity.

σ = the solid/liquid interface energy.

R = the particle radius.

α = the ratio of the particle radius to the interface radius.

Fp = is the volume fraction of particles a head of the interface.

do = interatomic distance.

g = accleration due to gravity.

Kp = thermal conductivity of the particle.

Kl = thermal conductivity of the liquid.

ηr= relative viscosity of the melt ahead of the interface.

$\Delta\rho$= density difference between particles and liquid.

ρp&ρpl = density difference between particle and liquid.

V = Velocity of Soldification.

$\Delta\sigma o$ = surface energy difference.

LIST OF FIGURES

CHAPTER I

CHAPTER III

CHAPTER IV

Note: Magnifications quoted for all optical micrographs in the figure captions above represent the original magnifications. (Prints shown are fifty percent reductions of the originals).

LIST OF TABLES

ABSTRACT

ABSTRACT

The effect of the remelting process, casting conditions (mainly mold temperature, using a permanent mold) and different heat treatment tempers (solution time and aging time) on the microstructural characterization and mechanical properties of two Duralcan Al-Si-Mg/SiC_p metal matrix composites (designated F3A.10S and F3S.10S), containing the same level of SiC particles (11.4 vol.%), but different Si contents-7 and 10 wt.%, respectively, was studied in the present work.

The presence of high silicon improves the composite fluidity, allowing an increase in the mold temperature range from 350-450 °C for F3A.10S to 300-450 °C for F3S.10S. Following proper precautions, the void volume fraction can be maintained around 0.3%, even after 3 hr stirring time (interrupted by different pourings). Similarly, sedimentation of the SiC particles can be also largely avoided. The presence of these particles, however, encourages heterogeneous nucleation of pores at the particle-matrix interface, leading to a very fine dispersed porosity as compared to the base alloy A356, where a large central shrinkage cavity associated with gas porosity is mainly observed. The average pore size in the composite alloys is about one tenth that in the base alloy.

Higher solidification rates promote homogeneous distribution of the SiC particles with less denuded zones. Holding the melt for long times (3 hr) at high temperatures (around 740 °C) leads to the formation of fragments of Al_4C_3 phase in the case of the F3A.10S alloy. This reaction, however, is suppressed in F3S.10S due to

the increased Si level in the alloy.

The spheroidization of the Si particles (judged from the roundness, aspect ratio and area size in μm^2 parameters) which occurs during the heat treatment temper is affected by both solution time and temperature and by the strontium (Sr) concentration within the casting.

The tensile properties (YS, UTS and EL%) of both composites in the as-cast condition are stable in the mold temperature range 300-450 °C. The presence of the SiC_p results in a 4 ksi increase in both YS and UTS compared to the base alloy. Prolonged solution heat treatment has no effect on the average mechanical properties (YS and UTS), but the ductility (EL%) is found to be sensitive to this parameter. Optimum values of elongation are obtained at times of 4-8 hr for both composites. The aging time (5, 12 and 24 hr) and temperature (155 °C, 160 °C) have a great effect on both YS and UTS compared to the solution heat treatment, while there is a large reduction in the elongation.

The presence of 3 wt% more Si in the F3S.10S alloy is enough to reduce the total heat treatment time from 60 hr (for F3A.10S) to 13 hr. (for F3S.10S). The YS and UTS values obtained from the two composites are about 10 and 4-8 ksi higher, respectively, than those obtained from the unreinforced A356 alloy treated similarly. However, the ductility is reduced from 6.0% to 1.0% in the composites.

The presence of the SiC_p appears to refine the Si particle size, more so in the case of F3A.10S than F3S.10S.

The fracture mode in these composites in the as-cast condition is complex. The

crack propagates through the matrix and the particle/matrix interface due to the opening-up of voids. Extension of cracked SiC particles and voiding depends on the localized stresses and degree of interfacial strength. In the heat-treated composites, the fracture behaviour is determined by the type of temper treatment applied to the composite i.e. ductile fracture in T4 temper and brittle fracture in T61 and T6 tempers for both composites.

CHAPTER I
DEFINITION OF THE PROBLEM

I.1. INTRODUCTION

Ceramic particle reinforced metal matrix composite (MMC) systems have been developed and implemented in a number of industrial applications. SiC_p has been one of the most successful reinforcement materials for aluminum alloys due to its high strength, stiffness and hardness as well as its chemical compatibility with aluminum alloys up to 500 °C [1]. SiC_p reinforced Al or Al alloys are characterized by their improved strength, Young 's modulus and wear resistance as compared to the unreinforced material [2]. Introduction of SiC-particles in aluminum alloys, however, results in a significant reduction in their ductility and fracture toughness. Flom and Arsenault [3] have related such reduction in ductility to the inhomogeneous distribution of the SiC-particles and void initiation at the reinforcement-matrix interface, which results, during straining, from a weak interfacial bond.

According to Lloyd and Chamberlain, [4] a castable metal matrix composite (MMC) has to satisfy certain criteria:

(a) It has to be remeltable and able to be held for a reasonable time above the liquidus without degradation of the reinforcement;

(b) It has to have good casting fluidity to fill the intricate passages of the mold;

(c) The shape casting has to have a suitable microstructure;

(d) The mechanical properties of the final casting have to be superior to those of the unreinforced casting.

The present work was undertaken with the aim of studying the effect of

remelting conditions as well as the mold temperature (permanent Stahl mold) on the mechanical properties of two Al-Si-Mg/SiC_p composites, containing the same volume fraction (11.4 vol%) of SiC particles and 7 and 10 wt% Si, respectively.

The effect of solidification rate (in a wide range of cooling rates from 0.1 to 100 °C/S) on the dendrite structure and redistribution of SiC particles and their influence on the mechanical properties and rupture mechanism was also investigated.

The effect of solutionizing at a temperature, quenching and natural and/or artificial aging on the average mechanical properties, namely the yield strength (YS), ultimate tensile strength (UTS) and elongation (EL%) were also studied. Variations in each of these steps, result in corresponding variations in the mechanical properties, and thus the conditions can be manipulated to derive a particular combination of strength-ductility required of a specific cast component.

The effect of the presence or absence of SiC-particles on the silicon morphology for different stirring and solution heat treatment times and varying Sr concentrations of the melt was also investigated.

Before proceeding to describe the experimental details of the present work and results obtained, a general background on composites, with particular emphasis on ceramic particulate reinforced metal matrix composites on which this study is based, is given in the following sections.

I.2. BACKGROUND

I.2.1. Composite Materials

Composites may be classified as being either natural composites (i.e. those occurring naturally, e.g. wood, rocks, minerals, bone tissue, etc.) or artificial composites (i.e. those that are man-made). The material science development of many engineering materials has made it easy to produce the latter type, by combining two (or more) constituents which are different in form, composition and essentially insoluble in each other to result in a material whose properties are different from those of either constituent.

Figure I.1. shows the five different classes of composites that are available in general : fibre-reinforced; particulate; laminar; flake; and filled composites [5]. All types are composed of an additive constituent or "reinforcement" (e.g. fibres or particles) embedded in the "matrix" or other major constituent of the composite.

I.2.2. Metal Matrix Composites

Metal matrix composites or MMCs constitute one of the more popular and extensively investigated category of composites on account of their capability to suit diverse combinations of properties that cover high modulus, strength, hardness, toughness, wear resistance and low coefficients of thermal expansion, which are of particular interest to the aerospace and automotive industries [6,7].

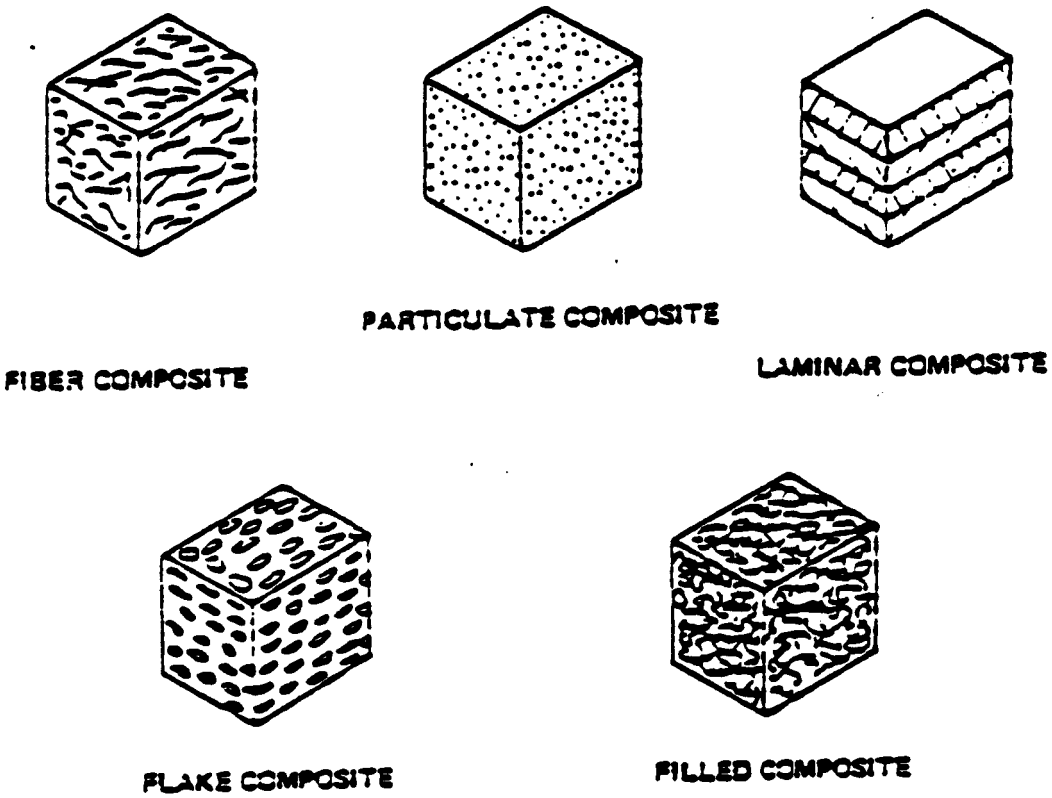

Figure.I.1.Different Classes of Composites [5]

In general, a metal matrix composite consists of at least two components : one, the metal matrix (in most cases an alloy) and the other, a reinforcement (in general, an intermetallic compound, e.g. an oxide, carbide or nitride). There are three basic types of composite materials that meet the above-mentioned criteria [8]:

(a) Dispersion-strengthened composites, which consist of an elemental matrix within which fine particles of the reinforcement are uniformly dispersed. The particle diameter can range from 0.01 to 0.1 μm and the volume fraction can vary from 1 to 15 percent.

(b) Fibre (or whisker)-reinforced composites, which consist of fibres that are either continuous or range in length from 0.1 to 0.25 μm, with a volume fraction of a few to > 70 percent. Obviously, in this composite type, the reinforcement is different in nature than that of the other types in that one of the dimensions is much longer.

(c) Particulate reinforced composites, which consist of dispersed particles with sizes ranging from 3 to 19 μm and volume fractions ranging from 5 to 40%.

I.2.3. Role of Metal Matrix and Reinforcement

The behaviour of a composite material is a result of the combined behaviours of the matrix reinforcement and the interface between the reinforcement and matrix.

(A) Matrix

The role of the matrix is to:

(a) Transfer stresses between the reinforcement and matrix;

(b) Provide a barrier against an adverse environment;

(c) Protect the surface of the reinforcement from mechanical abrasion; and

(d) Hold the reinforcement phase in place [9].

The two most commonly employed matrices are aluminum (Al) and titanium (Ti), both of which have a low specific gravity and are available in a variety of alloy forms. Al-Si alloys (A356 and 359) contain varying amounts of impurity elements, while aluminum alloys such as 201, 6061, 1100 have been used for their higher tensile strength-to-weight ratios. Pure aluminum has been used for its good corrosion resistance [9-11]. The addition of silicon (Si) to pure aluminum imparts a higher fluidity to the melt, resulting in good feedability, low shrinkage in the casting and good hot cracking resistance [12,13]. Magnesium (Mg) is added as an alloying element to increase the strength and hardenability of the material.

Modification of the matrix is an important factor since it affects both the microstructure and the mechanical properties of the casting. Modification is an important step towards the achievement of certain microstructural characteristics that can lead to improved mechanical properties [14]. In (Al-Si-Mg) alloys, in the unmodified case, the eutectic is acicular and contains large brittle plates of silicon which cause the casting to exhibit poor ductility. Modification with Sr or Na results in changing the unmodified acicular form of the eutectic silicon to a fine fibrous

structure. Such modification of the microstructure, i.e. Si spheroidization, can also be achieved with the use of high cooling rates [15,16]. This spheroidization is necessary to achieve optimum microstructure and hence, mechanical properties.

Referring to the two composite alloys studied in this work, the higher Si level of the F3S.10S alloy will require a larger amount of modifier to completely modify the eutectic structure : it was found that an increase of almost 50 percent in the amount of strontium needed was observed when the silicon level changed from 7 wt.% in the F3A.10S alloy to 11 wt.% in the F3S.10S alloy. Modification is also important from the point of view of heat treatment, a procedure to which as-cast material is normally subjected, to enhance the mechanical properties. In Al-Si or Al-Si-Mg alloys, modification can result in a reduction of the total solution time necessary, as mentioned above.

(B) Reinforcement

There are many reinforcement types that are commonly used in metal matrix composites. Among the four groups-continuous fibres, discontinuous short fibres, whiskers and particulates-discontinuous fibres are popular due to the advantage that they can be shaped by standard metallurgical processes such as forging, rolling, extrusion, etc. Particulates, however, are the cheapest form of reinforcement. Although many ceramics are available in a wide range of sizes, SiC and Al_4O_3 are mainly of interest for MMCs. For many years, Al_2O3 has been recognized as a promising

reinforcement for high-temperature applications of MMCs and also in various chemically aggressive environmental applications. Below 900 °C, it retains most of its elastic stiffness strength, and abrasion resistance [17].

Due to their ease of formability and relatively modest cost, SiC_p/Al and SiC_w/Al composites have been used in various applications ranging from tennis rackets to automobile engines. SiC is produced in the form of continuous filament and two useful particulate forms, alpha-SiC (α-SiC), which has a hexagonal (hcp) structure and beta-SiC (ß-SiC) which has a face centred cubic (fcc) structure. Both the volume fraction and the particle size control the proof stress of the composite. Particle size must be limited to maximize strength and minimize fracture, without adversely affecting processibility. Particulate reinforced composites have been under extensive development during the last two decades, primarily because of their ease of fabrication, an important cost consideration. They are produced by either powder metallurgy or liquid phase processing methods. Tables I.1 and I.2 show different properties of various continuous and discontinuous fibres and particles used as reinforcements in metal matrix composites [18-25].

Table I.1. Different Properties of Various Discontinuous Fibers [18-22].

Type	Diameter (μm)	Density Mg m^{-2}	Modulus GN m^{-2}	Breaking Strength MN m^{-2}	Breaking Strain (%)
Boron, Single, SiC Coated	100-150	2.70	400	3100	0.77
α-Al_2O_3 tow	20	3.95	379	1380	0.36
γ-Al_2O_3 tow	17	3.25	210	1800	0.85
Carbon, HM, tow	8	1.85	400	2300	0.58
Carbon HT, tow	8	1.75	235	2800	1.10
Silicon Carbide, tow	13	2.55	196	2550	1.00
Silicon Carbide, Single	100-140	3.50	400	2700	0.68

Table.I.2. Different Properties of Various Discontinuous Particles [22-26].

Type	Diameter (μm)	Density Mg m^{-2}	Modulus GN m^{-2}	Breaking Strength MN m^{-2}
δ-alumina, short fiber	3.0	3.30	300	2000
Silicon carbide, whisker	0.2-1.0	3.20	~450	10000
Silicon Carbide, abrasive grade	10.0	3.20	.....	.....
Potassium titanate, whiskers	0.5	3.30	280	7000

I.2.4. Reactivity of the Reinforcement with the Molten Melt:Interface Behaviour.

Most reinforcements of interest are not thermodynamically stable in molten aluminum, and reaction will occur between the melt and the reinforcement. Under the typical molten metal processing conditions (i.e. high metal temperature and long processing times) involved in the production of particulate-reinforced composites, the reinforcement particles undergo reaction at the metal/ceramic interface [27]. In the case of an Al/Al alloy matrix reinforced with SiC particles, the reaction results in the formation of Al_4C_3 :

$$4Al+3SiC \rightarrow Al_4C_3+3Si \qquad (1)$$

This reaction is harmful in several ways as: (a) it produces the reaction product Al_4C_3 at the interface between the reinforcement and the matrix, which could result in a degradation of the reinforcement strength and the interfacial strength; (b) Al_4C_3 is unstable in certain environments and so it increases the corrosion susceptibility of the alloy; and (c) the reaction changes the silicon content of the alloy and in cases when extensive reaction takes place, the matrix composition of the alloy can change significantly. The kinetics of the reaction depend on the Si level of the matrix alloy, the Si level required to inhibit the reaction being a function of the melt working temperature. The silicon level required can be calculated from the excess molar free energy for the reaction and the activity coefficient. The Si levels required at different temperatures are shown in Fig. I.2. The results show that casting alloys with high

silicon contents will have a high resistance to Al_4C_3 formation.

Lloyd has reported that in A356-15 vol% SiC_p composite, no detectable Al_4C_3 formation occurs during/up to 2 hr. at temperatures below 750 °C, as shown in Fig I.3. When Mg is present in the matrix alloy, $MgAl_2O_3$ (spinel) and MgO can also be formed, according to the following reactions:

$$3Mg+4Al_2O_3 \rightarrow 2Al+3MgAl_2O_4 \qquad (2)$$

$$3Mg+Al_2O_3 \rightarrow 2Al+3MgO \qquad (3)$$

The Al_2O_3 is supplied through the oxide film layer that is formed at the melt surface and which can be drawn into the melt at any stage of stirring during the melting/casting process. Wang et al. [28] have quoted a number of possible chemical reactions that could occur at the interface during the processing of such Al alloy/SiC_p composite systems. Equations (2) and (3) particularly apply in the present studies, where the working melt temperature is 735 °C (> 1000 K), at which temperature of the molten alloy is rapidly oxidized at the surface and forms a continuous Al_2O_3 layer that can later be drawn into the melt and gain access to the SiC/matrix interface. According to McLeod [29], Mg levels of only 0.03 wt pct are sufficient for spinel formation and it is the stable interphase phase observed in AA-6061 and AA-2014 Al matrix alloys.

Samuel et al. [30] have reported the presence of spinel both at the SiC/matrix interface and within the matrix in F3S.10S composite. At the interface, the spinel is present in the form of very fine crystals (> 2 μm), whereas within the matrix, it can

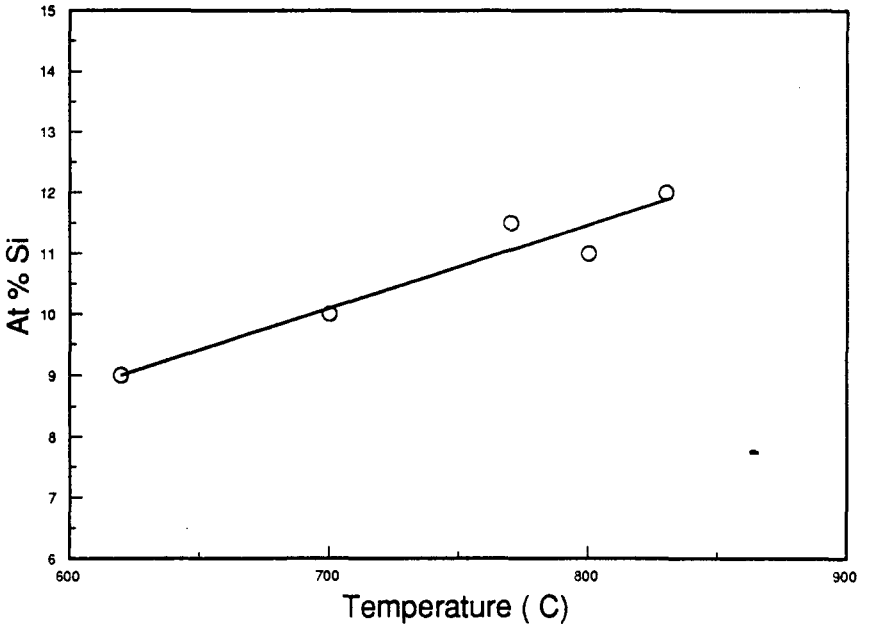

Figure.I.2. Theoretical silicon levels required to prevent Al_4C_3 formation [27].

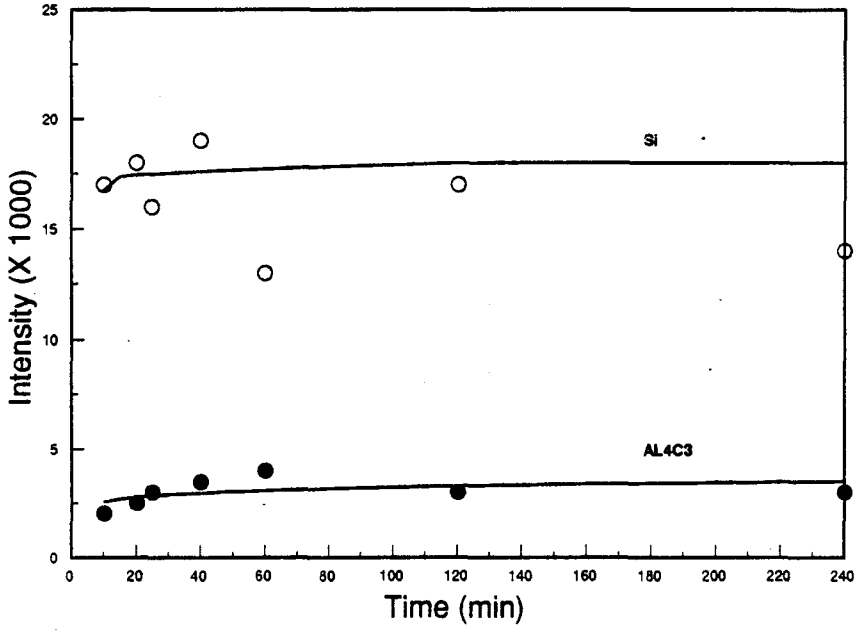

Figure.I.3. Variation in silicon and Al_4C_3 X-ray peak intensity with time at 800°C in Al-Si-Mg/SiC_p composites [27].

exist in much longer dimensions, in some cases almost 200 μm in length, and with different morphologies.

I.2.5. Fabrication of Metal Matrix Composites

The main purpose of producing MMCs is to increase the strength stiffness of the matrix alloy. The yield strength of the heat-treated MMCs is typically 40-65% and their modulus 30% higher compared to those of unreinforced standard aluminum foundry alloys. An additional benefit that metal matrix composites have is that they can be tailored to produce various combinations of stiffness and strength and different values of thermal coefficients of expansion. Also, they can be used in wear applications.

MMCs have several advantages that are important for their use as structural materials, and which include a combination of the following properties:

(a) high strength, elastic modulus, toughness and impact properties compared to the non-reinforced alloy;

(b) low sensitivity to temperature change or thermal shock;

(c) high surface durability and low sensitivity to surface flow; and

(d) high electrical/thermal conductivity and high vacuum environment resistance.

Despite the fact that MMCs have some disadvantages such as low ductility and fracture toughness, they are still considered to be more reliable high-temperature material systems than ceramic matrix composites.

There are many methods for the production of metal matrix composites as

shown in Table I.3 [31-46] In the case of Al/SiC_p or Al/SiC_w composites, the most important methods of fabrication include pressure casting, reocasting (a) mixing fibres (or particulates) with metal, followed by (b) die casting, powder metallurgy and superplastic forming, shown schematically in Fig. I.4. [47-50].

In the particular case of particle reinforced MMCs, there are various methods used for introducing the particles into the molten melt [51]. These methods include :

(a) Injection of powders entrained in an inert carrier gas into the melt with the help of an injection gun. The particles are transferred from the gaseous phase to the melt as the bubbles rise through the melt [52];

(b) Addition of particles to the molten stream filling the mold [53];

(c) Mechanical stirring of the molten alloy with a suitable impeller to create a vortex in the melt and simultaneous addition of solid dispersoid to it. This method has been used most extensively [54];

(d) Forming pellets or small briquettes by co-pressing powders of the base alloy and solid reinforcement particles, and subsequently plunging these pellets into the melt, followed by slow hand or mechanical stirring [55];

(e) Using centrifugal acceleration to disperse particles in the melt [56];

(f) Using high intensity ultrasound with or without mechanical force (e.g. injection of particles through a shotgun while the melt is being irradiated with ultrasound) [57].

The above section covers the general background on composites and MMCs. Other aspects, like the melt procedures followed, the reactivity of the reinforcement

Table.I.3.Various Fabrication Methods for MMCs [31-46].

Fabrication method	Reinforcing morphology	Examples of MMC systems
Diffusion bonding (vacuum, or air hot press)	Laminated composites	B/Al B-SiC/Ti
Squeeze casting	Generally applicable to any type of reinforcement	δ-Al_2O_3/Al C/Mg SiCw/Al Si_3N_4w/Al
Pressure casting	Generally applicable to any type of reinforcement	SiC/Al γ-Al_2O_3/Al
Hot isostatic pressing (HIPing)	Generally applicable to any type of reinforcement	W/Fe-alloy α-Al_2O_3(FP)/ FeCrAlY
Reocasting (compocasting)	Particulates, short fibers composites	Al_2O_3/Al SiCw/Al
Powder metallurgy	Particulates, short fibers composites	SiCw/Al K_2O–$6TiO_2$w/Al
Arc spray forming	Unidirectional and woven composites	W/super-alloy
Superplastic forming	Particulates short fibers and unidirectional composites	SiCp, SiCw/Al Stainless Steel/Al

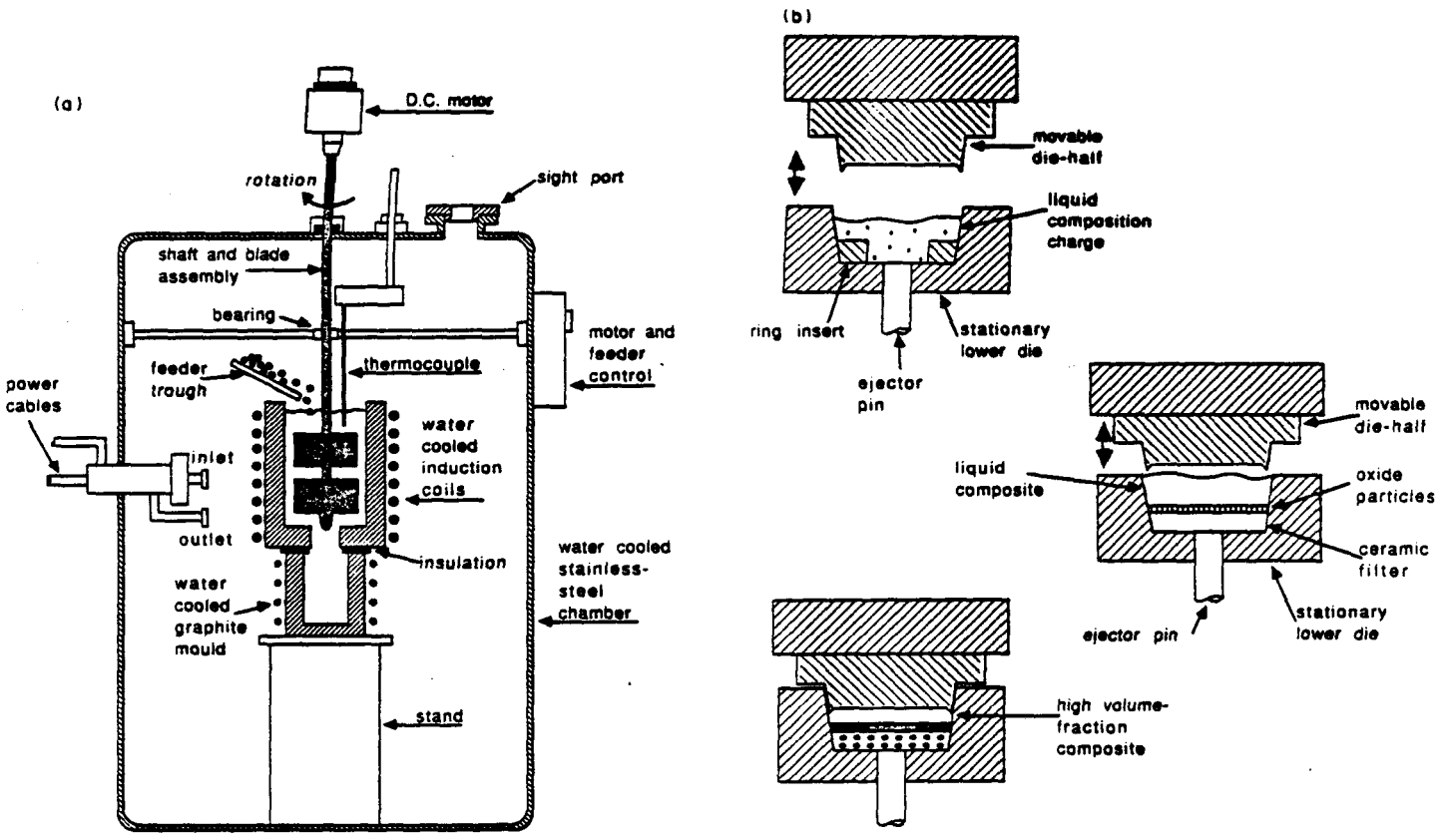

(a) Reocasting [49]

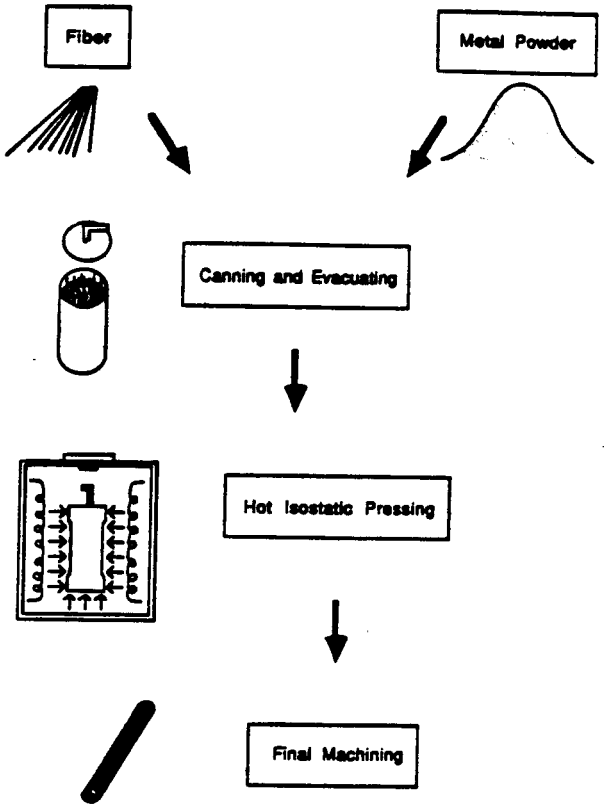

(b) Hot Isostatic Pressing [48]

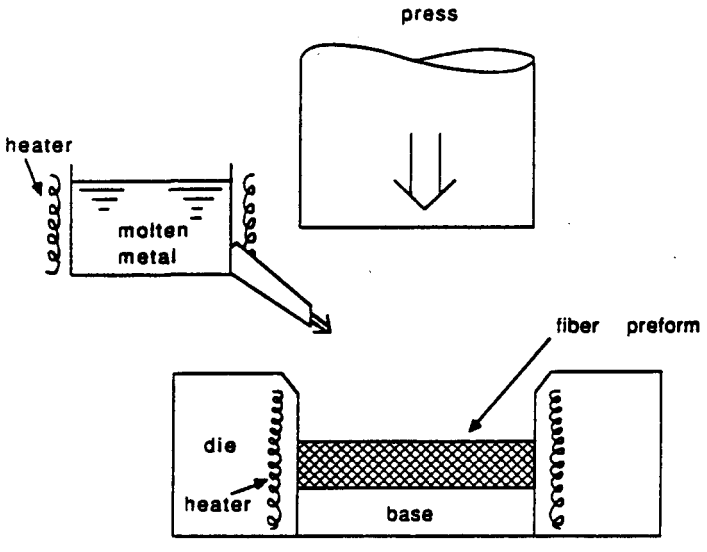

(c) Squeeze Casting [47]

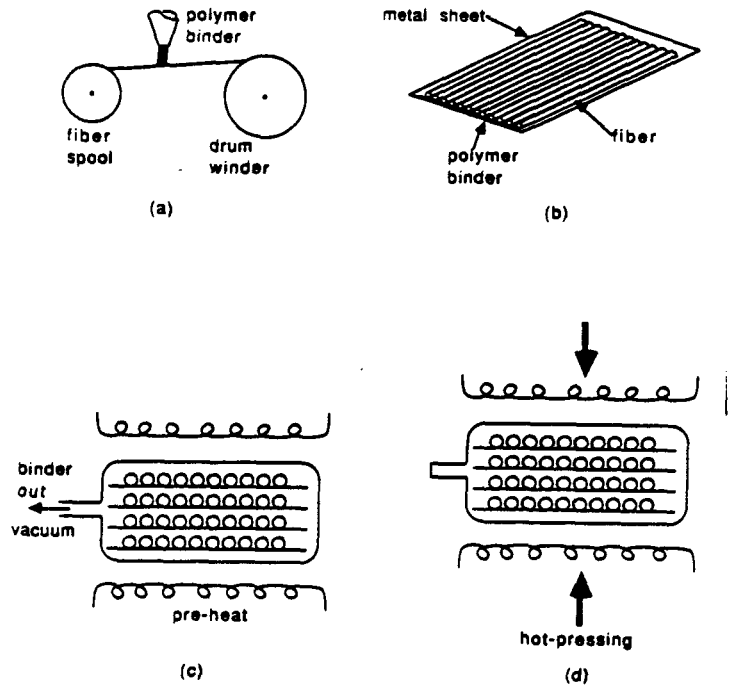

(d) Superplastic Forming [50]

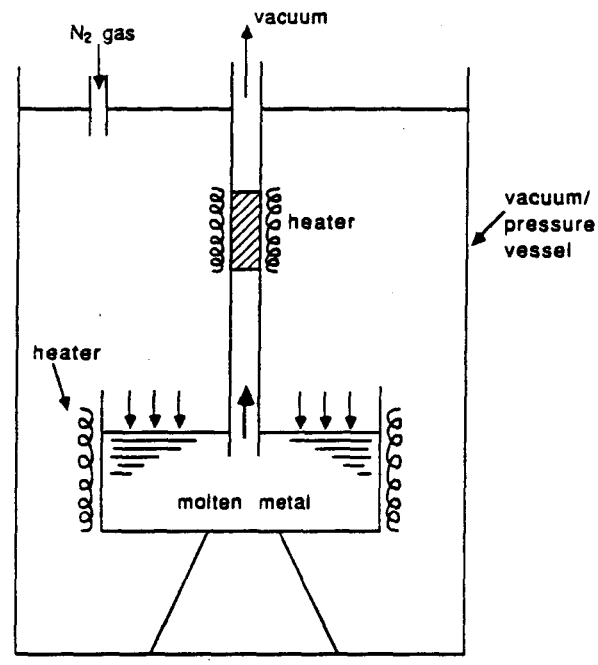

(e) Presure Casting [38]

Figure.I.4.Various Fabrication Methods for MMCs [38, 47-50].

with the melt the solidification and thermal characteristics, etc. are discussed in the next section, in the particular context of Al-Si-Mg/SiC_p composites which form the subject matter of this study.

I.3. Al-Si-Mg/SiC_p METAL MATRIX COMPOSITES

I.3.1. The Al-Si Alloy System

Many foundry alloys are based on the Al-Si system. The commercial importance of Al-Si alloys is based on their high fluidity and low shrinkage in casting, welding and other applications. The hardness of silicon particles imparts wear resistance. The main feature of these alloys is that a eutectic is formed at 580 °C (1080 °F) between aluminum and silicon at a silicon content of 12.5% as shown in the phase diagram of Fig. I.5 , with limited solid solubility at both ends. From this diagram, Al-Si alloys can be divided into three groups as follows [58]:

(a) hypo-eutectic alloys, containing 5 to 10% Si;

(b) eutectic alloys, containing 11 to 13% Si; and

(c) hyper-eutectic alloys, containing 14 to 20% Si.

The alloys A356, 357, 319 and 359 are examples of hypoeutectic alloys. Modification with sodium or strontium (< 0.02%) results in a fine distribution of silicon particles in the hypoeutectic alloys. Alternatively, phosphorous (< 0.01) can be added as a nucleating agent in hypereutectic alloys [45].

I.3.2. The Al-Si-Mg Alloy System

The Al-Si-Mg system forms the basic of a major class of heat treatable alloys used for both wrought and cast products. These alloys combine many favourable characteristics, including moderately high strength, relatively low quench sensitivity, and good corrosion resistance.

Fig. I.6. displays the equilibrium phase diagram. The precipitation reactions in this alloy system have been studied in detail [59, 60]. The normal sequence of precipitation reactions is as follows:

Supersaturated solid solution (SS) → semicoherent β'' rods // <001> Al

→ semicoherent β' (Mg_2Si) needles

// <001> Al

→ semicoherent β(Mg_2Si) needles

// <001> Al

→ non-coherent β(Mg_2Si),

where β'' is thought to have the same structure as $\beta'Mg_2Si$, but there is some evidence that it contains ~ 20% Al. The β' and β are, respectively, hexagonal and fcc Mg_2Si. It is the Mg_2Si precipitates that result in strengthening of the alloy. The above sequence can be better understood if we consider the mechanism of strengthening, details of which are given below.

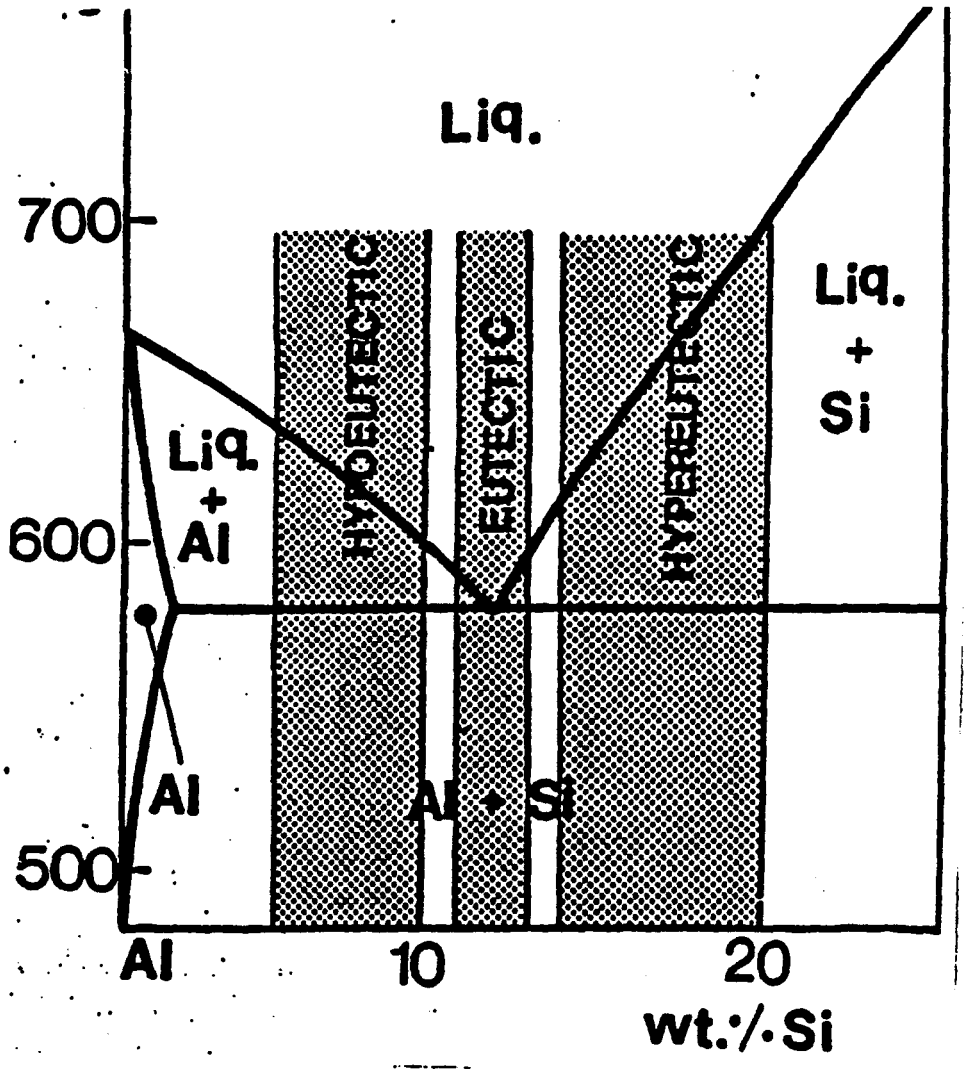

Figure.I.5.Equilibrium Phase Diagram of the Al-Si System [58].

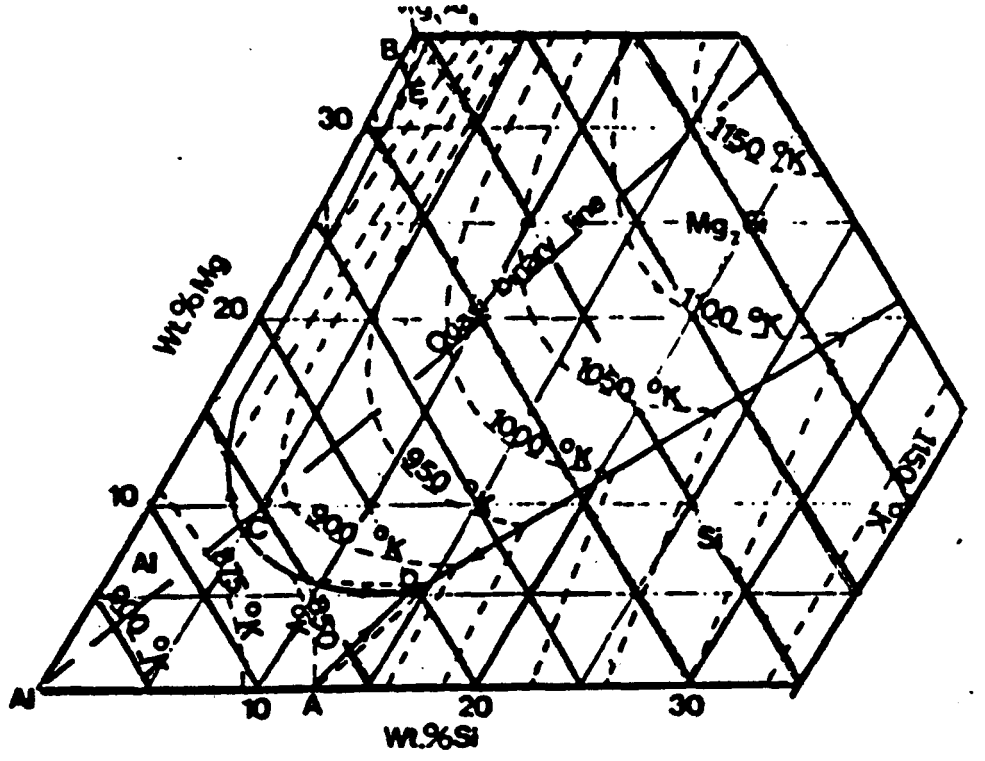

(a)

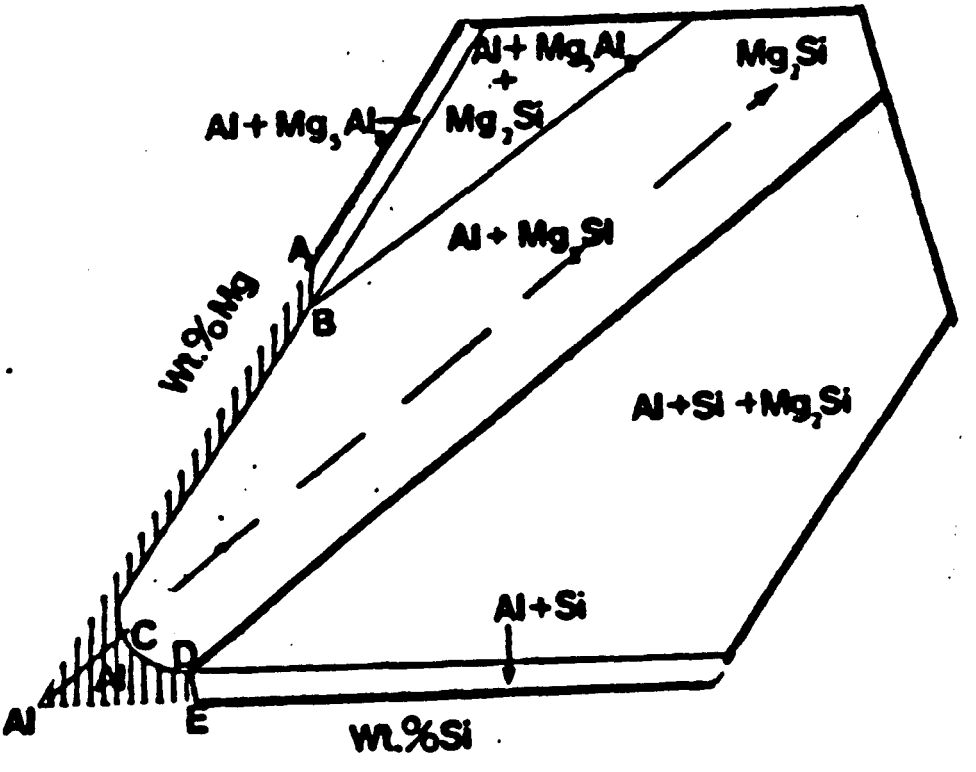

(b)

Figure.I.6. (a) The Al-Si-Mg System (b) Distribution of the Phase in the Solid Solution in the Aluminum Corner of the Equilibrium Diagram [59]

I.3.2.1. Mechanism of strengthening

In most heat-treatable alloys or precipitation-hardenable systems, a complex sequence of time-and temperature-dependent changes is involved. At relatively low temperatures and during initial periods of artificial aging at moderately higher temperatures, the main change is a redistribution of solute atoms within the solid-solution lattice to form clusters or GP (Guinier-Preston) zones that are much richer in solute. This local clustering of solute atoms produces a distortion of the lattice planes within the zones and in the surrounding matrix. The strengthening effect of the zones results from the additional interference with the motion of the dislocations when they cut the GP zones. In most systems, as aging temperatures or time are increased, the zones are either converted into or replaced by particles having a crystal structure distinct from that of the solid solution and also different from the structure of the equilibrium phase. These are called ß transition precipitates. In most alloys, they have specific crystallographic orientation relationships with the solid solution, such that the two phases remain coherent on certain planes by adaptation of the matrix through local elastic strain. The strengthening effects of these semicoherent transition structures are related to the impedence to dislocation motion provided by the precipitate particles and the presence of lattice strains. Strength continues to increase as the size of these precipitates increases, as long as the dislocations continue to cut the precipitates [59].

Further progress of the precipitation reaction produces growth of transition

phase particles, with an accompanying increase in coherency strains, until the interfacial bond strength is exceeded and coherency disappears. This usually coincides with a change in the structure of the precipitate from transition to equilibrium form. With the loss of coherency strain, strengthening effects are caused by the stress required to cause dislocations to loop around rather than cut the precipitates. Strength progressively decreases with growth of equilibrium phase particles and an increase in interparticle spacing.

In the Al-Si-Mg system mentioned above, the GP zones are reported to be of spherical shape and convert to needle-like forms near the maximum strength inflections of the aging curves. Further aging converts the zones to rod-shaped particles. At higher temperatures, this ß′ transition phase undergoes diffusionless transformation to the equilibrium Mg_2Si phase [60].

I.3.3. SiC_p as Reinforcement and its Advantages

The advantages of using particulate SiC as a reinforcement for aluminum alloys (in particular, the Al-Si-Mg alloys studied here) may be summarized as follows:

(a) SiC_p is an optimal reinforcement for aluminum alloys because it has a density only slightly higher than aluminum (cf. 2.7 g/cm^3 for Al vs 3.2 g/cm^3 for SiC).

(b) It has a high modulus and strength, a lower coefficient of thermal expansion and greater wear resistance.

(c) SiC powders are produced in a range of purities, sizes and aspect ratios which

can be used to achieve optimal mechanical properties. Also, it is readily available at low cost.

(d) The yield strength of SiC_p reinforced MMCs is typically 40-65% and their modulus 30% higher compared to those of unreinforced standard aluminum foundry alloys.

(e) SiC_p act as nucleation sites for gas porosity. The coarsening of both gas and shrinkage pores is restricted by the surrounding SiC_p, leading to a well distributed and finer porosity, compared to that formed in A356 alloy (40 μm and 400 μm, respectively). In the case of A356, the porosity is mainly central shrinkage type, linked with gas porosity [61].

(f) It can be used in a certain applications such as aircraft camera gimbals, belt pulleys, gearboxes, brackets, suspension arms, pistons, disk brake rotors, electrical housing and aerospace/defence which required certain mechanical and physical properties that can not be achieved by the ordinary alloys.

I.3.4. Effect of SiC_p on the Precipitation Kinetics

The presence of SiC-particulates or fibres in a ductile matrix significantly alter the response to aging treatment, and an understanding of this response is essential to a rigorous development of composite strengthening theories [62].

The difference between the precipitation kinetics in metal matrix composites and ordinary alloys may be summarized as follows:

(a) The rod-shaped precipitation density is higher in the composites than in the unreinforced material, their size is similar in both matrix and composite, small rounded precipitates are present in the case of composite.

(b) The nucleation of the precipitates during the high-temperature tensile deformation test seems to be favoured by the fibre reinforcement [51].

I.4. SOLIDIFICATION OF CAST METAL MATRIX COMPOSITES

(A) Effect of Chemical Composition

The chemical composition of the melt prior to casting is determined primarily by the purity of the charged materials. Both the mechanical properties and physical properties attainable in the cast component are strongly influenced by the alloy composition. The chemical composition of the two composites are the same as A356 and A359 base alloys, containing, in excess 10% SiC_p. That is, the two composites contain various chemical elements such as Si, Fe, Cu, Mn, Mg, Ti, Sr and SiC-particles. Each element plays a role in solidification, modification, precipitation during heat treatment and the mechanical properties.

Si is the main alloying element in both matrices; it has been reported [64] that for Si additions up to 7%, both UTS and YS increase, with Si additions greater than 7% , both elongation and charpy impact values decrease rapidly, this may be explained by the fact that the excess Si refers to any dissolved Si in the solid solution

which influences the precipitation behaviour during the heat treatment of the alloy.

Mg is the most important element in Al-Si-Mg systems, the Mg concentration is 0.3 and 0.7% for A356 and 359, respectively. The main purpose of Mg addition is that Mg reacts with Si to form the age-hardening compound Mg_2Si which is precipitated from solid solution during heat treatment. This compound is responsible for the improvement in the mechanical properties in the as-cast condition. After solidification Mg is present as large particles of Mg_2Si; depending on the cooling rate, some Mg is also retained in solid solution. An increase of around 0.01% Mg results in an increase of yield strength of about 1000 psi combined with a decrease in the ductility of the alloy. Increasing the Mg concentration more than 0.9% leads to a higher wear resistance than alloys containing 0.3-0.7% Mg [65].

Fe is always present in the melt, and its concentration in the melt plays a role in determining the mechanical properties. The Fe concentration in the melt lies in the range 0.13-0.14% for A356 and A359, respectively; at levels greater than 0.5%, Fe has a strong detrimental effect on elongation and impact strength due to the formation of Iron-rich compounds such as $FeSiAl_5$ and $Al_{10}Si_4Mg_4Fe$; at lower cooling rates they taken large needle shapes and are concentrated at the grain boundaries, at higher cooling rates these Iron-rich compounds are quite small and interspersed more evenly and do not dissolve after solution heat treatment [66].

Cu and Zn are often present in the melt, both reduce ductility and should be maintained within specified limits in order to minimize the effect of room temperature (preaging) on the mechanical properties during the heat treatment tempers.

Sr or Na is always present in the melt in the range 0.01-0.02% in order to alter the microstructure of the Si particles during solution heat treatment. Increasing the strontium content to greater than the indicated amount leads to a high reduction in the mechanical properties. The addition of strontium has been reported not to increase the hydrogen concentration or the rate of repassing for both alloys [67, 68].

SiC-particulates is the main reinforcement element for both the base alloys (i.e. A356 and A359). SiC_p has been one of the most successful reinforcement materials for Al alloys because of its high strength, stiffness and hardness and it is chemically compatible with Al alloys up to 500 °C. For the present two composite materials, the size of the silicon carbide particles meet with FEPA standard 42-6 B-1984 for F 600-grit powders. The particle size distribution has a median of 9.3±1.0 μm with 3% of the particles larger than 19.0 μm and 94% larger than 3.0 μm. The particle shape aspect ratio is from 2:1 to 5:1 and volume percent is 10±2%. They have the following chemical composition [69]:

SiC_p	Free Si	Free SiO_2	Free C	Fe(total)
98.0 %	0.3 % max.	0.5 % max.	0.2 % max.	0.2 % max.

(B) Effect of Cooling Rate

The properties of a casting are determined, in large measure, by the nature of the solidification process, where the factors involved in the transformation from liquid to solid are of the utmost importance. The solid/liquid interface morphology influences

the formation of the dendritic net work upon solidification. During solidification, dendrites grow from the mold wall and fluid flow should also occur in the transverse direction; this flow includes both liquid transport and liquid/solid transport. Fluid flow parallel to the primary dendrite arms/inter-dendritic arms (inter-dendritic flow) is termed as microfeeding.

I.4.1. Experimental Studies in Particle Pushing

Several experimental studies have been carried out in order to determine the critical velocity V_{cr} necessary for complete solidification of metal matrix composites containing different volume fractions of SiC-particles (from 10 to 20 %). Rohatgi et al [70] have studied the relation between the dendrite arm spacing and movement of the SiC-particles (average particle size 12 μm) and their results can be summarized as follows:

(a) At a solidification rate greater than 100 °C/s, the solidification front is planar and rejects the SiC-particles ahead of it.

(b) If the DAS is less than 12 μm, the SiC-particles are expected to be pushed into the intercellular regions. Due to the finer dendrite arm spacing, the number of SiC-particles which could be accommodated at each dendrite boundary is very low.

(c) If the DAS is approximately the same as the SiC-particle size, the particle will be incorporated into the solid by geometrical trapping between converging

dendrites.

(d) For dendrite spacings several times larger than the particle size, particle pushing is more extensive and the reinforcement distribution would be more clustered.

(e) When dendritic spacings are of an order of magnitude larger than the SiC particle size, the particle pushing during solidification will result in a SiC_p network delineating the intercellular regions.

Rohatgi et al. and Lloyd [70, 71] have reviewed the existing theory regarding particle trapping or pushing, over a wide range of freezing rates, where the SiC-particles appear to be rejected by the growing aluminum dendrite interface. According to them, the Jackson model [72], which is a kinetic approach to particle pushing, has failed to predict the particle pushing for the SiC_p/Al system.

Bolling and Cisse [73] have proposed a model which concentrates mainly on the shape of the solid/liquid interface behind the particles, and which is good for predicting the particle entrapment. Predictions of Zubkov's model [74], based on the thermal conductivity of the particles and the melt, and the Surappa and Rohatgi model [75] which employs a heat diffusivity criterion, agree with the experimental observations. However, all these models disregard thermal convection, body forces and breakdown of the solidification front. After diffusion of hydrogen from the interdendritic region to the bulk liquid, hydrogen atoms rise. If the passage of hydrogen is blocked because of solidification, then hydrogen can be trapped in the casting and may promote porosity formation. In discontinuously reinforced cast metal-

matrix composite, the SiC_p are in the intercellular regions, so that the particles are being rejected from the melt and being pushed ahead of the meniscus, to be finally geometrically trapped by converging solidification fronts.

I.4.2. Theoretical Studies in Particle Pushing : Prediction of Critical Velocity V_{cr}

Several theoretical studies have been made in order to determine the critical velocity (V_{cr}) necessary for complete solidification of metal matrix composites containing different volume fractions of SiC-particles (from 5 to 40%). Uhlmann et al. [72] proposed a model for predicting the critical velocity (V_{cr}) during the solidification process of MMCs taking into consideration diffusion in the liquid metal forming the gap between the particle and the solid/liquid interface, by solving the mass conservation equation and the chemical potential equilibrium condition in the gap. They arrived at the equation :

$$V_{cr}=0.5(n+1)\frac{LA_OV_OD}{KTR^2} \qquad (4)$$

where:

n = positive number near 4 or 5

L = the latent heat of fusion per unit volume.

A_O = the atomic diameter of the liquid

V_O = the atomic volume of liquid

D = the diffusivity of the liquid

R = the radius of irregularities on the particle surface

K & T = Boltzman constant and temperature

Bolling and Cisse [73] considered their model based on the viscous drag on the particles as a function of interface shape, and then the effective contact radius in the gap beyond which the interaction between the particle and the growth front is negligible, and they estimated the critical velocity (V_{cr}) for a smooth spherical particle by this equation:

$$V_{cr}^2 = \frac{4KTA_O\sigma\alpha(1-\alpha)}{9\pi\eta^2R^3(1-3\alpha)} \qquad (5)$$

where:

η = the liquid viscosity

σ = the solid/liquid interface energy.

R = the particle radius

α = the ratio of the particle radius to the interface radius.

This model was tested against many experimental results and extended to take into account the effect of gravity. They concluded that V_{cr} decreases as the liquid viscosity increases and the particle size increases, regardless of particle type. The Stefanescu et al. models [76, 77], assumed a planar solid/liquid interface and a gap distance of (1 or 2 atomic diameters). The critical velocity equation obtained by this method can take different forms, depending on the factors involved in the model and the approximations used in the calculation. Potschke and Rogge [78] obtained the critical velocity as follows:

$$V_{cr}=\frac{1.3\Delta\sigma_O}{n}[16(\frac{R}{a_O})^2\lambda_r(15\lambda_r+X^2)]^{-0.5} \qquad (6)$$

$$\textit{Where} \qquad \lambda_r=\frac{K_p}{K_L} \quad , \quad X=\frac{X_\infty/M_1/\Delta\sigma_\infty}{K_o G_n D}$$

where:

F_p = is the volume fraction of particles ahead of the interface

d_O = interatomic distance

g = acceleration due to gravity

K_p = thermal conductivity of the particle

K_L = thermal conductivity of the liquid

V = solidification velocity

V_{cr} = critical velocity for particle engulfment

η = viscosity of the melt

η_r = relative viscosity of the melt ahead of the interface

Δ_ρ = density difference between particles and liquid

λ_r = density difference between particle and liquid

$\Delta\sigma_O$ = surface energy difference

Stefanescu et al. [76, 77] have predicted the critical velocity V_{cr} by taking into account the role of drag forces on the particles, surface energies, buoyant forces and the thermal conductivities of the components in calculating the V_{cr} at which particles are engulfed by the growing solid-liquid interfaces, which is given by the equation :

$$V_{cr}=\frac{1}{6r\eta}\left[\frac{\Delta\sigma_o d_o}{2}(2-\lambda_r)-\frac{4r^3 g\Delta_p}{3}\right] \qquad (7)$$

This equation takes into consideration a single particle at the interface. The liquid viscosity (η_r) when several particles are involved at the interface can be obtained by using the equation:

$$\eta_r=\eta(1+2.5F_p+10.5F_p^2)$$

where F_p is the volume fraction of particles ahead of the interface, which varies during the solidification process, being altered by either engulfment or pushing.

From the last two equations, if we assume that the thermal conductivity of the particle and the liquid are approximately equal (i.e λ_r = 1), and using the relative viscosity calculated in the previous step, the equation can be reduced to the following equation:

$$V_{cr}=\frac{1}{6r\eta_r}\left[\frac{\Delta\sigma_o d_o}{2}-\frac{4r^3 g\Delta_p}{3}\right] \qquad (8)$$

Table I.4. shows the data necessary for calculating the critical velocity V_{cr} during the solidification of different alloys [76].

Table.I.4. Data Necessary for Calculating the Critical Velocity V_{cr} [76]

System	σ_{PS} (N/m)	σ_{PL} (N/m)	σ_{SL} (N/m)	η (Pa/s)	ρ_L (kg/m3)	ρ_P (kg/m3)	k_L (W/mK)	k_P (W/mK)
Al-2%Mg/ graphite	-0.007	1.70	0.093	0.002	2309	2000	109.5	86.5
Al-2%Mg/ SiC	7.81	2.32	0.093	0.002	2695	3220	109.5	15.57
Al-17%Cu SiC	7.81	2.32	0.093	0.002	2309	3220	109.5	15.57
Al-6%W	7.81	2.32	0.093	0.002	2440	3220	109.5	15.57

I.5. HEAT TREATMENT OF METAL MATRIX COMPOSITES

I.5.1. General Principles of Heat Treatment

Heat treatment is one of the important factors that affect the resulting mechanical properties of a casting. In general, the three steps involved in any heat treatment are :

i) Solutionizing at a temperature close to the eutectic temperature;

ii) Quenching; and

iii) Subjecting the casting to natural and/or artificial ageing.

Variations in each of these steps can result in variations in the mechanical properties and can thus be manipulated to derive a particular combination of strength-ductility required for a given application.

The Al-Si-Mg alloy system has been widely investigated in this area, due to the many applications of its alloys where high strength/weight ratios are needed, and heat treatment of the castings has improved the required properties [79]. These alloys contain elements that decrease in solubility with decreasing temperature, and in concentrations that exceed their equilibrium solid solubility at room and higher temperatures.

The mechanism of strengthening (or precipitation strengthening as it is called) involves the formation of coherent clusters of solute atoms. This causes a great deal of strain because of mismatch in size between solvent and solute atoms. The clusters

stabilize dislocations, because dislocations tend to reduce the strain. When the dislocations are anchored or trapped by these clusters, the alloy is considerably strengthened and hardened. The heat treatment includes solution heat treatment at a high temperature to maximize solubility, followed by rapid cooling or quenching to a low temperature to obtain a solid solution supersaturated with both solute elements and vacancies [80].

Solution heat treatments are designed to maximize the solubility of elements that participate in subsequent ageing treatments. They are most effective near the solidus or eutectic temperature, where maximum solubility exists and diffusion rates are rapid. The maximum temperature may also be set keeping in mind grain growth, surface effects and economy of operation. The minimum temperature should be above the solvus, or the desired properties achieved from ageing will not be realized.

The high strength is produced by the finely dispersed precipitates that form during ageing heat treatments that can include either natural ageing or artificial ageing. This final step must be carried out below the equilibrium solvus temperature, as well as below the Guinier-Preston (G-P) zone solvus line. Natural ageing refers to the spontaneous formation of a G-P zone structure during exposure at room temperature. Artificial ageing includes exposure at temperatures above room temperature so as to produce the transitional (metastable) forms of the equilibrium precipitate of a particular alloy system. These transitional precipitates remain coherent with the solid solution matrix and thus contribute to precipitation strengthening.

Several different heat treatment tempers (i.e.T4 and T6) have been developed

for Al-Si-Mg alloys [79] (listed in Table I.1 and Table I.2, in the Appendix). These alloys display appreciable solid solubility of the precipitating Mg_2Si phase at the solidus temperature. The mechanism of strengthening in Al-Si-Mg has been described in detail earlier on, in Section I.3.2.1.

The solution treatment of the alloy casting a) dissolves the Mg_2Si particles, b) homogenizes the casting and (c) changes the eutectic Si morphology. In order to obtain a maximum concentration of Mg and Si particles in solid solution, the solution temperature should be as close as possible to the eutectic temperature. Temperature control is extremely important because if the melting point is exceeded, there is localized melting at the grain boundaries and the mechanical properties are reduced. In most cases, the 356 and 357 type alloys are solutionized at 540±5 °C. At this temperature, about 0.6% Mg can be placed in solution.

The eutectic Si morphology (characterized by particle size, shape and spacing) is an important factor in determining the mechanical properties. Under normal cooling conditions, Si particles occur as coarse acicular needles which act as crack initiators and lower the mechanical properties. Therefore the Si particle characteristics are altered by modification with Na or Sr being added in small amounts to the melt, or by subjecting the casting to a high temperature treatment for long times, where the Si particles break down into smaller fragments and gradually become spheroidized. Prolonged solution treatment leads to coarsening of the particles. The rate of spheroidization and coarsening increase with solution temperature [81].

I.5.2. Heat Treatment of SiC Reinforced MMCs

In contrast to the extensive data available on the heat treatment of Al-Si-Mg alloys, relatively little is documented for their composites, in particular SiC_p reinforced foundry Al-Si-Mg alloys [82, 83]. Most of the investigations reported on MMCs concern discontinuous (particulate or whisker) reinforced composites based on wrought Al alloys. It has been shown that the presence of reinforcement in a matrix alloy can alter the heat treatment response of an MMC. Therefore the optimum heat treatment procedure for any given MMC can differ from that of the unreinforced alloy [84-86]. The reported literature indicates that the presence of the brittle reinforcement particulates in the ductile (Al alloy) metal matrix can lead to accelerated ageing of the matrix in the composite compared to the unreinforced alloy. The accelerated ageing kinetics have been attributed to the high dislocation density generated from the thermal expansion (CTE) mismatch between reinforcement and matrix, and to the presence of highly diffusive interfaces in the composite [88,89], both of which would tend to increase the diffusion rate of precipitation-forming alloying elements. In addition, the dislocations could also serve as nucleation sites for the strengthening precipitates and facilitate faster attainment of peak hardness.

Dionne et al. [87] studied the age hardening behaviour of a 30 vol% SiC_p/7091 composite and found that the ageing response was very rapid in that only after 1 hr ageing at 120 °C, 45% of the peak tensile strength and 69% of the peak hardness were attained compared to the unreinforced alloy.

Cottu et al. [88] showed that the hardening kinetics of an AS7G06 Al alloy/10vol% SiC fibre composite were enhanced by the presence of the reinforcement during the heat treatment. They explained this in terms of the plastic deformation induced during the heat treatment due to the CTE mismatch between matrix and reinforcement, as well as the higher dislocation density in the composite that supplied preferential precipitation sites.

Srivatsan and Mattingly [89] also attributed the enhanced properties of their heat treated 2124 Al alloy composites reinforced with SiC particulates to the CTE mismatch and higher dislocation density factors.

On the other hand, Skibo et al. [90] have reported no difference in the ageing response of cast unreinforced 6061 and 10 and 20 vol% SiC reinforced materials in their studies of the strength and elongation as a function of ageing time at 175 °C in these materials. Lloyd and Chamberlain [91] have reported similar behaviour in 15vol%SiC_p/A356 aluminum composites.

The investigations described above indicate that further detailed studies on the heat treatment of Al-Si-Mg composites are required, to obtain the optimum heat treatment procedure that would result in achieving enhanced mechanical properties.

I.6. FRACTURE MECHANISMS IN METAL MATRIX COMPOSITES

The fracture of unreinforced alloys is associated with void nucleation and growth and the inclusions present in the casting. Fracture of MMCs can occur, due to the formation of reaction products like Al_4C_3 in the case of Al/SiC_p composites at the interface between the reinforcement and the matrix, which can give rise to interfacial failure. Achievement of good wettability between the reinforcement and the matrix is very important because it can prevent such interface reaction which can result in degradation of the reinforcement; this is particularly a problem when continuous reinforcements are used. The fracture is also very sensitive to the distribution of the particulates. Segregation of SiC-particulates during solidification can lead to particle clusters in which the particles are very closely spaced or even touch each other, with voids being nucleated in these clusters. Such segregation of particles can substantially lower the fracture toughness of the composite. Lloyd et al. [92] have proposed a model for the fracture behaviour in Al/SiC composites, as shown in Fig. I.7. Three basic fracture modes are possible :

(a) along the SiC_p/matrix interface : this can happen if the interface is weak and the crack will propagate through the interface (type 1).

(b) along the particles themselves : if the interface is strong together with a strong matrix, the particles will be loaded to their fracture stress and crack (type 2).

(c) along the matrix itself : if the matrix is weak relative to the interfacial and particle strengths, the fracture will occur in the matrix by normal void

nucleation and growth (type 3).

In the fracture mechanism of Al/SiC_p for non-aged composites (i.e. T4 temper), the crack moves through the aluminum matrix by forming microcracks at stress concentration sites in front of the major crack and the major crack advances by crack linkage. The plastic deformation occurs throughout the gauge length, the extent of SiC particles cracking increasing with increasing strain. In the age hardened composite (i.e. T6 and T61 for F3S.10S and F3A.10S, respectively) fracture does not arise from a single major crack but from a large number of microcracks that nucleate in the vicinity of the Al/SiC interface; these microcracks tend to link together leading to catastrophic fracture. Strain becomes localized and particle cracking is more concentrated close to the fracture [93]. Distribution and segregation of SiC_p during solidification leads to particle clusters in which the particles are very closely spaced or even touch each other. Voids are nucleated in these particle clusters and the crack can propagate easily through the particle and result in lowering the fracture toughness of the composite.

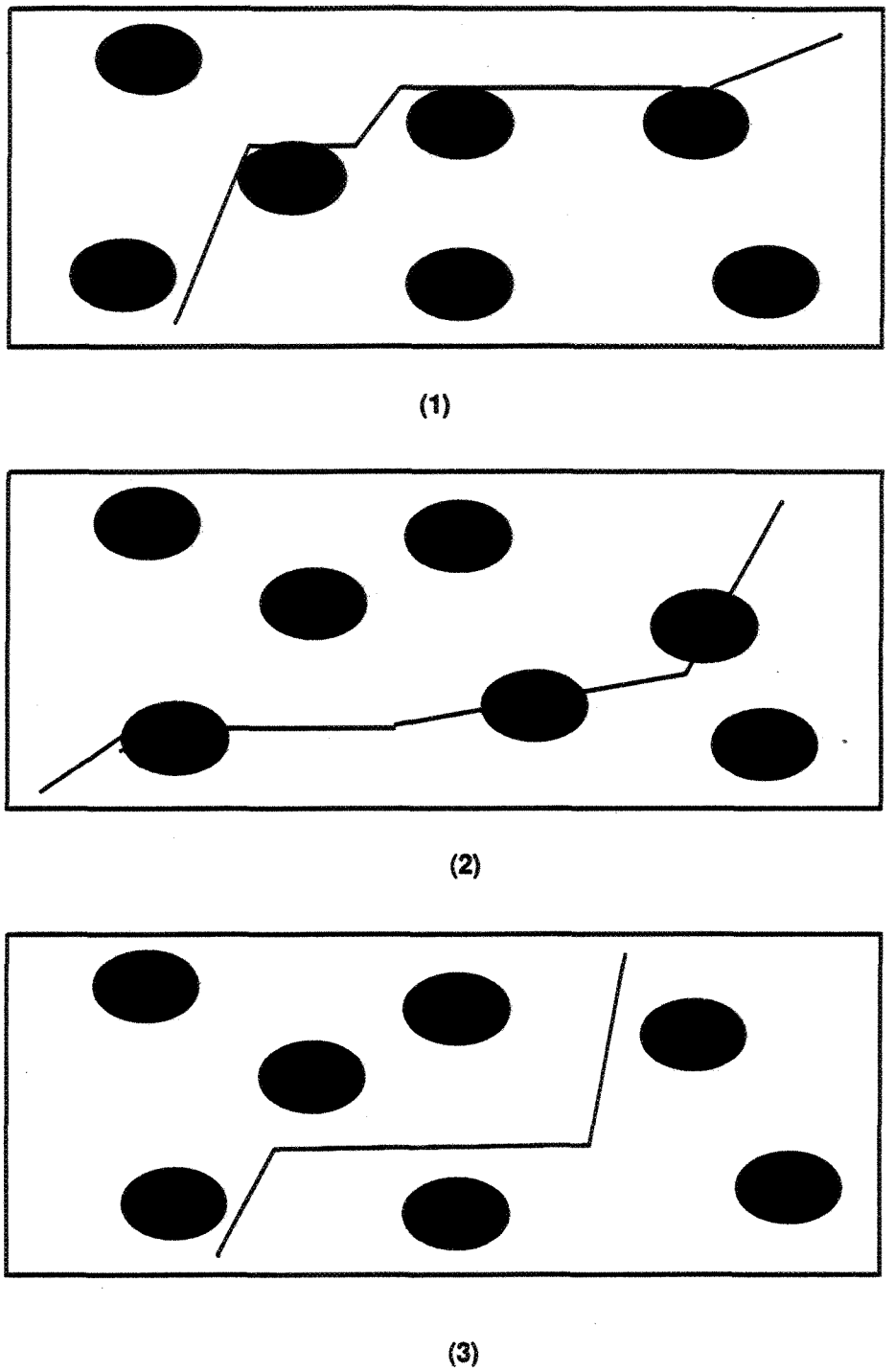

Figure I.7. **Basic fracture modes that can possibly occur in particulate composites [92].**

CHAPTER II
EXPERIMENTAL PROCEDURE

II.1. MATERIALS

The chemical compositions of the two composites studied are given in Table II.1. The composite materials were received in the form of 12.5 kg ingots from Duralcan Canada, Usine Dubuc, Chicoutimi, Québec. In Table II.1, the composites are designated by both their Duralcan names and the currently accepted Aluminum Association (AA) nomenclature for composites, which is of the form:

Alloy/Reinforcement type/Volume percent $_{\text{Morphology}}$-Temper

In the Duralcan system of designation, the composite are designated according as the Al-Si-Mg base alloy contains 7 wt.% Si (F3A.xxS) or 10 wt.% Si (F3S.xxS) and is reinforced with xx.vol.% SiC particulates (10 vol.% in the present case, hence F3A.10S and F3S.10S). Thus F3A.10S designates an Al-Si-Mg/SiC_p composite that contains 10 wt pct silicon and 10 vol pct SiC-particles.

The given Si and SiC contents correspond to the standard specifications; actual values can differ from ingot batch to ingot batch, as is observed in Table II.1. Nevertheless, the composites are still referred to by their standard codes for convenience.

Besides using the as-received ingots, cut-off material from cast test bars (e.g. risers, gates and runners) was also used for preparing melts. Thus, starting material using as-received (supplied) ingots is termed "fresh material" whereas the cut-off material obtained from the fresh material castings and used for further casting is termed "recycled material", to distinguish the two types of castings.

Table II.1. Chemical Compositions of the Two Matrix Alloys.

Duralcan Spec. / AA Spec.	Spec.	Element (wt%)								SiC Vol (%)
		Si	Fe	Cu	Mn	Mg	Zr	Ti	Sr	
F3A.10S	Stand	6.5	.15	.20	.10	.30	.10	.20	-	10
Al-7.0Si-Mg /SiC/10_p	Conc	7.5	max	max	max	.45	max	max	-	
	Anal	7.5	.13	.019	.003	.40	-	.10	.01	11.3
F3S.10S Al-10.0Si-Mg /SiC/10_p	Stand	8.5	.30	.20	-	.45	-	.20	-	
	Conc	9.5	max	max	-	.65	-	max	-	10
	Anal	9.4	.14	.002	.30	.58	-	.11	.13	11.4

II.2. MELT PREPARATION

The supplied ingots were cut into small pieces (about 3in x 3in x 3in (76.2 mm^3)) and heated at 400 °C for at least 2 hr prior to remelting in either 7 or 25 kg capacity silicon carbide crucibles, using an electrical resistance heating furnace, the charging being done when the temperature inside the crucible reached 550 °C. All casting tools such as ladles and skimmers were coated appropriately using Wear-Life mold coating and preheated similar to the ingots (at 400 °C for about 2 hr). During remelting, when the composite was above the mushy zone, the melt was stirred with a graphite impeller specially designed for this purpose, to obtain homogeneous mixing of the SiC particles throughout the melt crucible and to avoid their settling or sedimentation to the bottom of the melt. The impeller was also preheated by positioning it just above the melt surface prior to use. As pointed out in the previous chapter, it is important that stirring be commenced as soon as the metal is fluid enough, to avoid the formation of the harmful Al_4C_3 that can result as a side effect of this sedimentation. The melting temperature was usually kept close to 735±5 °C.

As the composite alloy melts could not be degassed following procedures used for the base alloy due to removal of the SiC-particles, the only means of reducing the hydrogen content in these melts was to take precautionary measures like preheating and proper stirring. Preheating ensures a dry atmosphere for the material, whereas a proper stirring speed allows for the maintenance of the stable oxide layer on the melt surface that serves to isolate the melt from the atmosphere above it. Taking these

precautions, the hydrogen level in the composite melts could be controlled to within 0.15-0.2 ml/100 g Al, an acceptable value. A low hydrogen level is always aimed for, to avoid hydrogen-related gas porosity in the resultant casting.

The melting and casting conditions are summarized below:

Melt holding temperature	735±5 °C
Crucible diameter	172 mm
Impeller/crucible diameter ratio	3/7
Stirring speed	125±5 rpm
Duration of stirring (continuous mode)	20, 40, 60, 120, 180 min.
Pouring temperature	725 °C
Mold temperature range	300-450 °C

II.3. CASTING PROCEDURE

(A) For Tensile Testing and Melt Analysis

Castings were done in a Stahl mold (permanent cast iron mold, ASTM-B-108-85A) to produce test bars for tensile property measurements. Depending upon the study being conducted, melt and mold temperatures were varied accordingly. The pouring temperature was usually very close to 725 °C. Specimens for chemical analysis were also cast simultaneously for each pouring. The chemical analysis was carried out at Alcan International's Arvida R & D Centre (ARDC), Jonquière. The SiC content

was measured using inductive couple plasma (ICP) analysis, also carried out at ARDC.

(B) For Solidification Rate and Related Studies

To investigate the effect of solidification rate (in the range 5-25 °C/s) on the dendrite structure and SiC particle distribution (and related mechanical properties), different molds were employed, and the mold temperatures varied.

The melt was held at 735±5 °C, the pouring temperature was very close to 725 °C. For mold temperatures in the range 300-450 °C, the molten metal was poured into the central zone of a Stahl mold. In connection with the solidification studies, the effect of mold temperature on the castability of these composites was investigated, where the mold temperatures were kept at 300, 350, 400 and 450 °C, respectively. From these studies, it was determined that the F3A.10S composite required a mold temperature of 400-450 °C to produced optimum castings, whereas the F3S.10S composite could be cast at or below 400 °C [94].

II.4. HEAT TREATMENT

All test bars of F3A.10S and F3S.10S were subjected to different solution and aging treatments as follows, as well as the T6 and T61 heat treatments recommended by the manufacturer (Duralcan) for these composites:

- Solution time 4, 8, 12 and 24 hr at 540 °C

- Preaging + Artificial aging	24 hr at room temperature + 24 hr at 160 °C.
- Artificial aging only	5, 12 and 24 hr at 155 °C.

T6 (For F3S.10S) [69]:

(i)	Solution treatment	8 hr at 538 °C (±2 °C)
(ii)	Quenching	Water at 60 °C
(iii)	Artificial aging	5 hr at 155 °C

T61 (For F3A.10S) [69]:

(i)	Solution treatment	12 hr at 540 °C
(ii)	Quenching	Water at 60 °C
(iii)	Natural aging	24 hr at room temperature
(iV)	Artificial aging	24 hr at 160 °C

where treatment involving steps (i) and (ii) only is termed as the T4 temper.

The heat treatment was carried out in a Blue M Ultra-Temp Oven (PRO-8 type). This system is fully linearized, offers thermocouple break protection and provides zero crossover SCR performance; accuracy is ±0.2% of the thermocouple span and repeatability is ±0.5 °F.

II.5. TENSILE TESTING

Tensile tests were performed under uniaxial tensile loading on specimens taken from as-cast or tempered test bars (specimen dimensions : 12.5 mm diameter and 50 mm gauge length), employing an Instron testing machine equipped with data acquisition system that supplied the stress-strain data during testing. All tests were conducted at room temperature at a strain rate of ~ 4 x 10^{-4}/s, using a strain gauge extensometer with a 2.0 inch gauge length, and a cross-head speed of 0.020 in/min. Mechanical properties, namely, yield stress at 0.2% offset strain (YS), ultimate tensile strength (UTS), and fracture elongation (EL%) as well as the plot of stress-strain were derived from the data acquisition and data treatment systems. Each reading in the measurements shown in the corresponding figures represents the average value taken from the two test bars that were simultaneously produced from the same Stahl mold casting.

II.6. METALLOGRAPHY

Samples for metallographic observation were taken at positions as close as possible to the fracture surface of the test bar so that the information near to the fracture surface could be obtained. Samples were also obtained from as-cast test bars and heat treated test bars for microstructural examination. These samples were polished using a technique specially developed for such (Duralcan) composites. The

steps followed in the polishing were as follows:

(a) Grinding the cut samples on a Leco Belt Grinder PSA-12 with Leco 240 and 320 grit SiC grinding paper at a pressure of 35-150 lbf and speed 150 rpm until a flat surface was obtained.

(b) Grinding at the same speed and higher pressure (around 40-180 lbf) for 7 min.

(d) Final polishing step was carried out by grinding at 100 r.p.m speed using magnesium oxide and/or colloidal silica with water at a pressure of 10-50 lbf for 2-5 min.

Keller's reagent was used to etch the samples, wherever required. The polished samples were then examined for SiC_p content and distribution, porosity, etc. using an optical microscope (Olympus PMG3).

The SiC_p and porosity volume fractions, as well as the Si volume fraction, particle size vs count distribution, roundness and aspect ratio were measured by means of a Leco 2001 image analyzer system attached to the optical microscope. Dendrite arm spacings (DAS) for these samples were also measured using the image analyzer. In each case, 100 fields were analyzed at a magnification of 200X, which covered about 12.24% of the total transverse section of the test bar. Although the volume fraction evaluations by image analysis are based on two-dimensional measurements, it is assumed that these are representative of the three-dimensional picture and hence the measurements are expressed in terms of volume fractions.

II.7. FRACTOGRAPHY

The fracture surfaces of the test bars were studied using an Hitachi S-2700 scanning electron microscope equipped with a Link-4 energy dispersive X-ray system to analyze the fracture features. In some cases, metallographic samples were prepared from longitudinal sections of the fractured test bars, as close to the fracture surface as possible, to study the fracture behaviour in the matrix immediately underneath the fracture surface.

II.8. OBJECTIVES OF THIS STUDY

The objectives of this study are: to determine the influence of melting and casting variables on the average (YS, UTS and EL%) and the microstructural characterization of two Al-Si-Mg/SiC/10_p metal-matrix composites (i.e.F3A.10S and F3S.10S); to determine the influence of solution treatment on the change in the Si particle morphology and the average tensile properties; to compare the effect of preaging (natural aging) and direct aging on these properties; to determine the factors which influence the aging response in both composites.

CHAPTER III
EFFECT OF MELTING AND CASTING VARIABLES

III.1. REMELTING AND CASTING TECHNOLOGY

Considerable progress has been made in developing foundry techniques for processing metal matrix composites. These techniques have the potential for low cost mass production and to produce near net shape castings with tailored property-performance characteristics. The composite foundry ingot can be remelted and shape cast easily using standard aluminum foundry practices and equipment [95]. The most significant requirement is stirring the melt to prevent settling of the SiC particles which are denser than the Al matrix. Stirring is accomplished with a motor-driven graphite impeller, except in most induction furnaces, where the convection currents make mechanical stirring unnecessary. The stirring rate must be sufficient to create visible turbulence (but not a vortex) at the surface of the melt.

Fluxing and degassing must be avoided because it would remove the SiC-particles along with everything else. An inert cover gas, such as dry argon, helps to prevent atmospheric contamination of the melt and ceramic filters can be used to trap any large inclusions. Good foundry practice is required, therefore, to keep the composite ingots and the melt itself as clean as possible. The main procedure adopted for the remelting of the composites was as follows:

(a) Materials were preheated at 540 °C for about 2 hr to remove all moisture and dirt.

(b) When the crucible temperature reached about 700 °C, the preheated materials were immediately transferred to the crucible.

(c) Once the composites started melting, the molten bath was stirred mechanically using a graphite stirrer. The impeller blades were designed in such a way (proprietary design) as to prevent sedimentation of the SiC_p. Two different stirring intervals were tried, 20, 40 and 60 min and 60, 120 and 180 min (i.e short and long intervals), respectively.

(d) The melt was held at 735±5 °C (to minimize the volume fraction of Al_4C_3) and the stirring speed did not exceed 125 rpm, to avoid any turbulence (vortex) that could cause contamination by surface oxide films.

(e) No degassing or fluxing was employed.

Fig. III.1 and Fig. III.2 show the melting and casting conditions followed in the present investigation. Before each casting, a sample for spectrometric analysis was prepared. It was noted that there was a slight tendency for SiC particle sedimentation in the case of F3S.10S alloy during the time required for casting. Therefore, in the case of F3A.10S, manual stirring was done before the mechanical stirring. This resulted in maintaining the volume fraction of SiC_p close to the normal level of around 10-12%.

The mold was preheated at the required casting temperature, for at least 3 hr, in an electrical resistance furnace controlled with ±5 °C precision. Before pouring, the surface oxide film was removed, the molten metal was slowly poured into the mold sprue to avoid turbulence, no ceramic filters were employed.

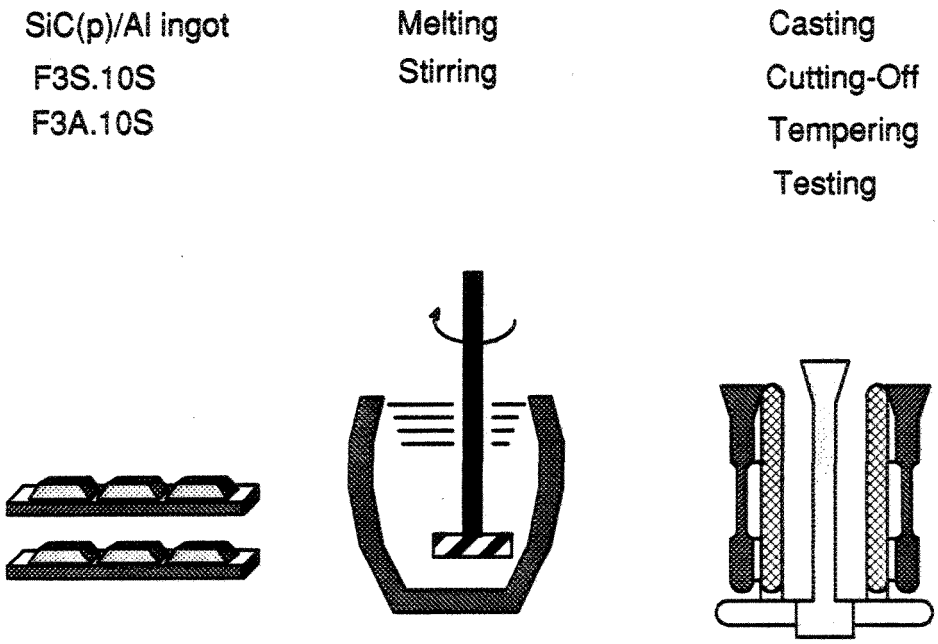

Figure III.1. **SiC_p/Al casting procedure followed in the present investigation: (a) SiC_p/Al Ingot, F3S.10S, F3A.10S; (b) melting, stirring (c) casting, cutting- off, tempering, testing.**

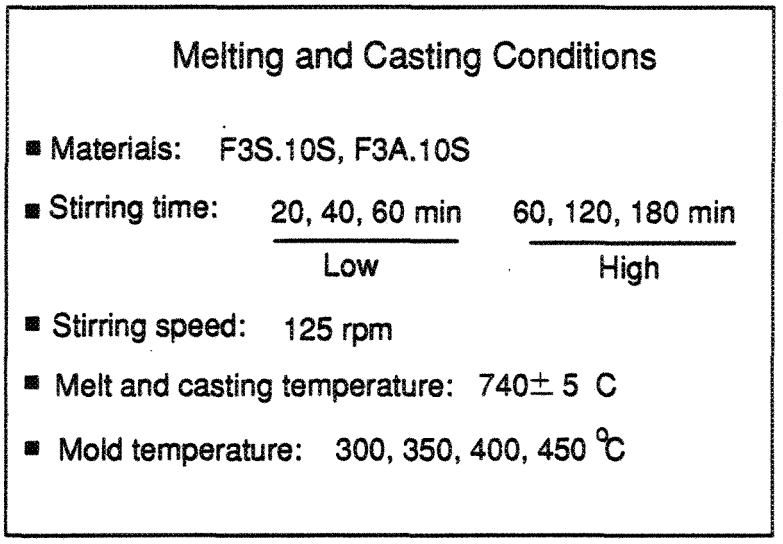

Figure III.2. **Melting and casting conditions followed in the present investigation.**

III.1.1. Estimation of the Motion of SiC_p Particles Within the Molten Melt

Simulation process has been carried out using fluent Logical (Suncao) system for F3A.10S alloy by using the physical properties for both A356 and F3A.10S alloys as given in Table III.1.[69] in the Appendix). The physical constants (density, viscosity, coefficient of thermal expansion and thermal conductivity) were calculated using the linear relationship:

$$Y = AX + B \qquad (11)$$

Assumptions:

(a) Velocity (i) beside the crucible wall: 0 m/s (ii) within the molten bath: 1.78 m/s (based on 125 rpm stirring time) (iii) at/near the top of the melt 0: m/s.

(b) Temperature (i) Crucible wall temperature: 1500°C (ii) molten metal temperature: 750°C (iii) Outer temperature: 50°C.

From the previous calculation and the above assumptions, the velocity vectors show that the motion of SiC_p within the molten bath occurs from the bottom to the top of the crucible and the impeller motion is from left to right; the SiC particles are always distributed homogeneously within the molten bath as show in Fig. III.3. Fig. III.4 shows the stream function representing the velocity vector contour lines within the crucible. From this figure it is clear that the velocity reaches a maximum value near the impeller and a minium value near the crucible walls, while the temperature contours show an opposite trend.

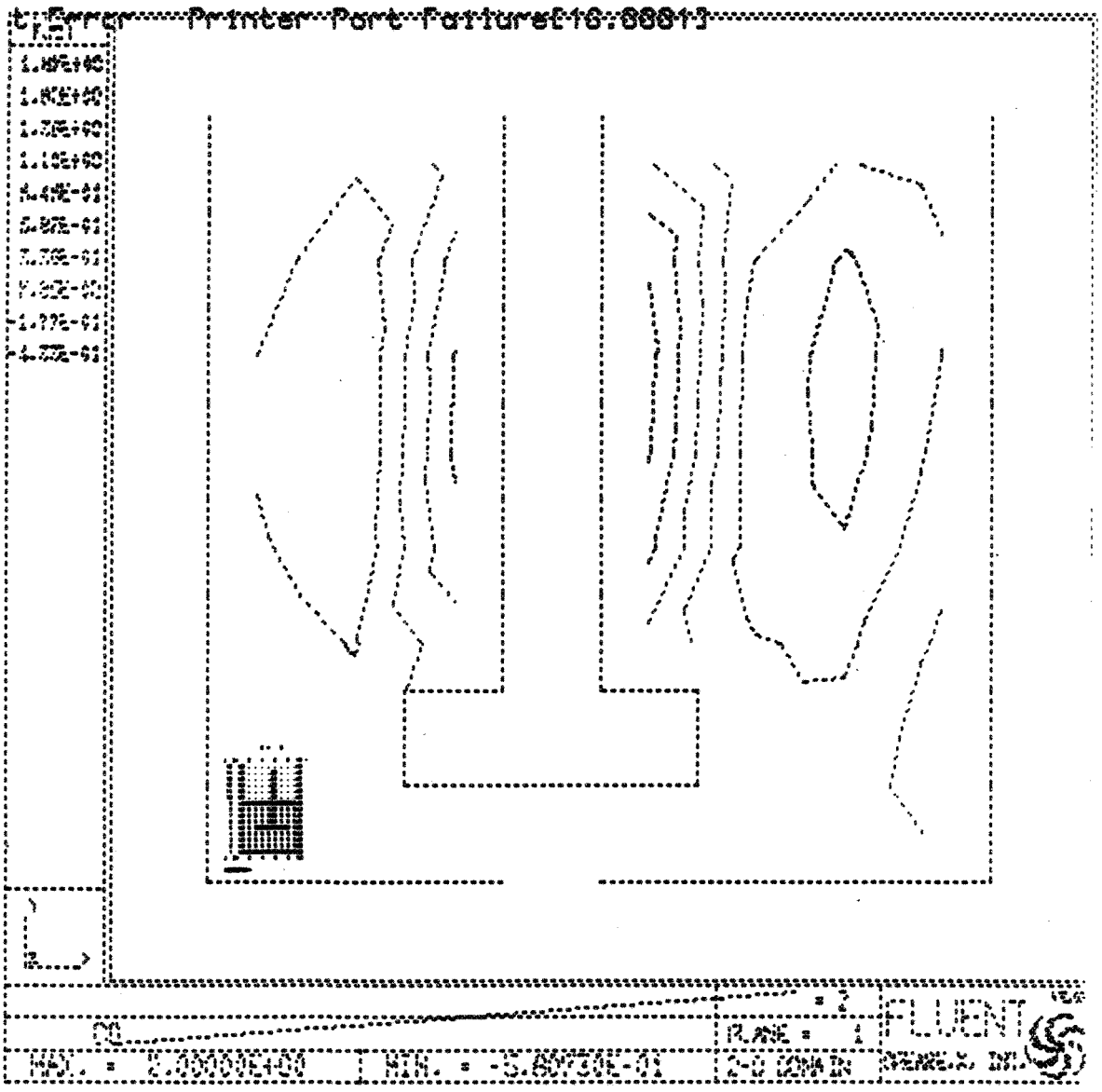

Figure III.3. **Velocity vectors of SiC_p within the molten Al-Si-Mg bath.**

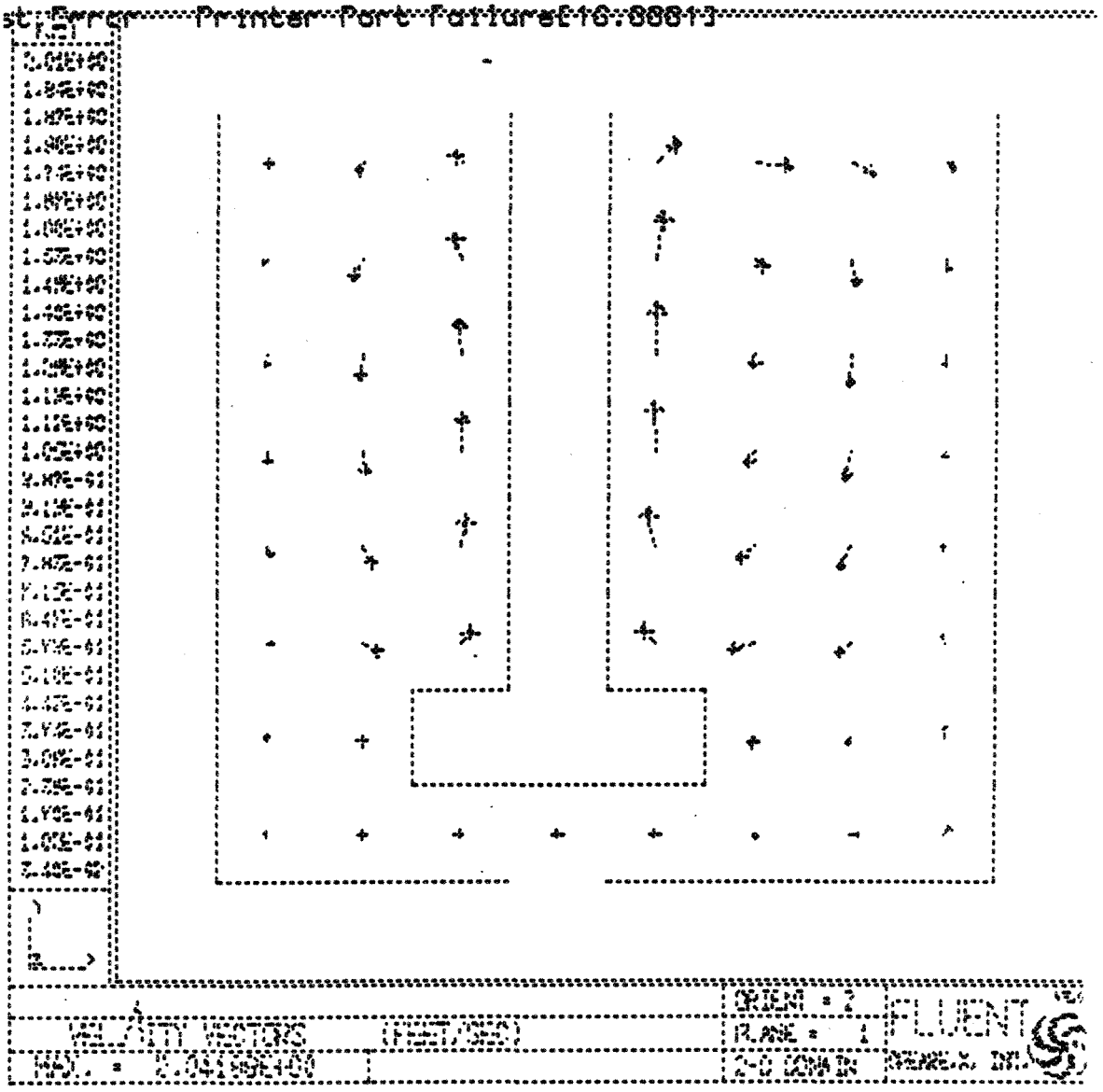

Figure III.4. **Velocity vector contour lines within the Al-Si-Mg bath.**

III.2. FLUIDITY MEASUREMENTS

Introducing SiC particles into the molten melt imparts a viscous slurry-like characteristic to them, affecting flowability or fluidity. There is a dramatic change of fluidity at higher temperatures. This may be attributed to an increase in the tendency of the alloy to form bubbles and oxides at higher temperatures. Fluidity is not the inverse of viscosity, rather, it is the ability of the melt to fill the mold or take a shape. The fluidity of the composite alloy is, in most cases, not significantly different from that of the unreinforced matrix. In the present study, the fluidity was measured in two ways :

(a) Using a Ragone fluidity tester at 200 mm Hg. In each case, the melt was stirred for 30 min (melt temperature range: 650-850°C).

(b) Measuring the ability of the liquid metal to fill the mold heated at 300, 350, 400, and 450°C.

The results obtained on employing the first technique are shown graphically in Fig. III.5. Two main observations can be made from this figure:

(a) The fluidity of F3S.10S alloy is much better than that of F3A.10S, probably due to the increase in Si content (10 vs 7 wt %).

(b) On cooling from temperatures higher than 800 °C, the fluidity of both alloys is significantly reduced.

This reduction may be explained in terms of the increase in the volume fraction of Al_4C_3 that normally forms at high temperatures [27]. Therefore, it is recommended

that the melting temperature of the composite should not exceed 725 °C. Similar results have been reported by Lloyd and Chamberlain [4] on the fluidity of A356 with ~ 10 vol% SiC_p as measured by the spiral length the metal traverses when cast into a spiral mold. Due to the formation of Al_4C_3 phase at temperatures higher than 725°C, especially for the F3A.10S composite, and its effect on the fluidity, another series of tests was carried out. In this series, the melt temperature was held at 735±5 °C for 20 min. Thereafter, the melt was poured into the mold preheated at 300, 350, 400 and 450°C. In this case, the fluidity was measured by the height of the mold riser, as shown in Fig. III.6, (a) for F3A.10S and (b) for F3S.10S, respectively. It is evident that there is a dramatic reduction in the riser height with mold temperature in the case of F3A.10S, whereas the effect is observed on a much lesser scale for the F3S.10S composite.

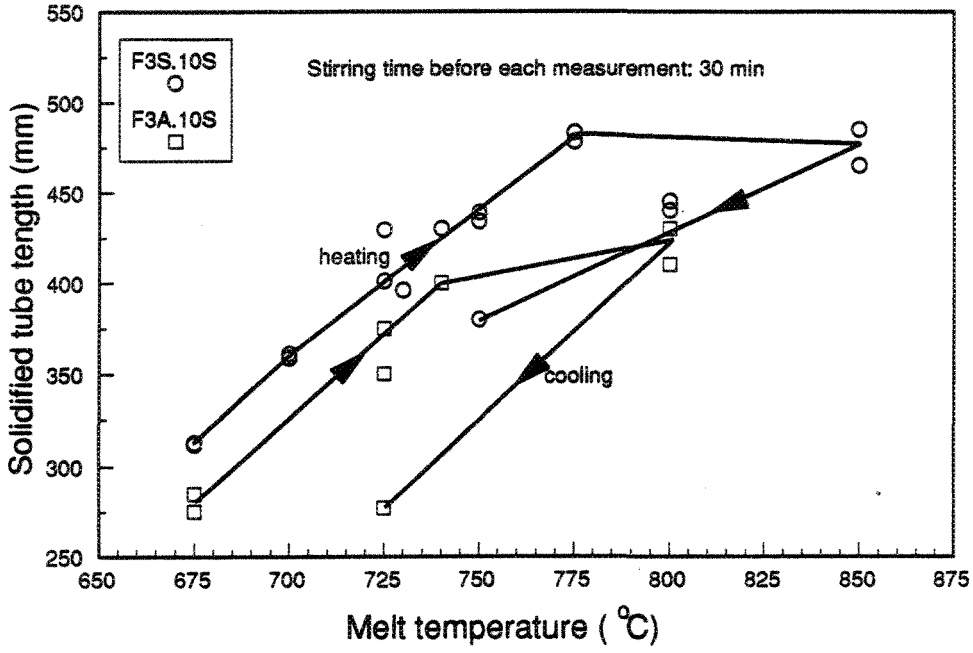

Figure III.5. Fluidity characteristics of F3A.10S and F3S.10S composites in the temperature range 675-850°C, measured by the solidified tube lengths in a Ragone Fluidity Tester (at 200 mm Hg).

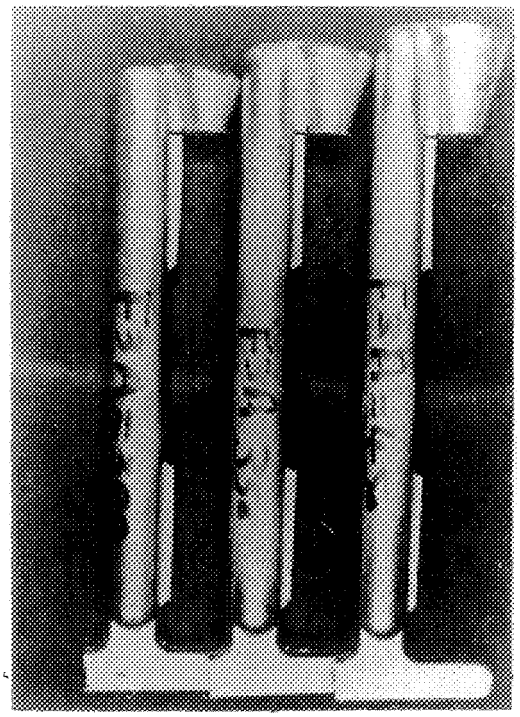

a

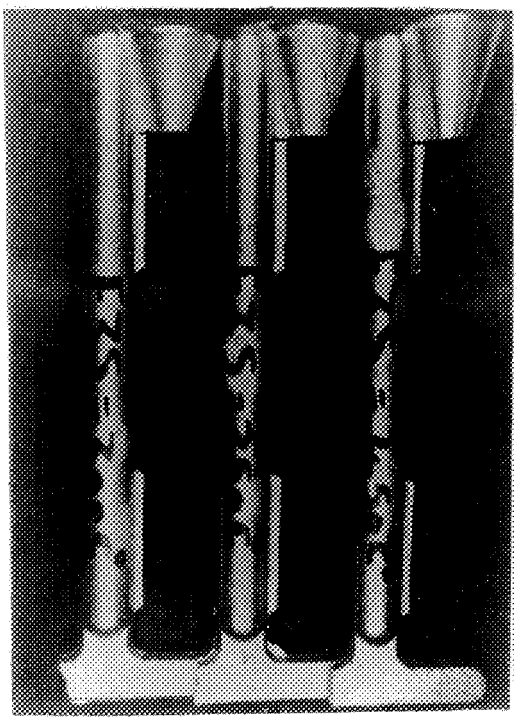

b

Figure III.6. Shape of the casting obtained at different mold temperatures in the range 300-450°C: (a) F3A.10S, (b) F3S.10S.

III.3. EFFECT OF MELT AND CASTING VARIABLES ON THE PROPERTIES OF THE AS-CAST COMPOSITES

The strength values depend somewhat on the uniformity of the particle distribution which in turn depends on the solidification rate of the casting. Castings that solidify rapidly exhibit very uniform distribution. When the solidification rate is very slow, the distribution is less than optimal. This is caused by the pushing of the SiC particles by the leading edges of growing aluminum dendrites. These factors control the mechanical properties of the as-cast composites. Particulate reinforced MMCs produced by foundry techniques find a wide variety of applications due to the low cost of their fabrication and specificity of achievable engineering properties. They have high longitudinal and transverse strengths at normal and elevated temperature [96]. A proprietary SiC_p/Al material has excellent high temperatures strength up to 500°C, above this temperature, however debonding and decohesion between reinforcement and matrix causes reinforcement pullout and failure of the material. The Al-Si-Mg matrix used in SiC_p/Al composites, coupled with mold temperature, are the most important factors affecting the tensile properties of these composites. From the stress-strain curves, it was observed that the proportional limit stress increased as the SiC_p reinforcement particles were introduced. Accordingly, a higher flow stress was required to reach a given plastic strain. As mentioned by McDanels [97], this indicates that the strength increase was probably caused by closer packing of the reinforcement and smaller interparticle distance in the matrix. This would cause an increased

interaction of dislocations with the SiC_p reinforcement, resulting in increased strain hardening.

Tensile properties - yield strength (YS), ultimate tensile strength (UTS) and percent elongation (EL%) for both F3A.10S and F3S.10S composites as a function of mold temperature and stirring time obtained in the present work are given in Fig. III.7 and Fig. III.8, for F3A.10S and F3S.10S, respectively (and listed in Tables III.2 to Table III.5. in the Appendix). Each reading is an average of two to four test bars. The results could be summarized as follows:

(a) Increasing the Si content from 7 to 10 wt% results in slightly higher YS and UTS values,~1.5 ksi, for mold temperatures below 450°C. This is coupled with a reduction in ductility of about 0.5%.

(b) At mold temperature 450°C, the F3A.10S composite reveals a better strength and ductility compared to the F3S.10S alloy.

(c) For clean metal, increasing the stirring time from 20 min to 3 hr does not cause any significant change in the mechanical properties.

(d) Comparing the mechanical properties of both A356 and F3A.10S alloys reveals that the presence of 11 vol% of SiC_p attributes, to a good extent, to the material strength. This however, is associated with a marked reduction in the alloy ductility. (see also Table IV.1 and Table IV.2 in the Appendix for properties of A356).

Fig. III.9 shows the relationship between stress (MPa) and elongation (%) for F3A.10S and F3S.10S in the as-cast condition at mold temperature 450°C.

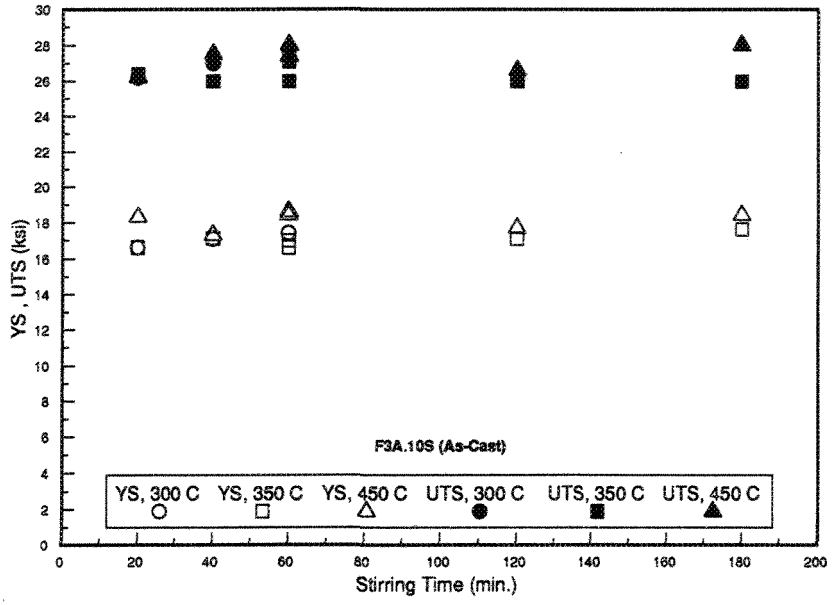

(a)

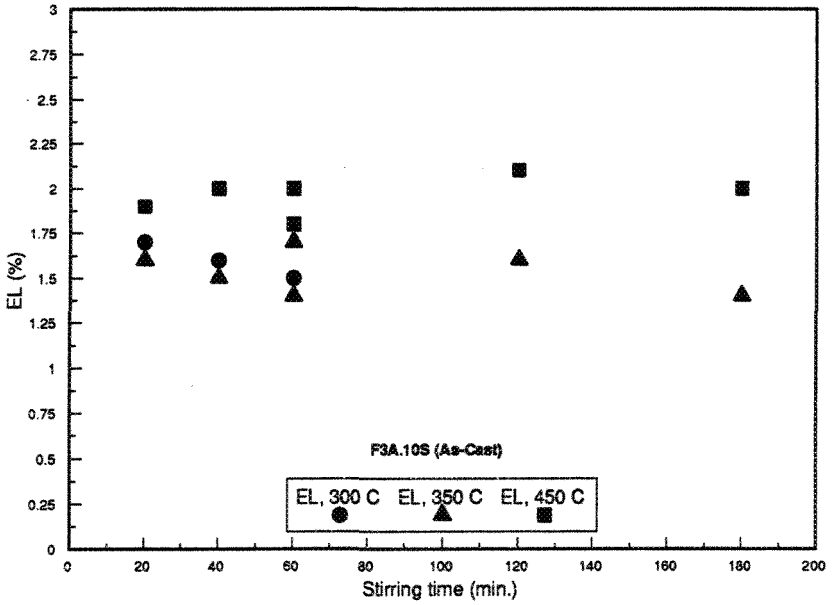

(b)

Figure III.7. Effect of stirring time and mold temperature on (a) tensile strength (ksi) (b) elongation (%) of F3A.10S composite in the as-cast condition.

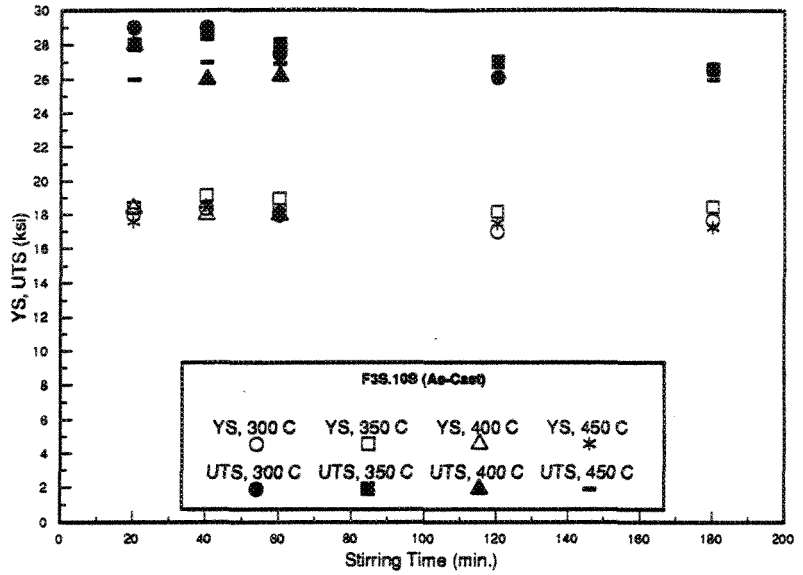

(a)

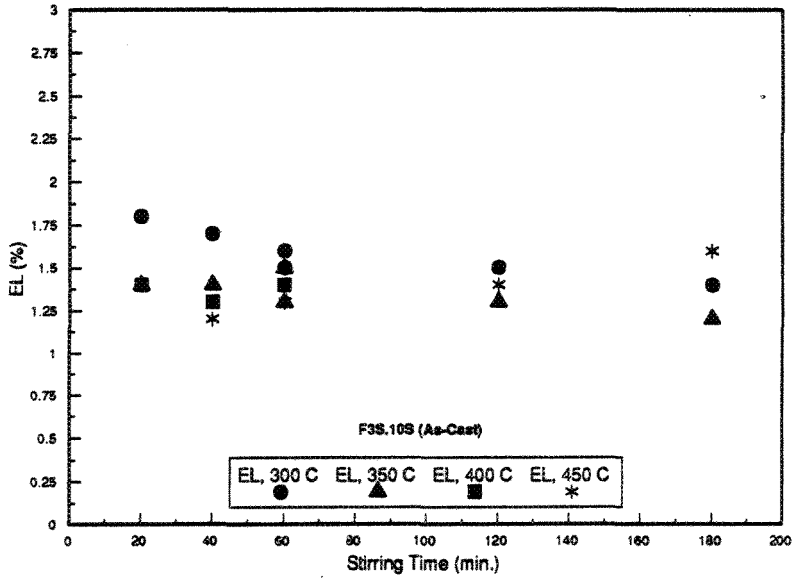

(b)

Figure III.8. Effect of stirring time and mold temperature on (a) tensile strength (ksi) (b) elongation (%) of F3S.10S composite in the as-cast condition.

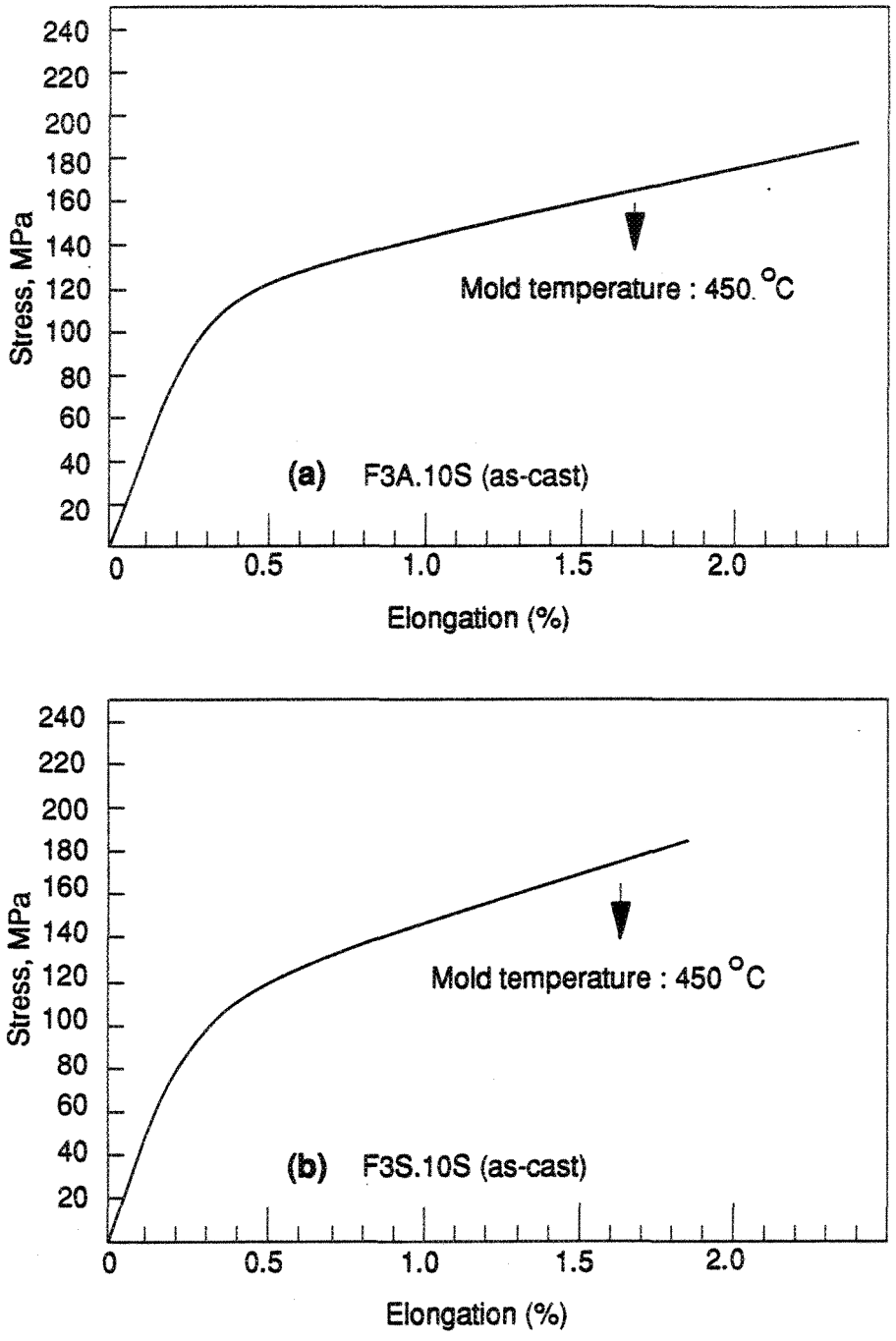

Figure III.9. Typical stress-strain curves obtained from 450°C mold temperature castings for (a) F3A.10S, (b) F3S.10S.

III.4. EFFECT OF MELT AND CASTING VARIABLES ON THE STRUCTURAL CHARACTERIZATION OF THE AS-CAST COMPOSITES

III.4.1. Porosity Formation

The void volume porosity fractions for F3A.10S and F3S.10S composites were measured from metallographic specimens obtained from the central portions of test bar gauge lengths, using image analysis. Porosity can occur in the composites due to several reasons, for example, hydrogen gas from moist air in the atmosphere surrounding the melt, oxides formed at the surface of the melt, the presence of foreign particles (inclusions) in the melt, graphite contamination from the shaft and impeller, as well as the shrinkage that arises from an improper mold temperature which affects the feedability of the as-cast composite.

Figs. III.10 and III.11 show the gas and shrinkage porosity observed in the casting after 20 and 180 min stirring time at mold temperature 450°C for F3A.10S and F3S.10S composites, respectively. Depending on how they are formed, the pores take different shapes. In the present work, the mold temperature was maintained constant at 450°C to minimize the latter (i.e. shrinkage porosity).

The dependence of porosity or void volume fraction on the mold temperature and stirring time is shown in Fig. III.12. The field numbers represent fields taken consecutively, traversing from edge to centre to the opposites edge, for each specimen. It is evident that irrespective of stirring time, the porosity is more or less distributed

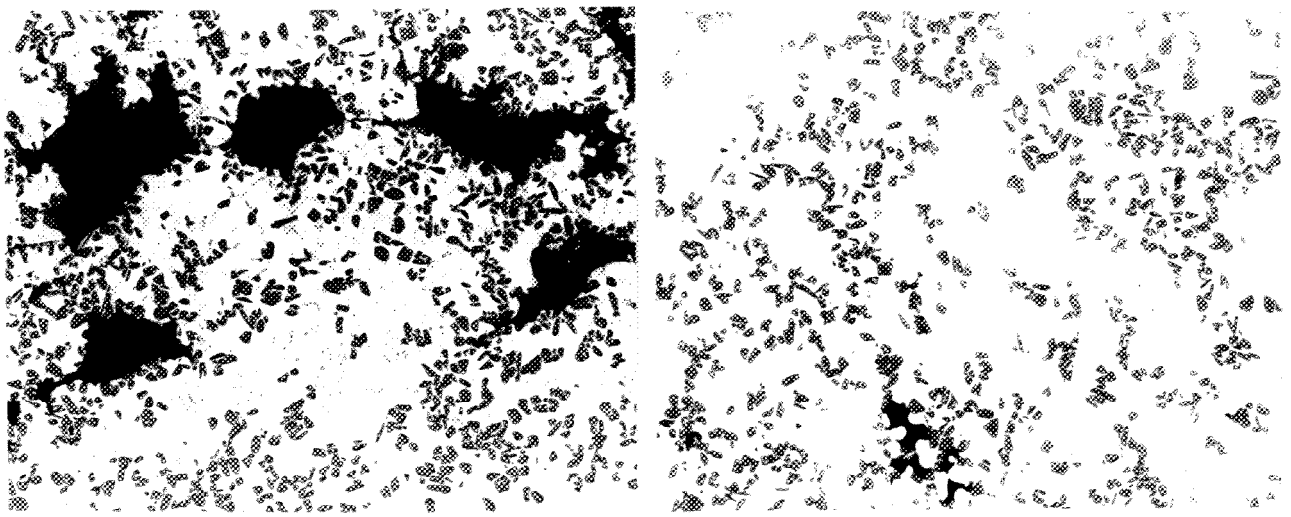

a

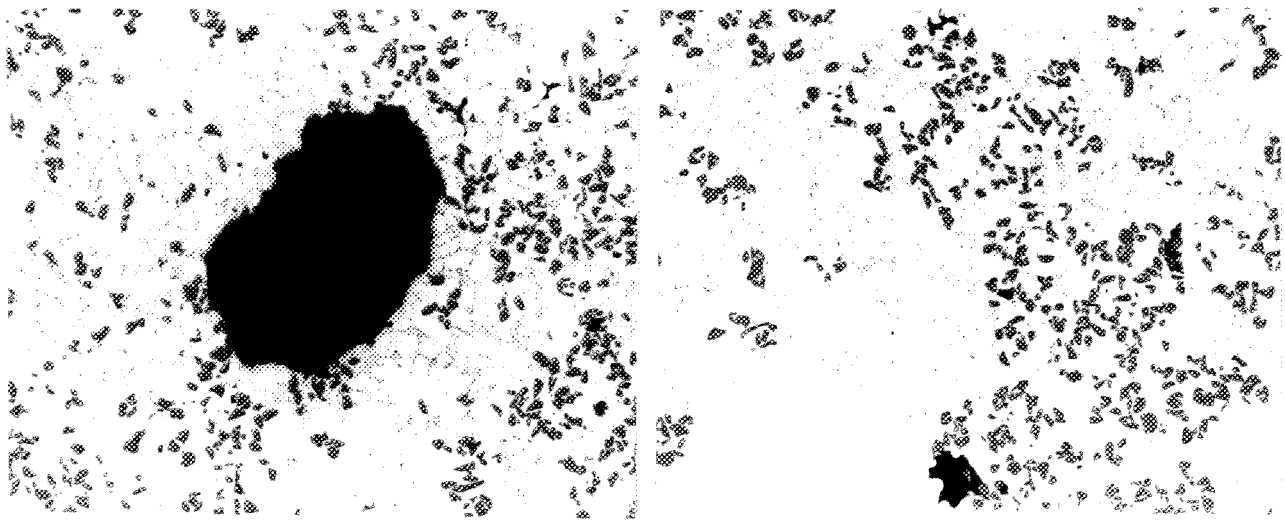

b

Figure.III.10. Optical micrographs showing the gas and shrinkage porosity in the casting (a) after 20 min stirring time, (b) after 180 min stirring time, for F3A.10S test bars at mold temperature 450°C (750 X).

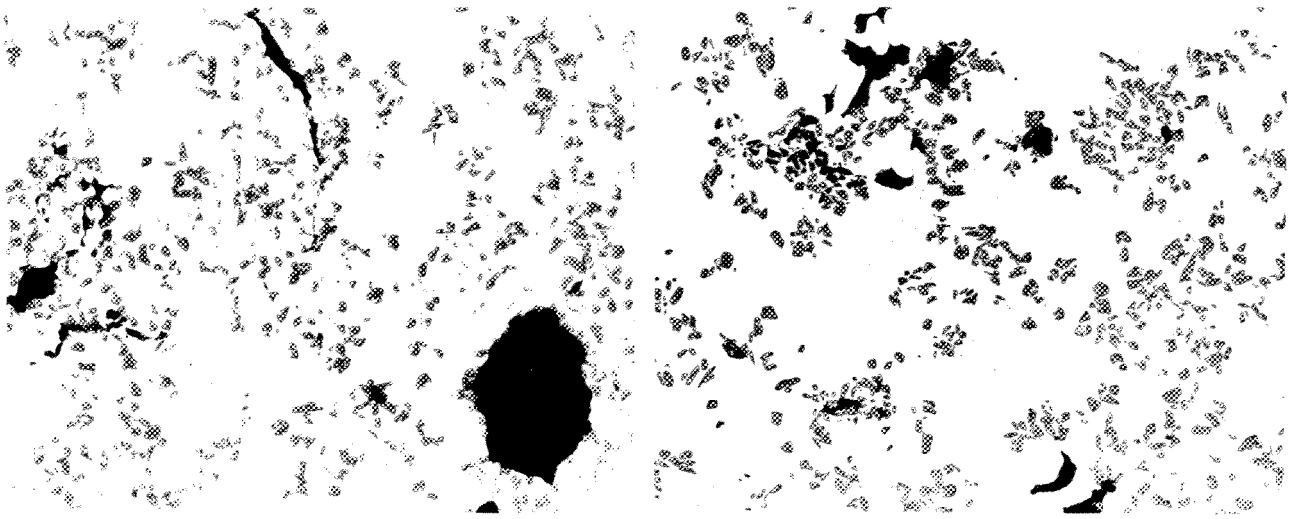

a

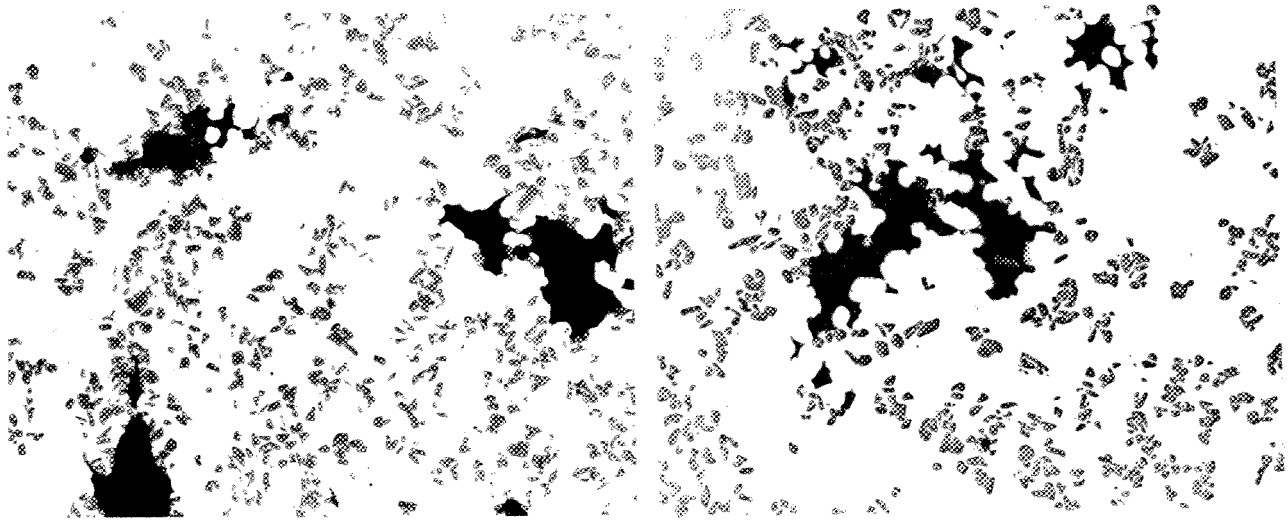

b

Figure.III.11. Optical micrographs showing the gas and shrinkage porosity in the casting (a) after 20 min stirring time, (b) after 180 min stirring time, for F3S.10S test bars at mold temperature 450°C (750 X).

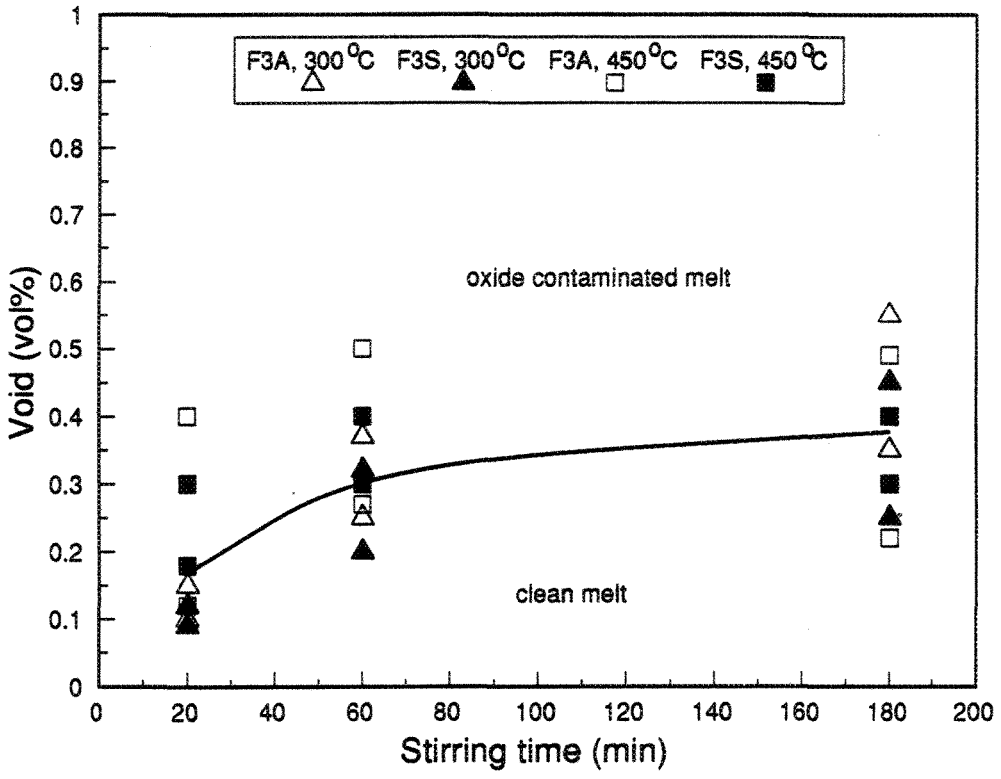

Figure.III.12. **Effect of mold temperature and stirring time on void volume fraction (obtained from image analysis). Each spot is an average of at least four specimens.**

across the cross section of the specimen. Increasing the mold temperature or stirring time only results in increasing the porosity level, without a significant effect on the porosity distribution. It is important to note, however, that oxides have a very pronounced effect on the porosity level, regardless of stirring time, the porosity level going up to 0.6% or even more. From Fig. III.6, one also observes that the F3S.10S alloy has a slightly better soundness, specially at low mold temperatures (300°C) than the F3A.10S alloy.

Fig. III.13 shows the void (porosity) area distributions for A356, F3A.10S and F3S.10S alloys, respectively. It is clearly seen from these distributions that the presence of the SiC particles leads to a marked reduction in the pore size (about 10 times smaller than those found in the A356 alloy. Fig. III.14 shows the effect of mold temperature on the void distribution in the two composites. In the optical micrographs shown in Fig. III.15, the voids are seen to occur at the SiC_p/matrix interface. In other words, the SiC particles act as nucleation sites for gas porosity. The growth/coarsening of the gas void is seen to be restricted by the surrounding SiC particles, as shown in the inset in Fig. III.15.

The optical micrographs of Fig. III.16 show the difference in void distribution obtained for clean versus oxide contaminated material; from Fig. 16 (b), the oxide films are always seen to be associated with gas voids. It is evident that localization of oxides results in the formation of large voids, leading to an overall increase in the void volume fraction to about 0.6%. On the other hand, the clean material displays a maximum void volume fraction of 0.3%, as shown in Fig. III.12.

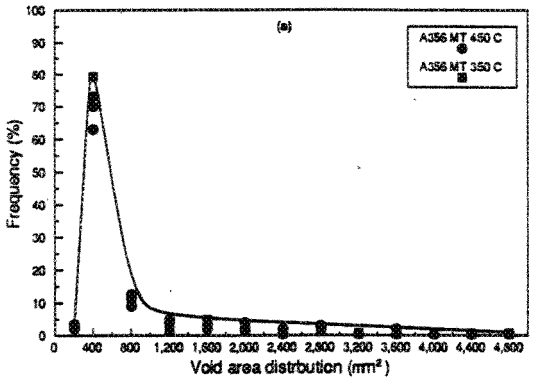

(a)

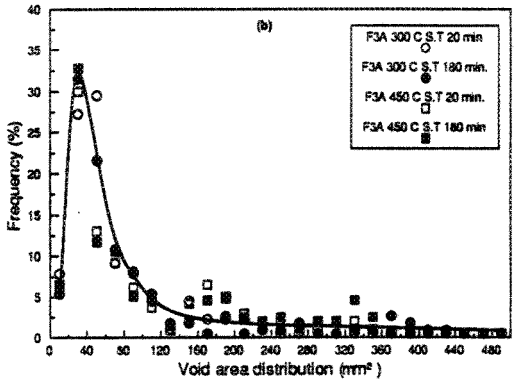

(b)

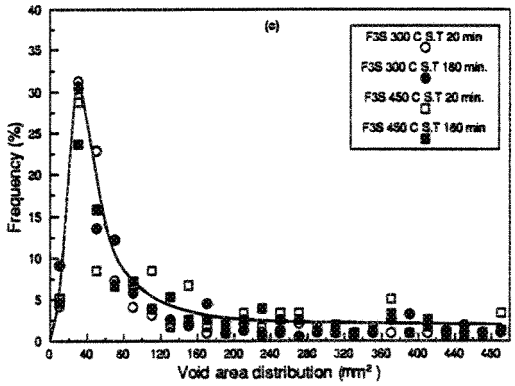

(c)

Figure.III.13. **Void area distribution measured from specimens prepared from (a) A356, (b) F3A.10S, (c) F3S.10S.**

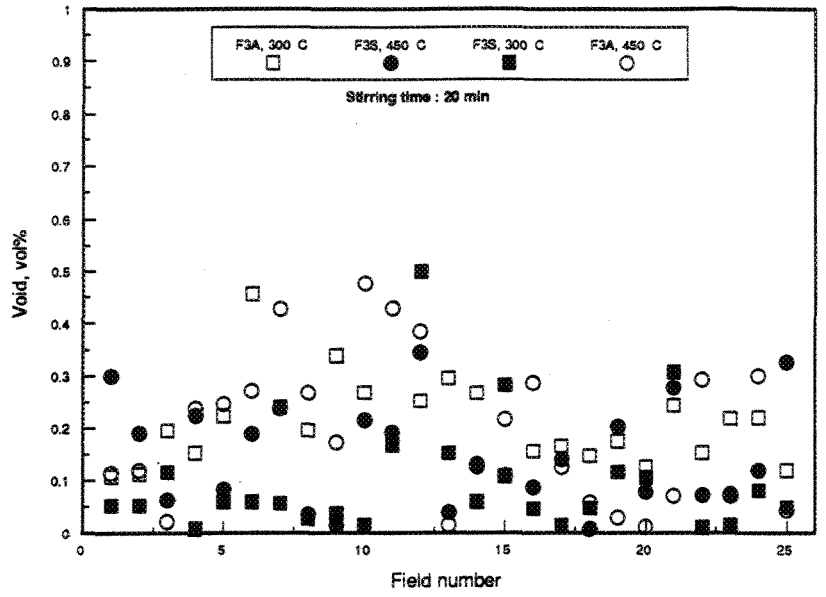

(a)

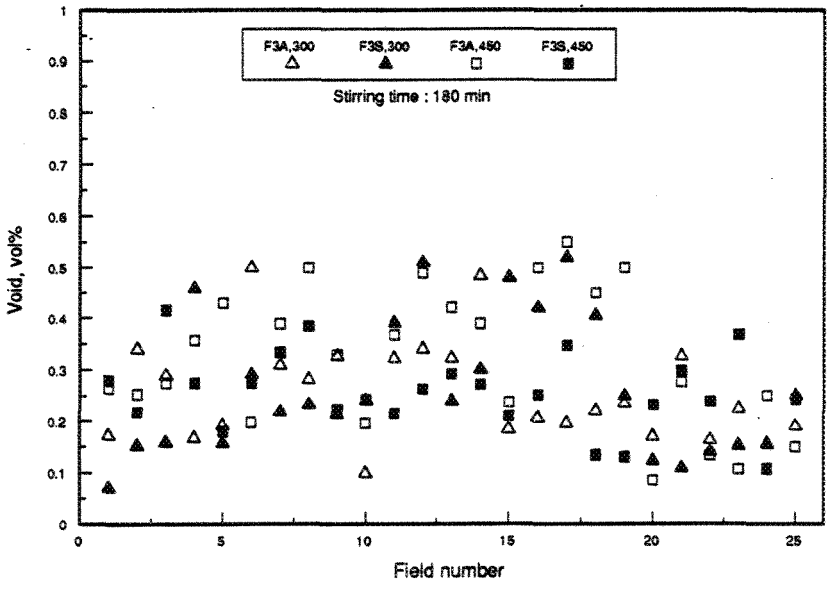

(b)

Figure III.14. **Effect of mold temperature on void distribution (obtained from image analysis): (a) 20 min stirring time, (b) 180 min stirring time, for F3A.10S and F3S.10S composites.**

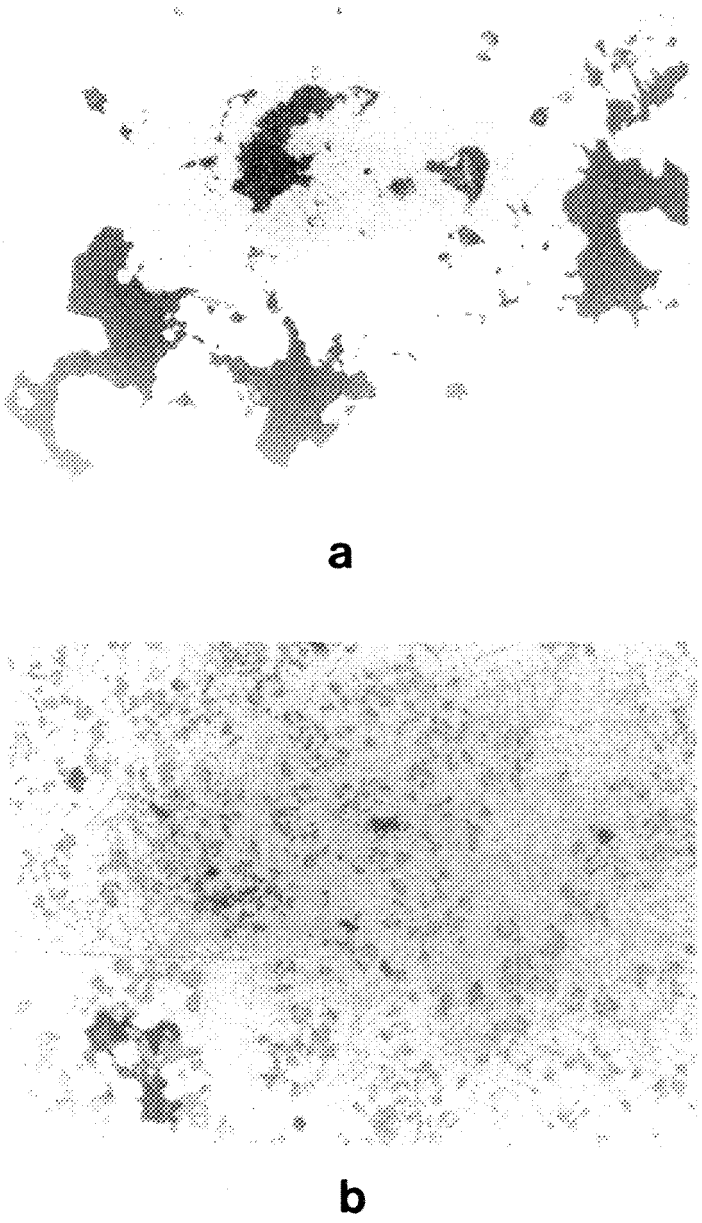

Figure III. 15. **Optical micrographs (after 3 hr stirring time at 740°C) taken from: (a) A356, and (b) F3A.10S composite (100 X). The inset in (b) shows how the SiC_p particles resist void coarsening (200 X).**

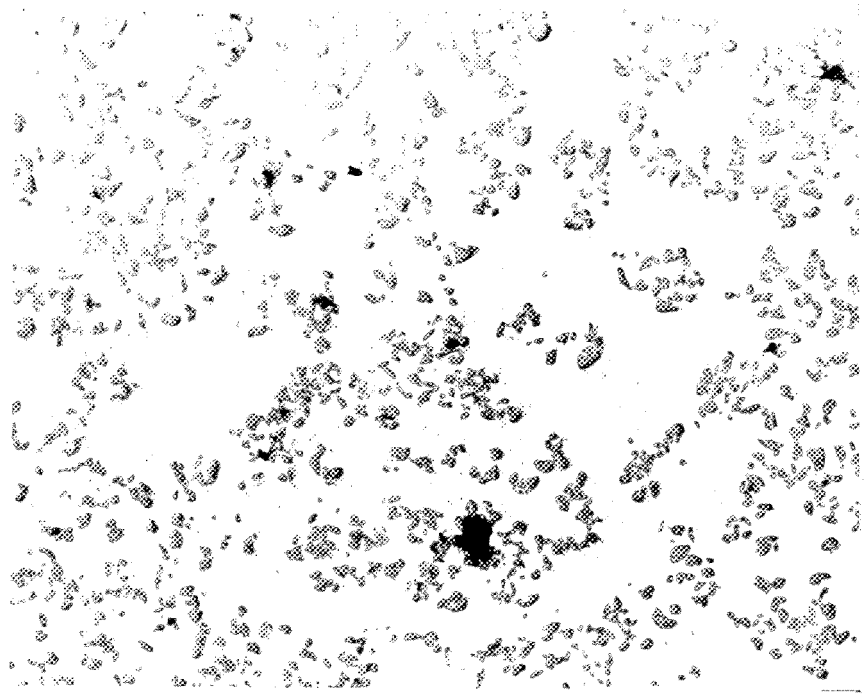

a

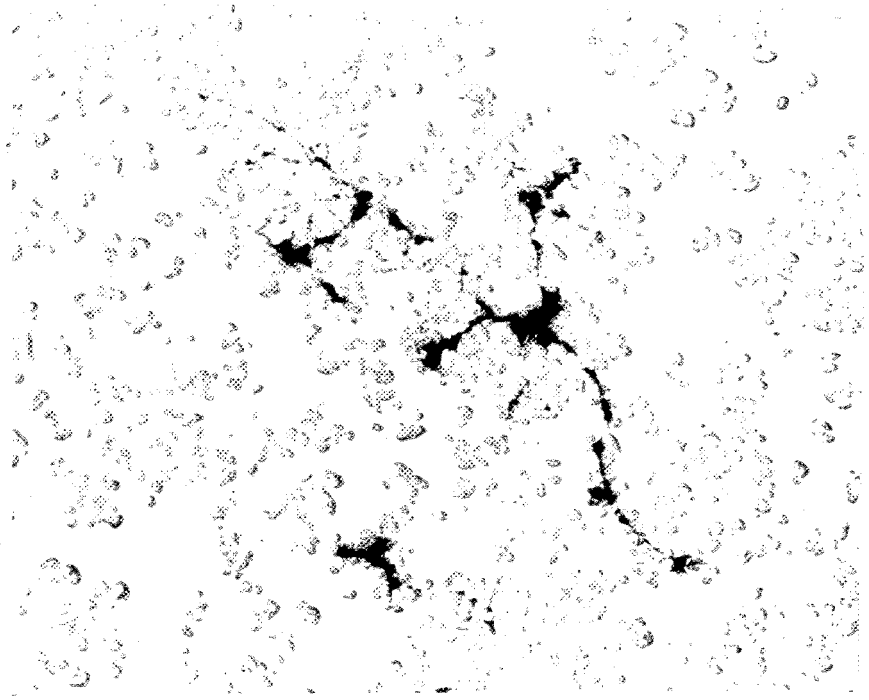

b

Figure III.16. Optical micrographs taken from: (a) clean, and (b) oxide contaminated melts (100X).

III.4.2. Al_4C_3 Formation

At high melting temperatures, SiC reacts with the molten Al matrix according to the reaction:

$$4Al+3SiC \rightarrow Al_4C_3+3Si \qquad (9)$$

where the Al_4C_3 forms a stable compound in the melt and the excess Si alloys with the matrix, increasing the Si level of the alloy. Lloyd and Dewing [98] have studied the Al_4C_3 reaction with respect to the melt temperature, holding time and Si level in the matrix alloy. Theoretically, silicon levels above 8 at% are required to prevent Al_4C_3 formation. From a study of holding times and temperatures, it is found that Al_4C_3 forms rapidly at temperatures above 790°C and 895°C for F3A.10S and F3S.10S composite alloys, respectively. The reaction also occurs below these temperatures but at much lower rates. For the short holding times involved in the present work (20 min) and relatively low melting temperatures (below 740°C), no significant Al_4C_3 was formed in both composites. Increasing the holding time to 3 hr resulted in the formation of small fragments or platelets of Al_4C_3, bridging the SiC particles at or between which the reaction was taking place, Fig. III.17(a), for F3A.10S composite. For the F3S.10S composite, increasing the Si content up to 10% resulted in a significant reduction in the amount of Al_4C_3 phase (hardly any Al_4C_3 is visible in Fig. III.17(b)). This may be understood from considerations of the theoretical Si levels required to prevent Al_4C_3 formation: approximately 12 at% Si is required for a melt temperature of 850°C.

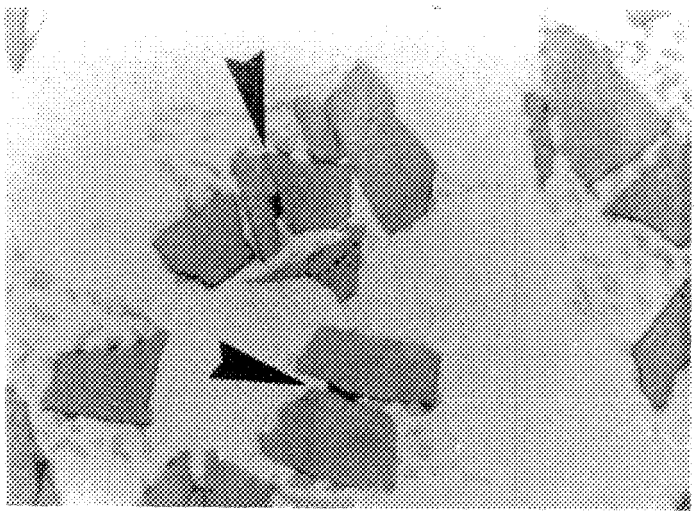

a

b

Figure III.17. **Optical micrographs (after 3 hr stirring time at 740°C) showing Al_4C_3 formation in: (a) F3A.10S, (b) F3S.10S composites. Arrows indicate the position of Al_4C_3.**

III.4.3. SiC-Particle Distribution

It is well established that the microstructure of an alloy is dependent on the solidification rate or the cooling rate of the casting. This effect becomes important in the case of composites because particle distribution is affected by the dendrite arm spacing (DAS) i.e. on the solidification rate. Fig. III.18 shows the dependence of the DAS on the mold temperature (cooling rate). It is an established fact that increasing the Si content refines the DAS value [99]. The DAS value is related to the solidification rate by the following expression :

$$DAS = A\, r^{n}$$

where: DAS = dendrite arm spacing in μm,

r = solidification rate, in °C/s,

A = constant,

n = 0.334 for F3S.10S composite.

From this equation, the estimated solidification rate for the mold temperature 300°C lies in the range 20-30°C/s, and for the mold temperature 450°C, in the range 10-15°C/s. The DAS can also be estimated from thermal analysis data. In the case of F3A.10S alloy, due to its low Si level, 7wt%, a coarser DAS is observed compared to the F3S.10S alloy.

The DAS is also affected by an increased SiC_p content in the Al matrix. The solidification rate of the casting is very important in controlling the SiC_p distribution.

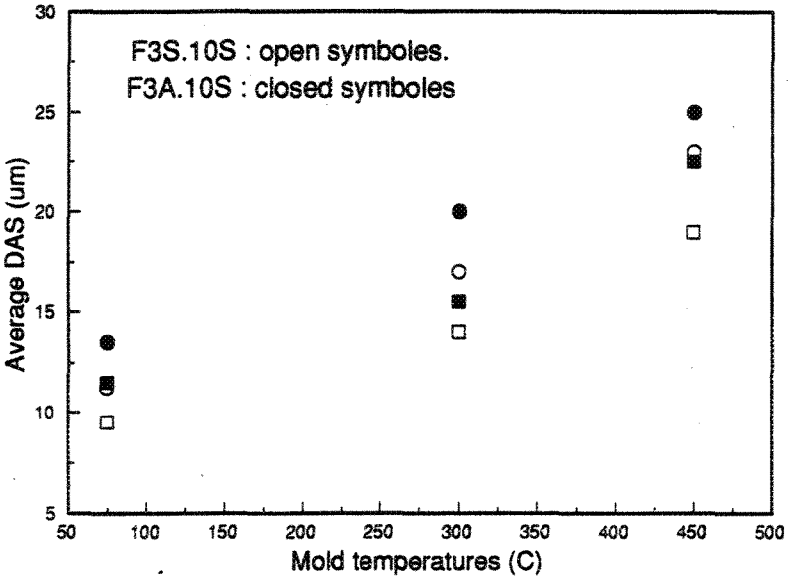

Figure III.18. **Dependence of DAS on solidification rate (75°C mold temperature readings are taken from Ref. 61).**

During solidification, the SiC_p distribution becomes more clustered as the solidification rate decreases. This affects the as-cast mechanical properties which are mainly controlled by the distribution of SiC_p. A uniform distribution of the SiC_p is essential to obtain good levels of strength and ductility. Several models have been proposed to explain particle entrapment and rejection by a solidifying interface, based on differences in thermal conductivity or thermal diffusivity and energy considerations.

Fig. III.19 shows the increase in the width of the SiC_p denuded zone around the periphery of the specimen cross-section, while Fig. III.20 demonstrates the SiC_p distribution across the specimen surface as a function of mold temperature. It is to be noted that the width of the denuded zone in each case was not uniform around the periphery but varied from place to place. Fig. III.21 shows the histograms of the SiC interparticle distance obtained at two different cooling rates (a) $25°C/s^{-1}$ and (b) $10°C/s^{-1}$. Fig. III.22 shows the corresponding microstructures taken from the central areas of the specimens solidified at the two cooling rates.

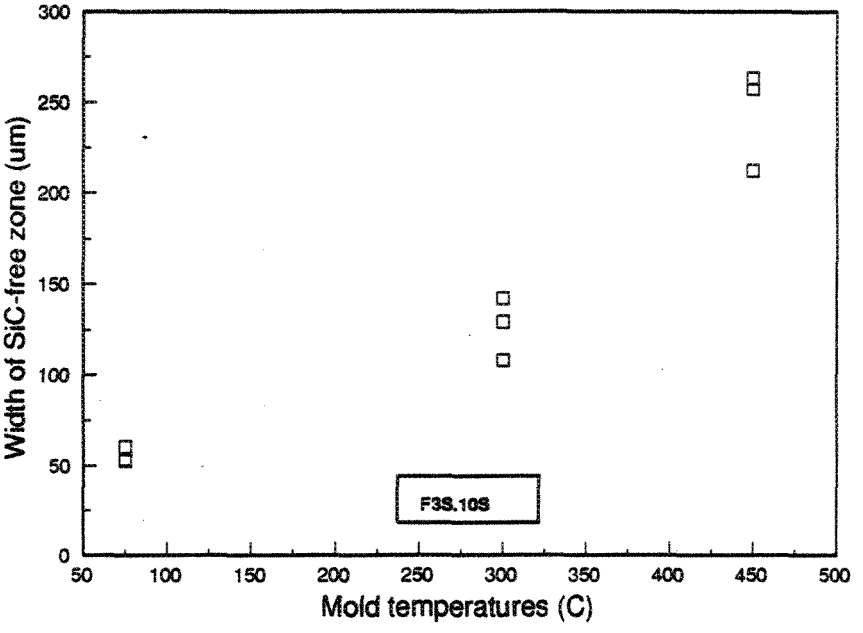

Figure III.19. **Dependence of the width of SiC_p-free zones on the solidification rate (mold temperature) of F3S.10S composite (75°C mold temperature readings are taken from Ref. 61).**

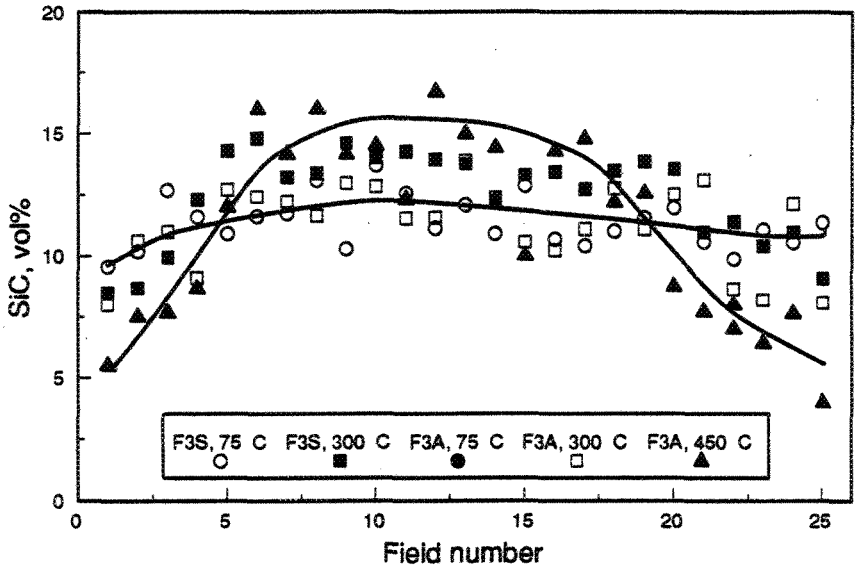

Figure III.20. **SiC_p distribution across the specimen surface as a function of mold temperature for F3A.10S and F3S.10S composites (75°C mold temperature readings are taken from Ref. 61).**

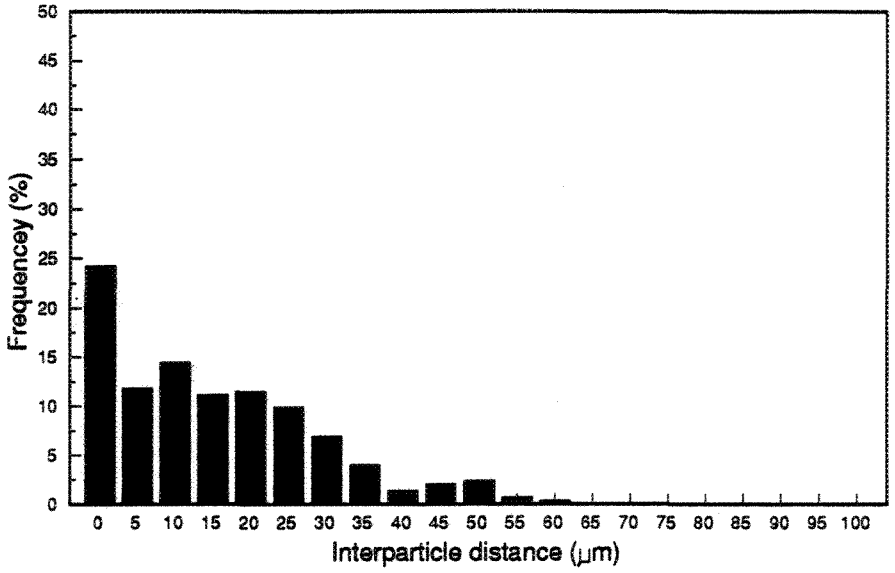

a

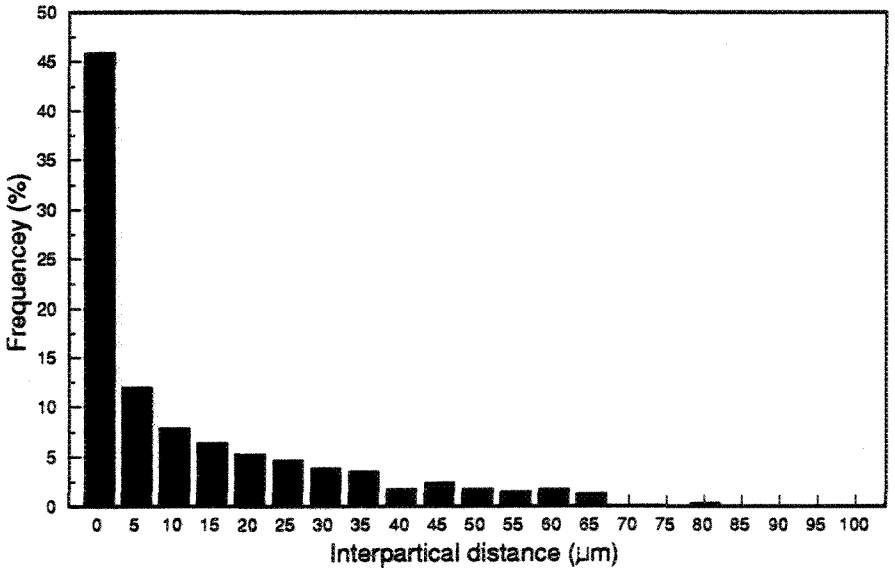

b

Figure III.21 **Histograms showing SiC interparticle distance in the central region of specimens solidified at:(a) 25°C/s^{-1}, and (b) 10°C/s^{-1}.**

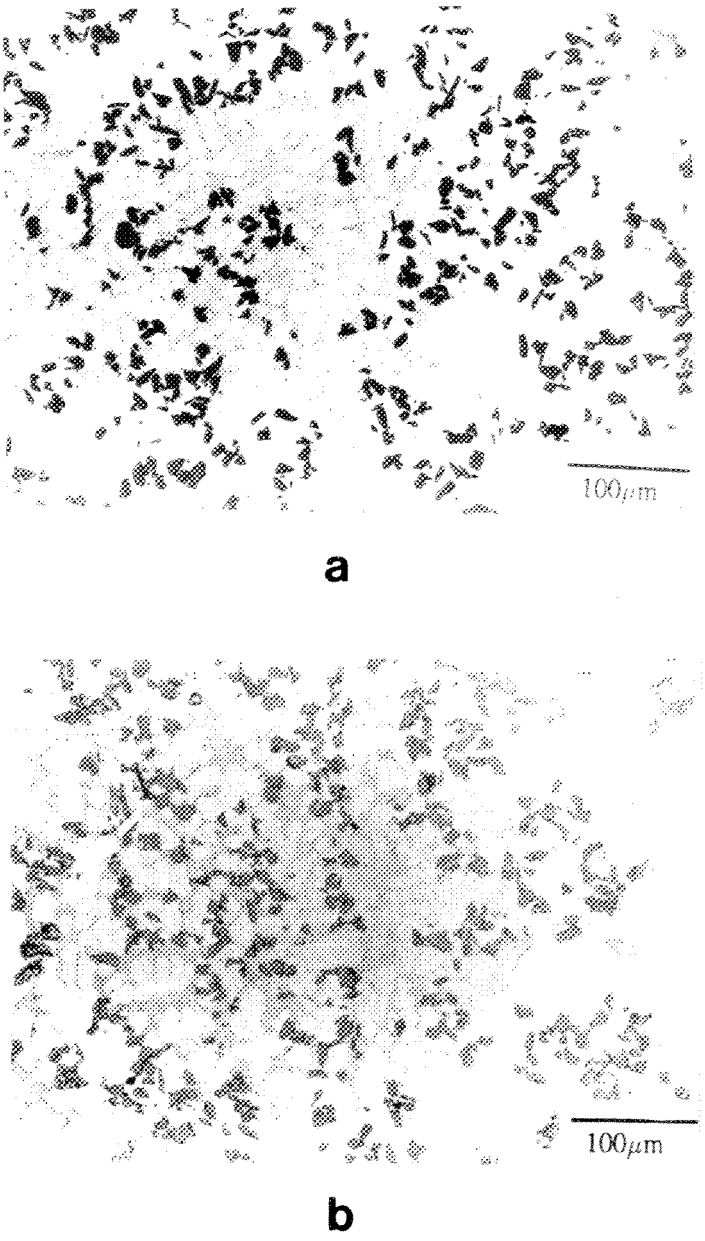

Figure.III.22. Corresponding microstructures taken from the central region of specimens solidified at: (a) 25°C/s^{-1}, and (b) 10°C/s^{-1}.

III.4.4. SiC_p Volume Fraction (Vol%)

The volume fraction of the SiC_p was evaluated employing a Leco 2001 Image Analysis system. For each successfully polished metallographic sample, 100 fields were analyzed under a magnification of 200X, which covered about 12.24% of the total transverse section of the test bar. The magnification was chosen taking into consideration both the largeness of the analyzed area and the accuracy of the evaluation. Although the evaluation of volume fraction of SiC_p is based on two-dimensional measurements, it is assumed that these are representative of the three-dimensional picture, and hence, the measurements are expressed in terms of volume fractions. The SiC_p volume fraction in the melt prior to casting (based on chemical analysis) was in the range 10-12%, depending on the stirring time and the dead time between one casting and another. Fig. III.23 shows the effect of stirring time on the SiC_p volume fraction (obtained from spectrometric analysis) of F3A.10S and F3S.10S composites for two different crucible capacities, 7 and 25 kg, respectively. From image analysis, it was observed that due to the pushing of the SiC_p by the moving solidification front during solidification, the SiC_p segregated towards the specimen centre, reaching volume fractions of up to 16% (cf. 10 vol% fraction specified for the as-cast composites) for both composites. Fig.III.24 shows the effect of stirring time on the SiC_p volume fraction obtained from image analysis for F3A.10S and F3S.10S composites. These results support the higher strength values achieved with 300°C compared to 450°C mold temperature, for F3S.10S, as reported in Chapter IV.

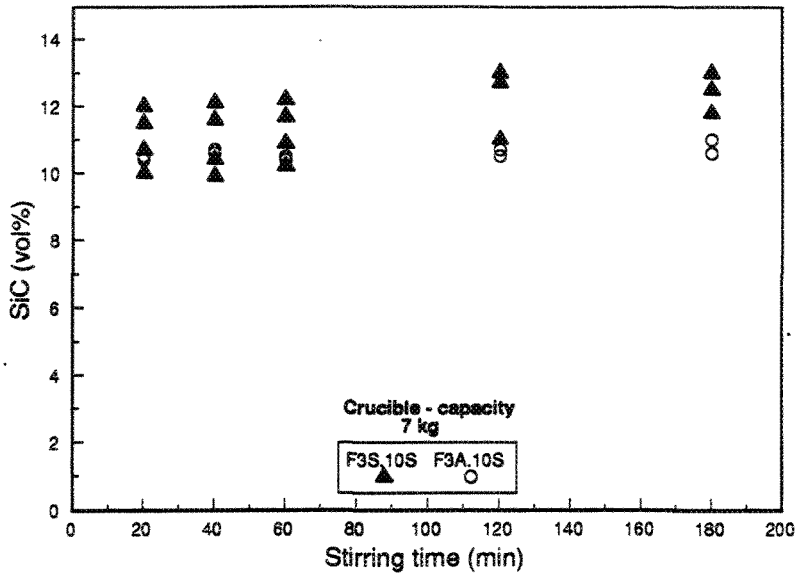

(a)

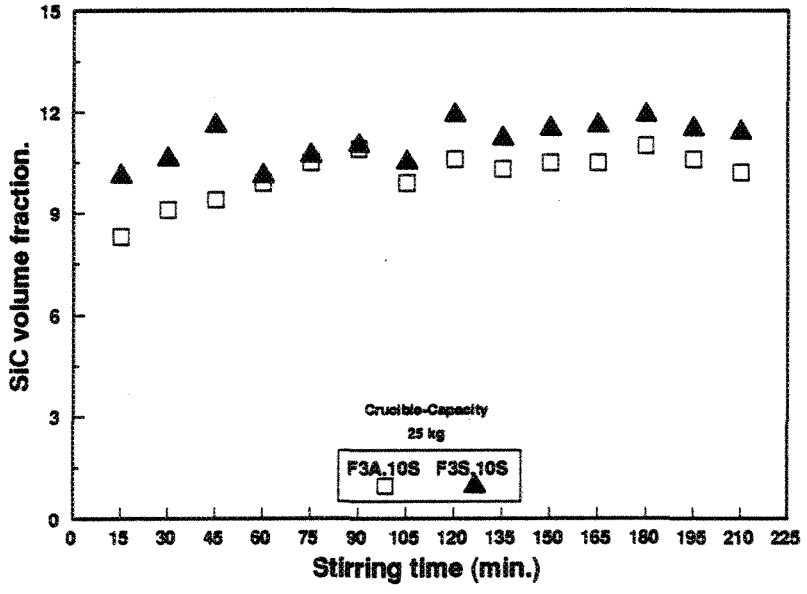

(b)

Figure III.23. **Effect of stirring time on the SiC_p volume fraction (obtained from spectrometric analysis) of F3A.10S and F3S.10S composites obtained from: (a) 7 kg, (b) 25 kg crucible-capacity melts.**

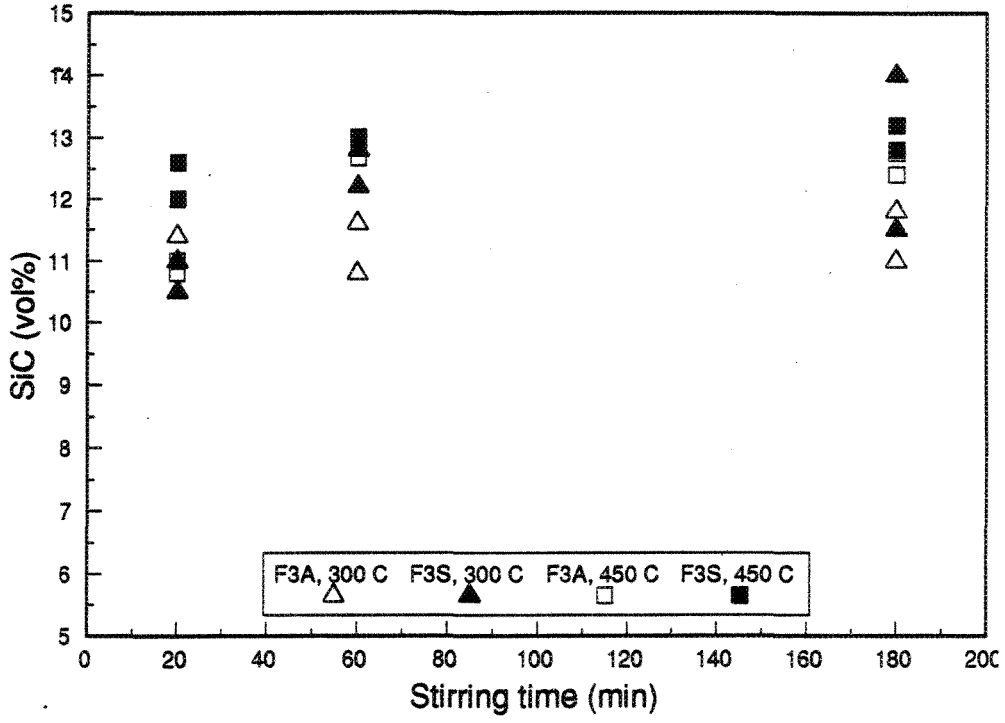

Figure.III.24. **Effect of stirring time on the SiC_p volume fraction (obtained from image analysis) of F3A.10S and F3S.10S composites.**

III.4.5. Fracture Behaviour

The fracture mode of the as-cast composites was examined using scanning electron microscopy (SEM). It was found that tensile fracture of test bars solidified at the three different mold temperatures showed a mixed fracture path, Fig. III.25, with crack propagation along the particle-matrix interface and through the matrix, with voids and/or cracks associated with the SiC_p.

Lewandowski and co-workers [100] have conducted studies on the fracture behaviour of particle-reinforced metal matrix composites. They suggest that there are a number of microcracks that form ahead of and near the initial crack tip. The crack propagation takes place by a process whereby some of these microcracks join via matrix failure ahead of the original crack tip, concurrent with the formation of additional microcracks ahead of the crack.

Lloyd [93] states that in cases when interfacial reaction is not too severe, a small amount of particle cracking occurs and the fracture is controlled by matrix metallurgy and particle distribution effects. Fig. III.26 shows the maximum extent of particle fracture and voiding observed in tensile fractured specimens corresponding to mold temperature 450°C. The fracture of test bars obtained from 450°C mold temperature revealed that failure was mainly initiated in the matrix, Fig. III.27. In scattered areas and because of localized stresses, some of the SiC_p are cleaved, see inset in Fig. III.27.

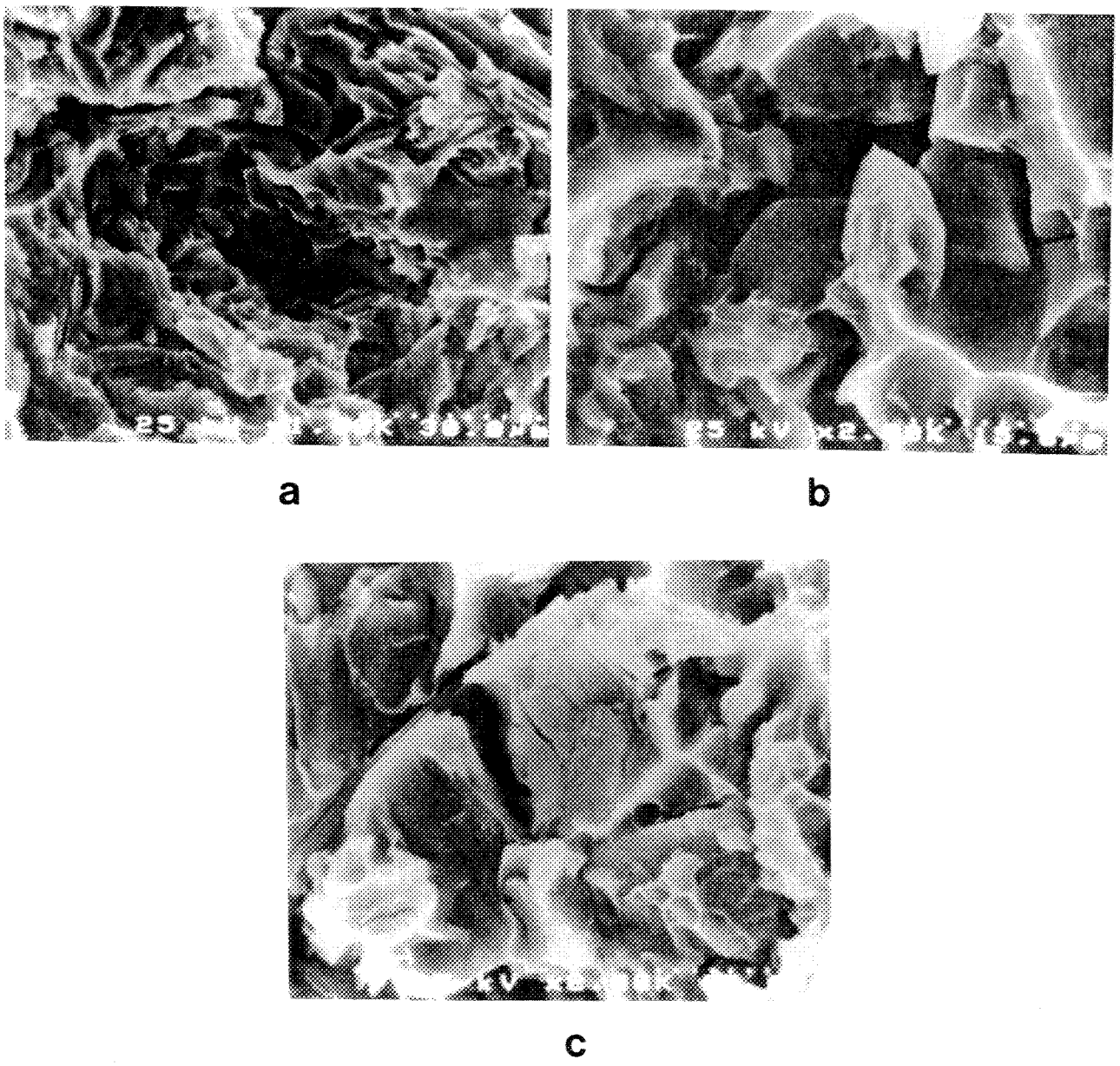

Figure III.25. Scanning electron micrographs obtained from the fracture surface of a 450°C specimen, showing: (a) matrix fracture, (b) matrix-SiC_p crack, and (c) SiC_p cracking.

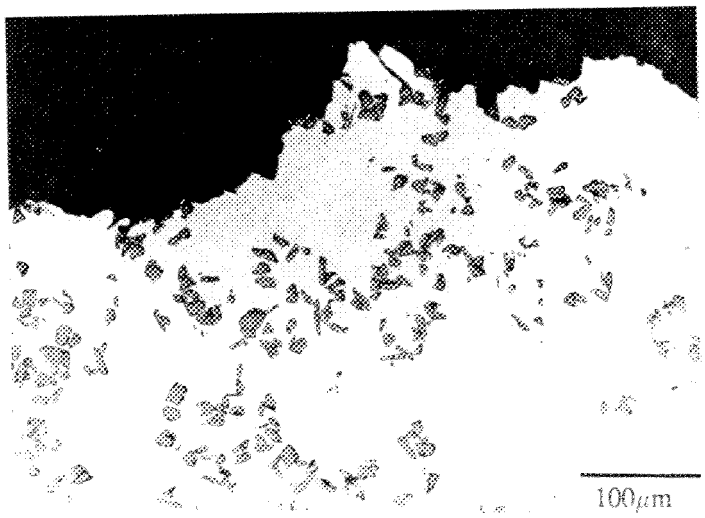

Figure III.26. Maximum particle fracture and voiding in specimen corresponding to 450°C mold temperature.

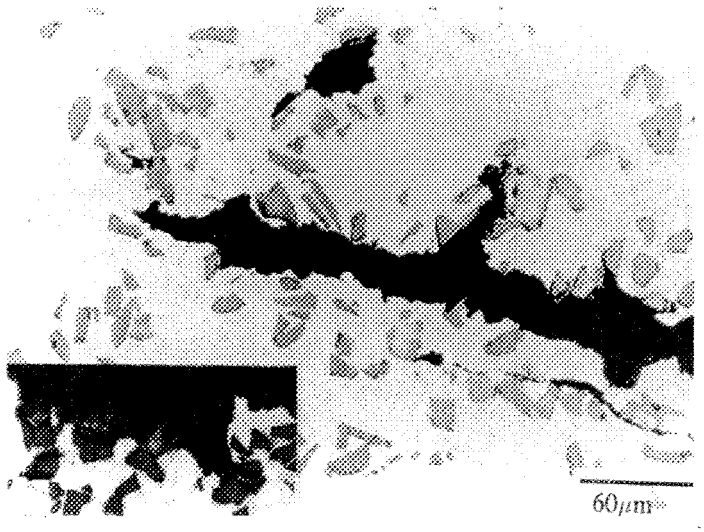

Figure III.27. Fracture path propagation in the matrix immediately underneath the fracture surface. The inset shows SiC_p fracture.

CHAPTER IV
HEAT TREATMENT

IV.1. OPTIMIZATION OF HEAT TREATMENT

The purpose of carrying out this heat treatment study was based on the fact that (a) the literature survey showed very few studies on such composites, and (b) most of the investigations conducted on SiC_p-reinforced Al-Si-Mg alloys utilized heat treatments very similar to those used for the unreinforced alloys. Thus, it was felt that further investigations were required in this area, which resulted in the work described in this chapter.

The heat treatment of the two composites (F3A.10S and F3S.10S) was studied with a view to optimizing the treatment in order to obtain optimum mechanical properties.

The main objectives of the study were:

(a) To determine the effect of solution heat treatment at 540 ± 2°C for different times (4, 8, 12 and 24 hr) on the average tensile properties (YS, UTS and EL%).

(b) To examine the spheroidization process and/or the change in the Si particle morphology (roundness, aspect ratio, particle size and numbers) during the solution heat treatment.

(c) To determine the effects of Sr concentration, stirring time and solution treatment on the spheroidization of the eutectic Si particles in SiC-free and SiC-containing areas.

(d) To determine the effect of preaging for 24 hr at room temperature on the

average tensile properties.

(e) To determine the effect of direct artificial aging at 155-160 °C for various times (5, 12 and 24 hr) on the average tensile properties.

(f) To determine which factors accelerated the aging kinetics of the two composites and under what conditions.

IV.2. EFFECT OF T4 TEMPER ON THE AVERAGE MECHANICAL PROPERTIES

Apelian et al [80] have reported on the effect of increasing the solution time and temperature on the average mechanical properties of Sr-modified A356 alloy Stahl mold castings (see Table IV.1, in the Appendix). The average mechanical properties show higher ultimate tensile strength (UTS) and elongation (EL%) after only 50 min solution treatment time compared to the as-cast values (i.e.36.7 ksi and 6.5% vs 29.5 ksi and 1.6%), while YS remains unaffected (16 ksi). Increasing solution time up to 24 hr at 540°C does not result in any significant changes in the average YS, UTS and EL% (see Tables IV.2 to IV.4 in the Appendix).

In most cases, Al-Si-Mg alloys are solutionized at 540°C. At this temperature, about 0.6% Mg can be placed in solution. The results of Closset et al. [102] suggest that Mg has substantial solubility in solid aluminum and the presence of Si does not alter the distribution of Mg between solid and liquid.

The effect of solution heat treatment at 540°C for different solution times (4, 8, 12 and 24 hr) is shown in Fig. IV.1 and Fig. IV.2 (and listed in Table IV.5 and

Table IV.6 in the Appendix) for F3A.10S and F3S.10S composites, respectively. The average tensile propertes (YS, UTS and EL%) improved after only 4 hr solution heat treatment, compared to the as-cast condition, viz. 17 ksi, 27 ksi and 1.6% vs 23 ksi, 37 ksi and 3.5% in the case of F3A.10S and 18 ksi, 27 ksi and 1.6% vs 23 ksi, 37 ksi and 3.5% in the case of F3S.10S for YS, UTS and EL%, respectively.The influence of solution treatment is significant, because it reduces the amount of intermetallics which form during solidification. Some of these intermetallics contain elements which are not part of the alloy specification, most likely they are contaminants.

Prolonged solution times up to 24 hr for both composites does not result in any significant changes in the elongation or ultimate tensile strength, while a noticeable increase in yield strength ~3 ksi is observed. Using a solution temperature close to the eutectic temperature (540 ± 2°C) leads to stabilization of the average tensile properties during the solution heat treatment process.

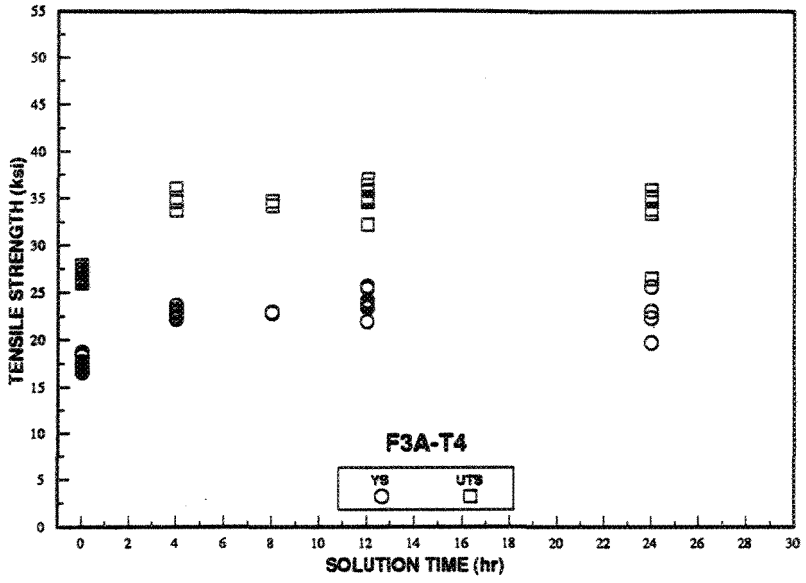

(a)

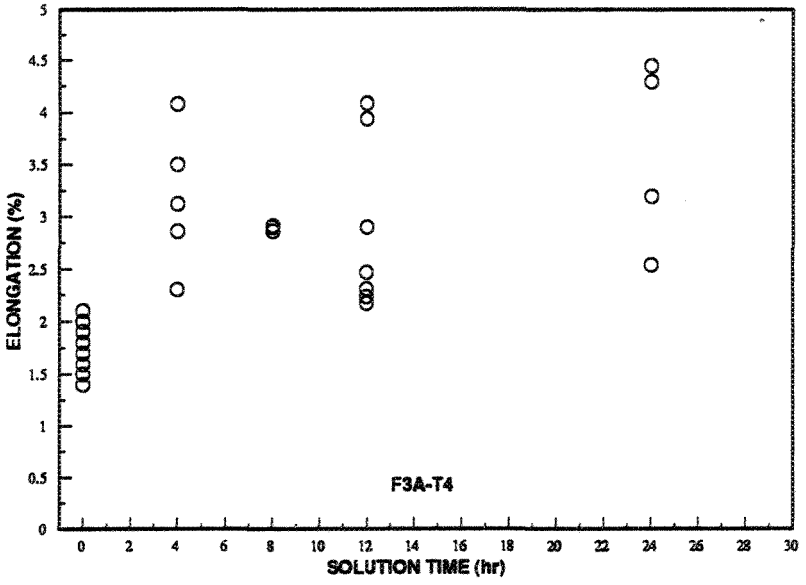

(b)

Figure.IV.1. Effect of solution time at 540°C on: (a) tensile strength (ksi), (b) elongation (%) of F3A.10S composite.

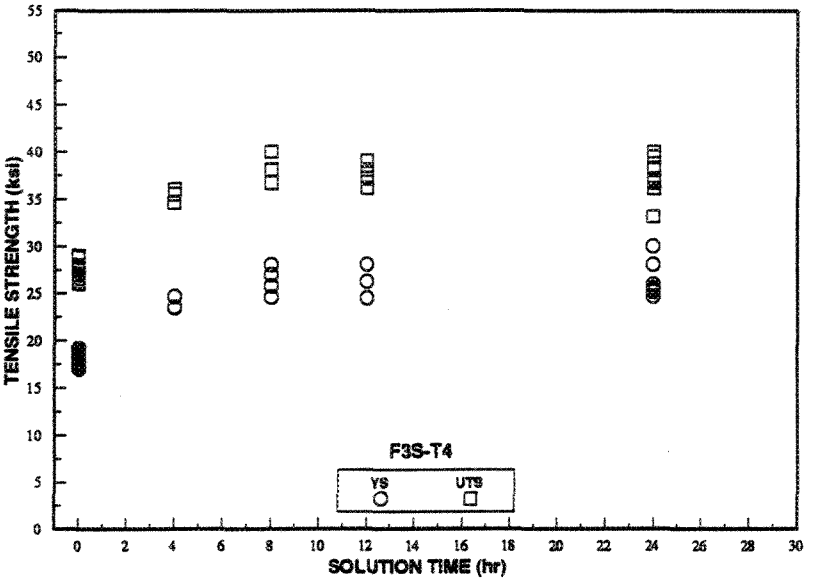

(a)

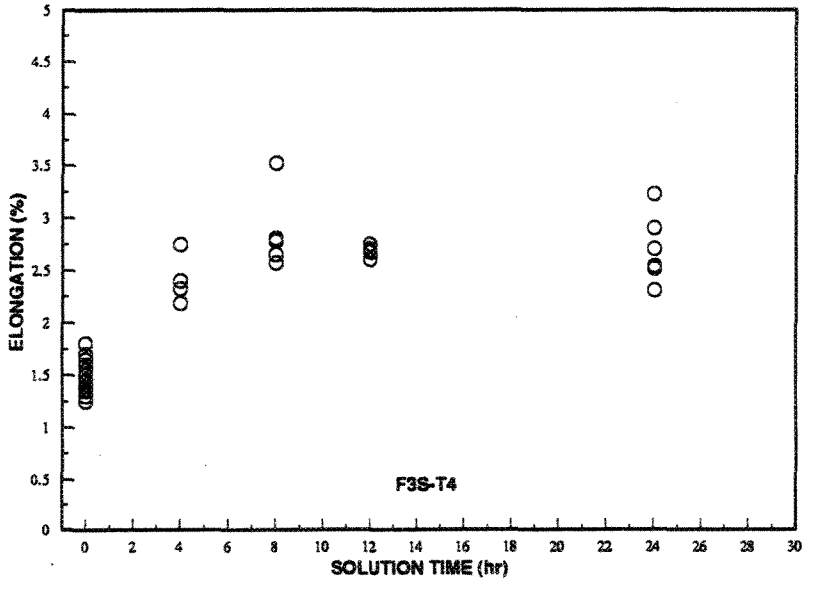

(b)

Figure IV.2. Effect of solution time at 540°C on (a) tensile strength (ksi),(b)elongation (%) of F3S.10S composite

IV.3. EFFECT OF T4 TEMPER ON THE EUTECTIC Si MORPHOLOGY

Modification with Sr in Al-Si-Mg alloys is an important key to improving ductility and machinability. The amount of modifier necessary to achieve complete modification generally depends on the type of modifier and the concentration of impurity elements in the alloy. It has been reported that the amount of Sr concentration sufficient to obtain complete modification in A356 base alloy lies in the range 100-200 ppm. Increasing the Sr concentration above this value leads to a coarsening of the eutectic Si particles [101,102]. Both particle diameter and aspect ratio begin to increase at strontium levels greater than 150-200 ppm.

As a result of high stirring times during the remelting and casting of the composites, the Sr concentration drops from 140 to 100 ppm in the case of F3A.10S and from 110 to 75 ppm in the case of F3S.10S after 3 hr stirring, Fig. IV.3.

Hogan et al. [103] and Denton and Spittle [104] have reported that during solution heat treatment of A356 alloy at 540°C (i.e. at the eutectic temperature) the Si particles that were initially coarse, acicular needles, undergo necking and break down into smaller fragments. These fragments are gradually spheroidized. Prolonged solution time up to 24 hr leads to extensive coarsening of the particles.

Rohatgi et al. [71] made a thorough analysis of the solidification process in SiC particulate MMCs. During solidification, these particulates result in particle refinement of both eutectic and primary Si which appears to nucleate preferentially on the surface

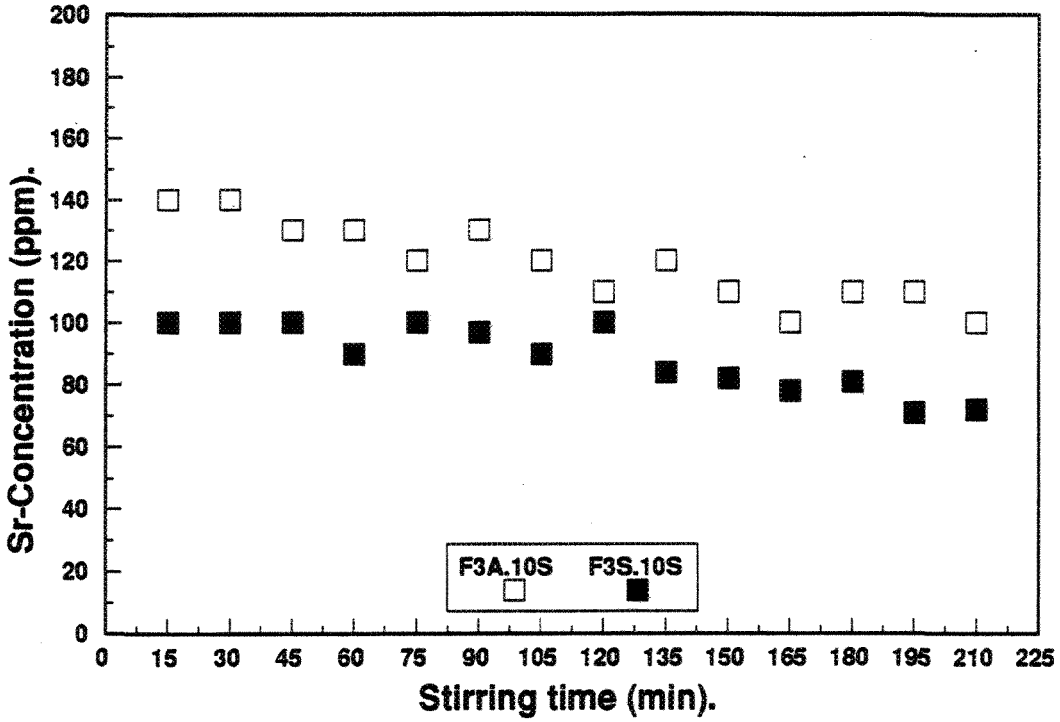

Figure IV.3. Relation between stirring time and Sr concentration for F3A.10S and F3S.10S composites.

of the dispersed SiC particulates.

The as-cast and solutionized microstructures of F3A.10S and F3S.10S composites, shown in Figs. IV.4 through IV.13, display the influence of solution treatment time (4, 8, 12 and 24 hr) on the change in the Si morphology in SiC_p-free and SiC_p-containing (i.e interdendritic) regions in the same sample. It is clearly evident from these microstructures that 8-12 hr solution time at 540°C is the optimum condition to produce homogeneous spheroidized Si particles, and that this process is not affected by the presence of the SiC particulates, whose main role is to refine the Si particle size in both composites.

The variation in Si particle average roundness, aspect ratio and area size as a function of solution time at 540°C is shown in Fig. IV.14. From this figure the average values of these parameters were found to be 80, 1.6 and 8 μm^2 vs 70, 1.8 and 12 μm^2 for SiC_p-free and SiC_p-containing areas, respectively in the case of F3A.10S and 80, 1.6 and 6 μm^2 vs 70, 2 and 8 μm^2 for SiC_p-free and SiC_p-containing areas, respectively in the case of F3S.10S.

The variation in the Si particle roundness as a function of solution time is shown in Fig. IV.14 (a) and (a_1) for F3A.10S and F3S.10S, respectively. The roundness is seen to increase sharply after only 4 hr solution treatment compared to the as-cast values (75 vs 45 in SiC_p-containing and 80 vs 45 in SiC-free areas). Thereafter, the roundness remains constant up to 24 hr for both composites, in the range 75-80.

The variation in the Si particle aspect ratio as a function of solution time at 540°C is shown in Fig. IV.14.(b) and (b_1) for F3A.10S and F3S.10S, respectively.

Starting from similar aspect ratios for the as-cast structure that decreased slightly after 4 hr solution treatment, the average values of these parameters were found to be 2 vs 1.8 in the case of F3A.10S and 2.2 vs 1.8 in the case of F3S.10S.

The variation in the Si particle average area as a function of solution time at 540°C is shown in Fig. IV.14.(c) and (c_1) for F3A.10S and F3S.10S, respectively. An initial decrease in the Si particle area can be observed up to about 4 hr compared to the as-cast condition. The particle area then increases slowly, up to 12 hr in the case of F3A.10S alloy, and up to 8 hr in the case of F3S.10S alloy, followed by a gradual increase up to 24 hr, ~10 μm^2, indicating particle coarsening in both composites. The variation in the Si particle average aspect ratio and area size in both SiC_p-free and SiC_p-containing areas for the two composites may be explained as a result of the following facts:

(a) The variation in the volume fraction of gas porosity and voids nucleated by the fracture of Si particles is much higher in the case of F3S.10S (0.3-0.6%) than in the case of F3A.10S (0.2-0.4%). These voids act as a resistance to the mass of heat which is transferred during heat treatment from one particle to another in the Al matrix in addition to the differences in the thermal conductivity and the coefficients of thermal expansion between the two composites.

(b) SiC particles are sites for preferential nucleation of eutectic particles in the as-cast condition. This process of nucleation enhances refinement of the Si particles within the areas containing SiC_p.

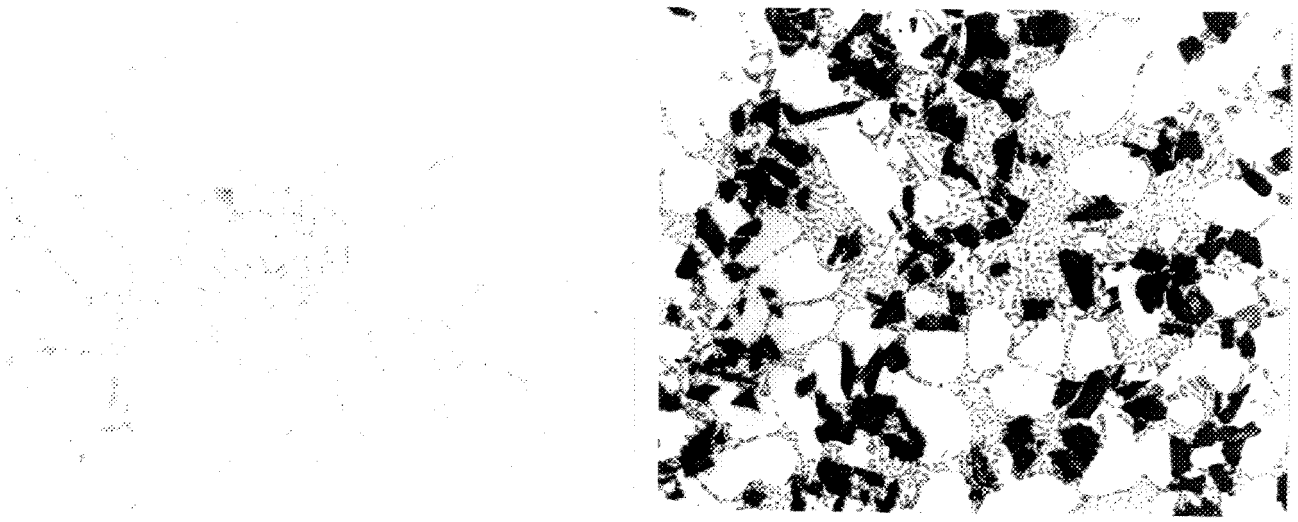

a

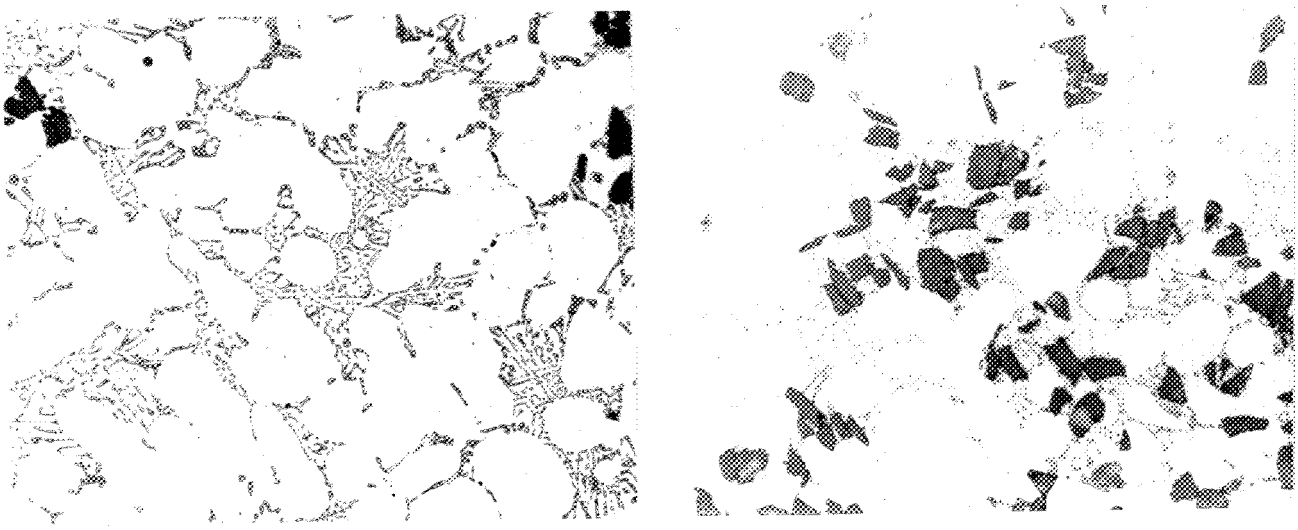

b

Figure IV.4. As-cast microstructures of F3A.10S composite permanent mold test bar samples taken from both SiC_p-free and SiC_p-containing areas:(a) Sr concentration: 140 ppm, (b) Sr concentration: 100 ppm (750 X).

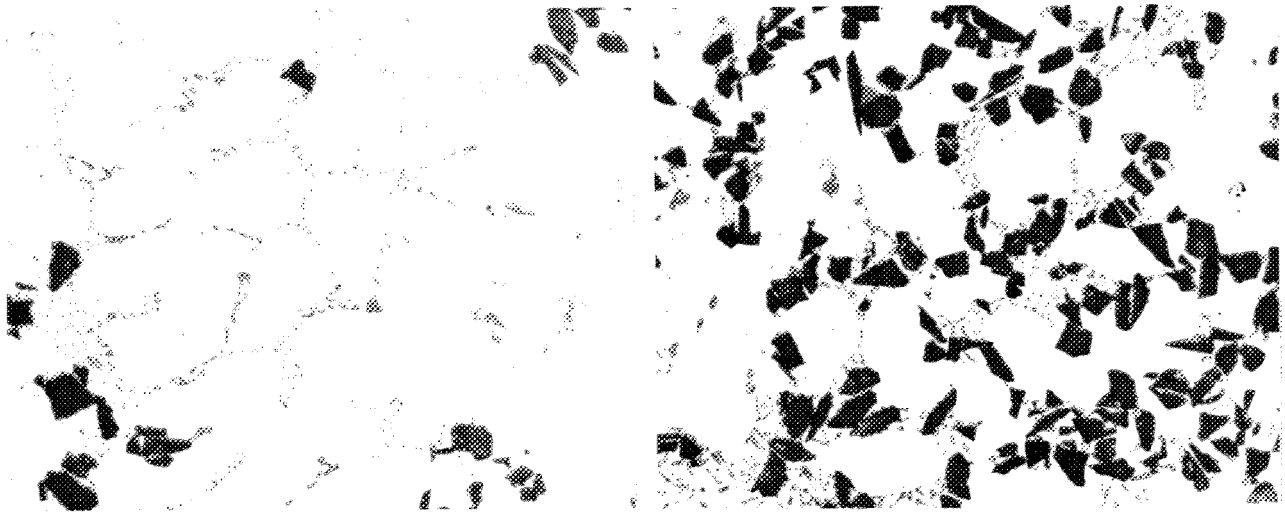

a

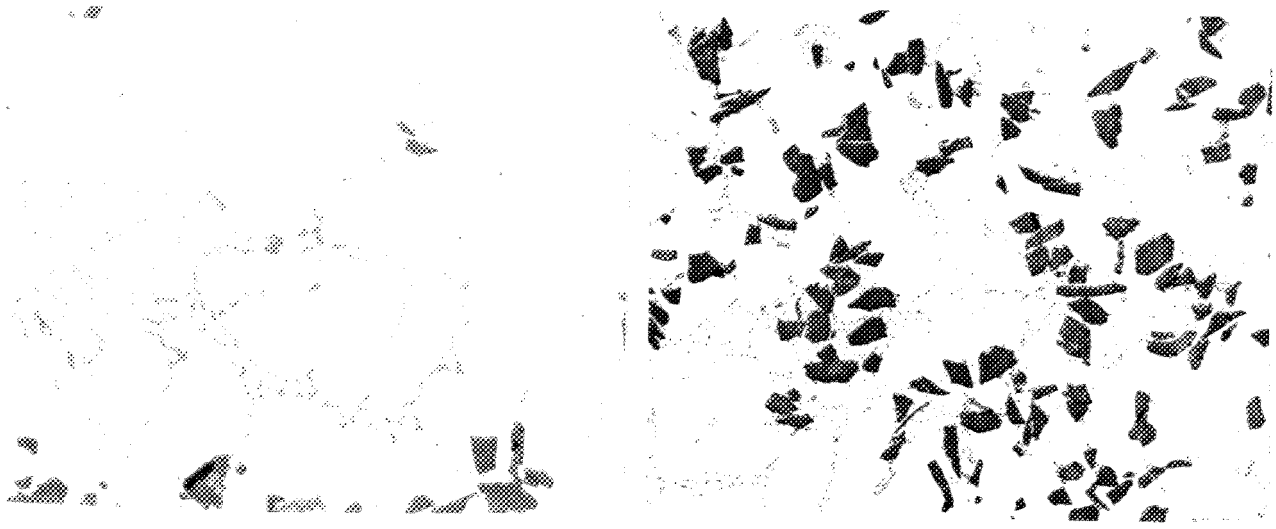

b

Figure IV.5. As-cast microstructures of F3S.10S composite permanent mold test bar samples taken from both SiC_p-free and SiC_p-containing areas: (a) Sr concentration: 110 ppm, (b) Sr concentration: 75 ppm (750 X).

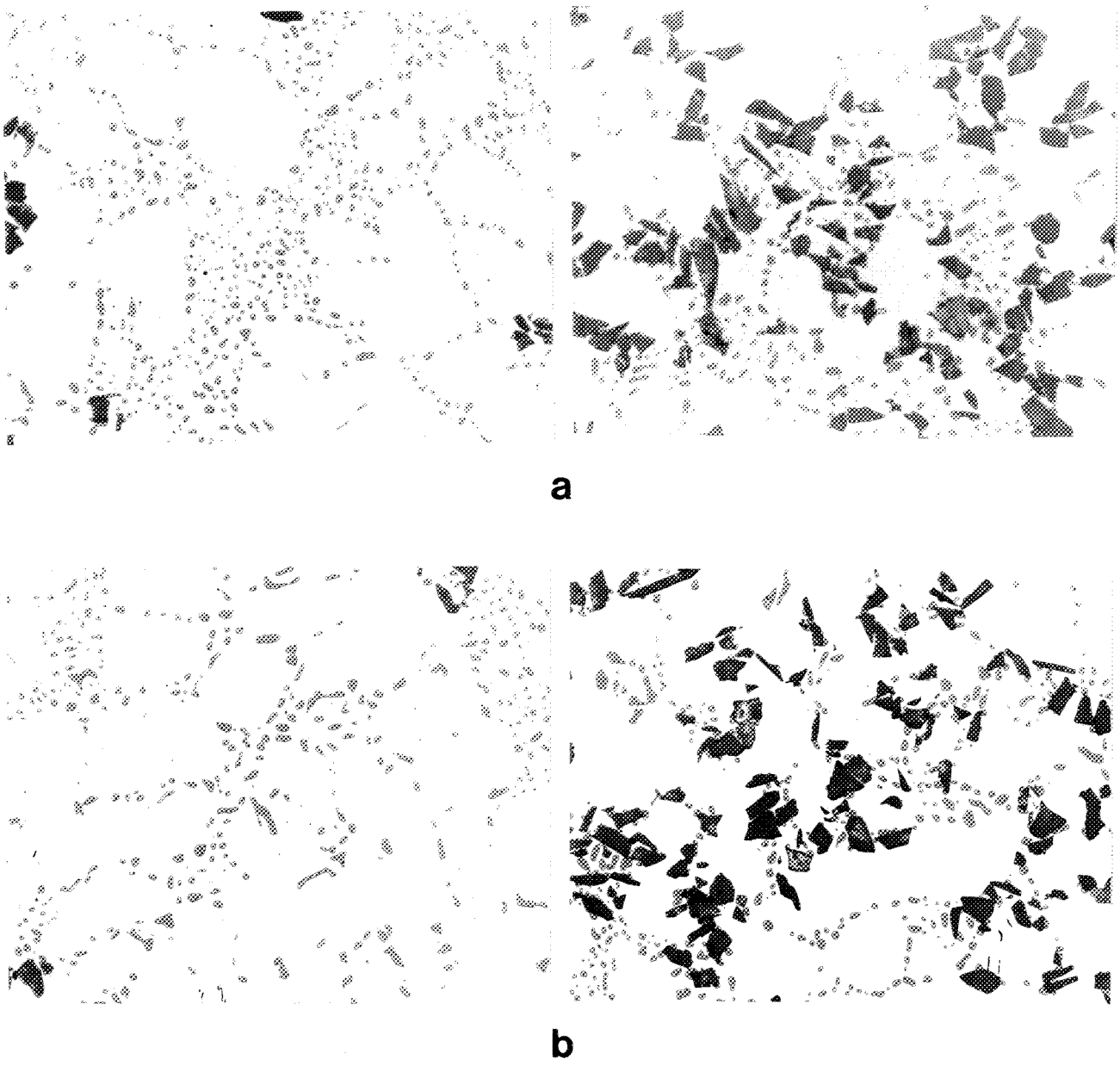

Figure IV.6. Microstructures of 4 hr solution heat treated F3A.10S composite permanent mold test bar samples taken from both SiC_p-free and SiC_p-containing areas: (a) Sr concentration: 140 ppm, (b) Sr concentration 100 ppm (750 X).

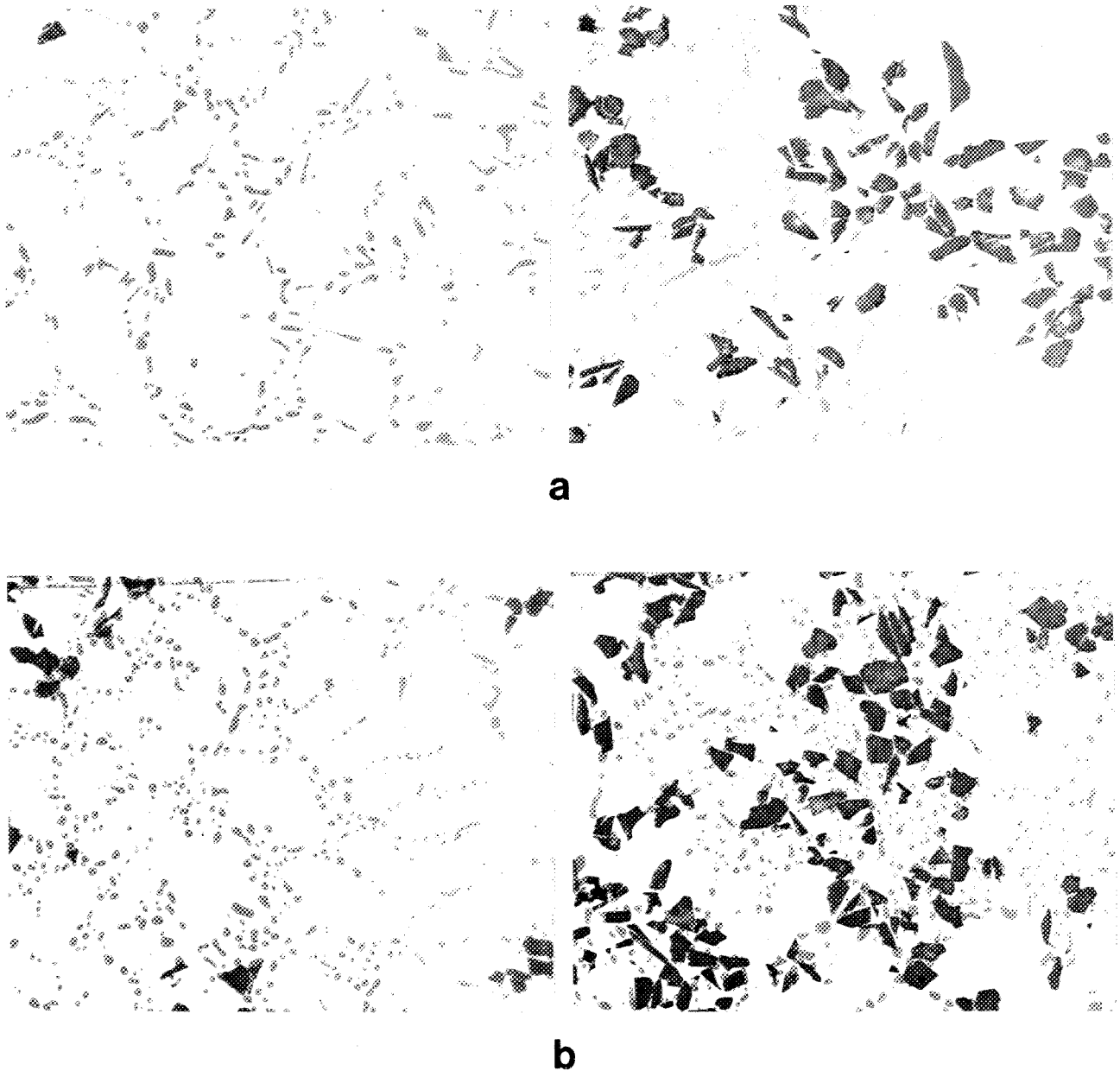

Figure IV.7. Microstructures of 4 hr solution heat treated F3S.10S composite permanent mold test bar samples taken from both SiC_p-free and SiC_p-containing areas:(a) Sr concentration: 110 ppm, (b) Sr Concentration: 75 ppm (750 X).

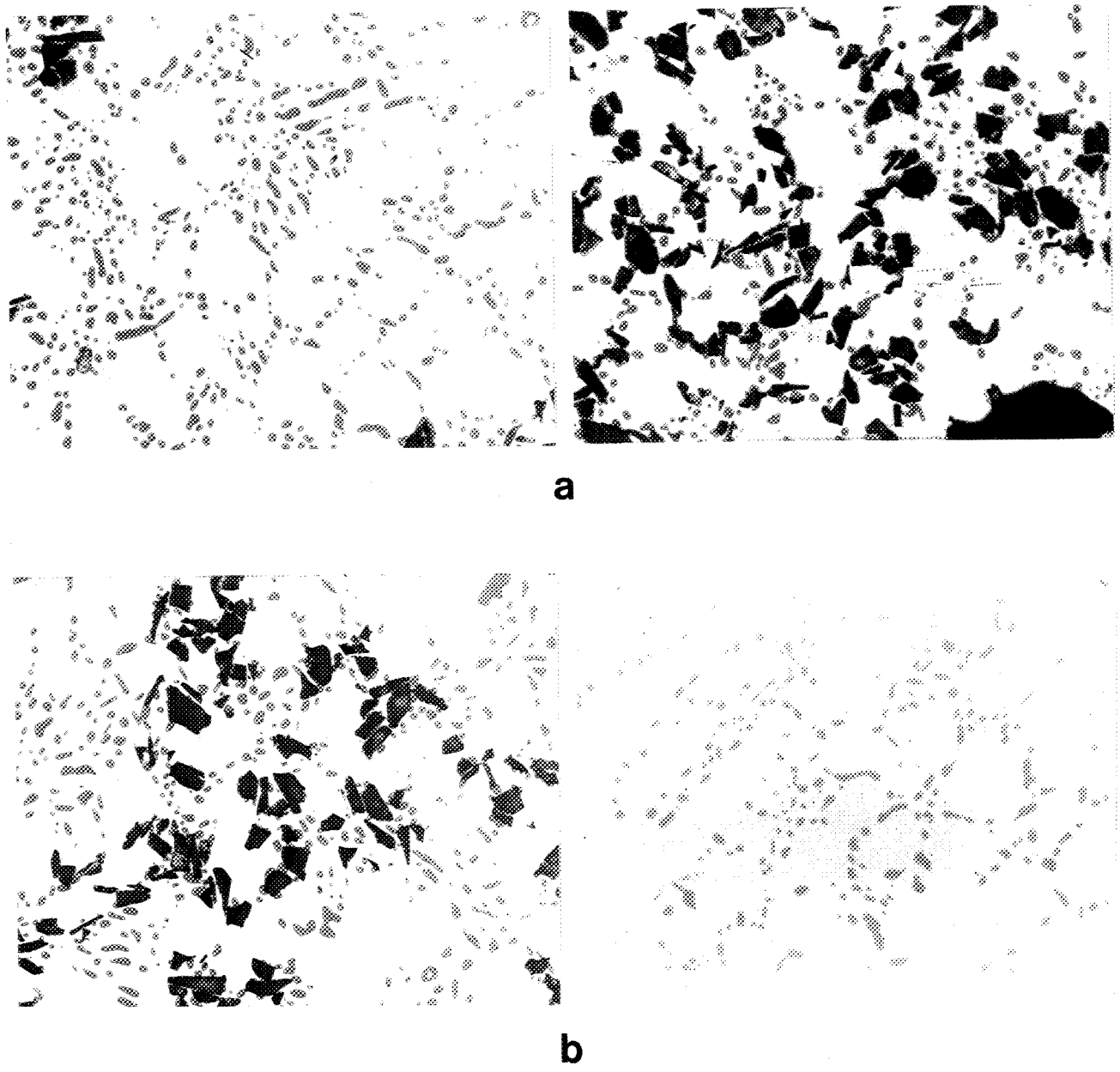

Figure IV.8. Microstructures of 8 hr solution heat treated F3A.10S composite permanent mold test bar samples taken from both SiC_p-free and SiC_p-containing areas:(a) Sr concentration: 140 ppm, (b) Sr concentration: 100 ppm (750 X).

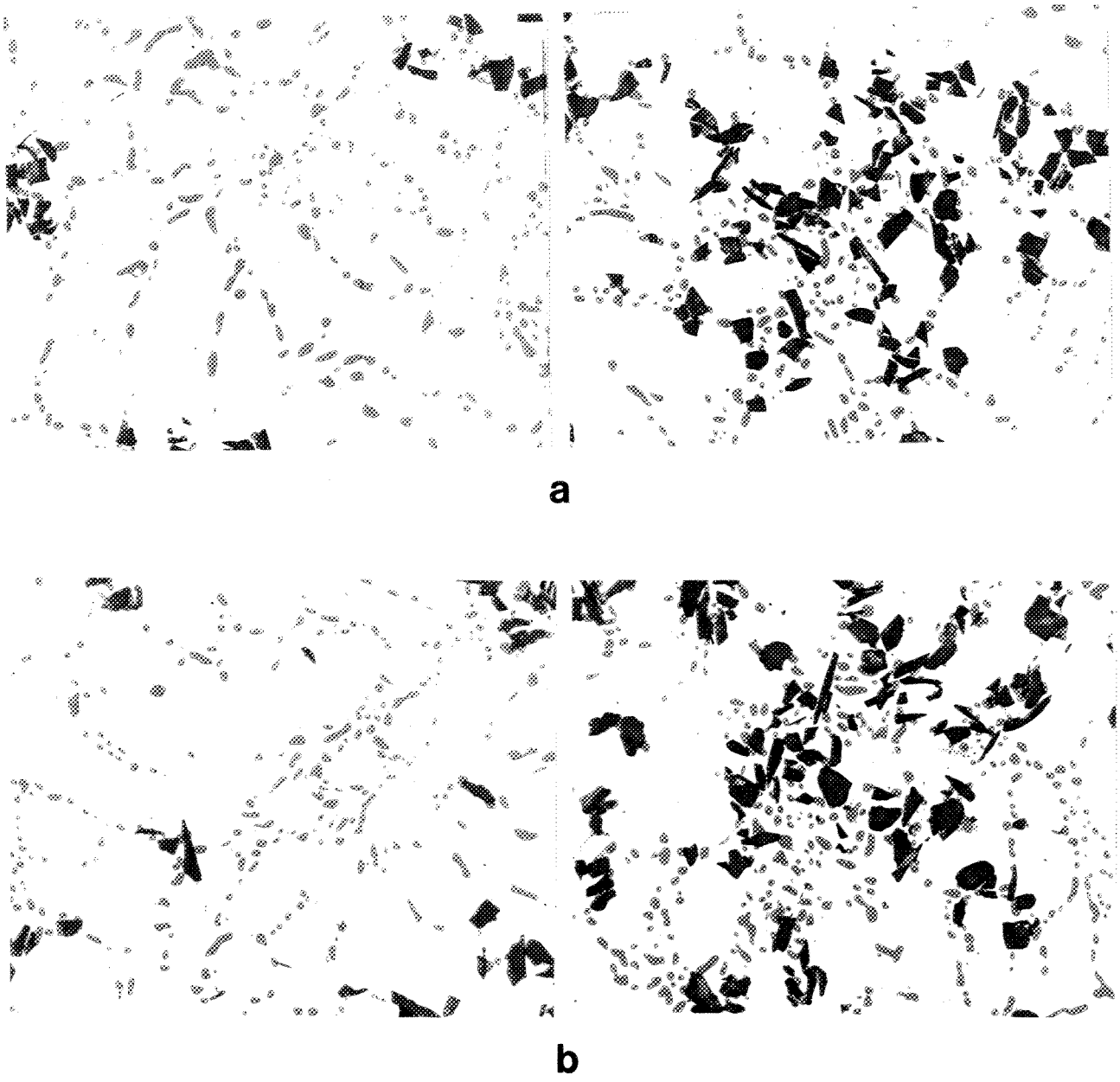

Figure IV.9. Microstructures of 8 hr solution heat treated F3S.10S composite permanent mold test bar samples taken from both SiC_p-free and SiC_p-containing areas: (a) Sr concentration: 110 ppm, (b) Sr concentration: 75 ppm (750 X).

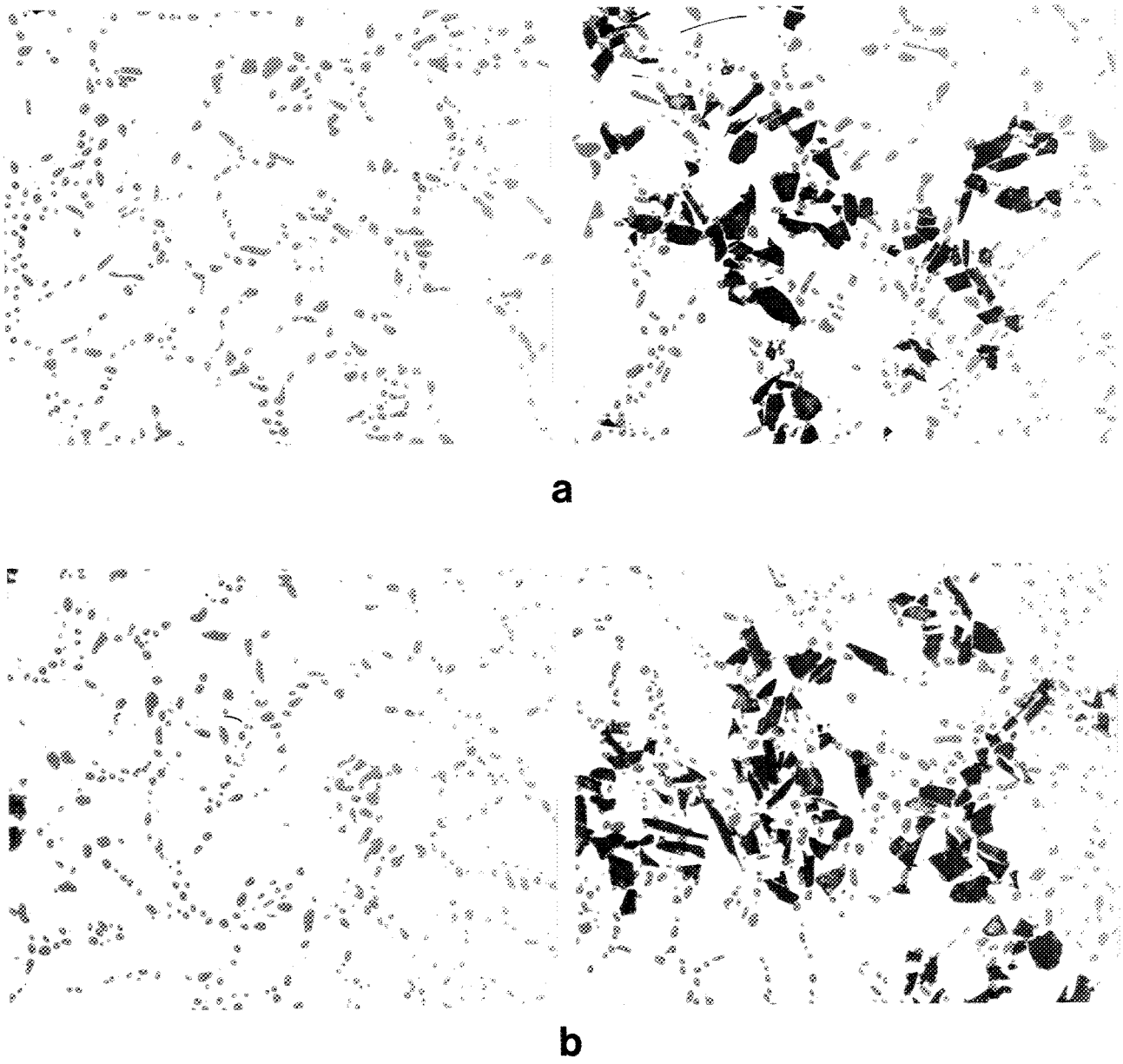

Figure IV.10. **Microstructures of 12 hr solution heat treated F3A.10S composite permanent mold test bar samples taken from both SiC_p-free and SiC_p-containing areas: (a) Sr concentration: 140 ppm, (b) Sr concentration: 100 ppm (750 X).**

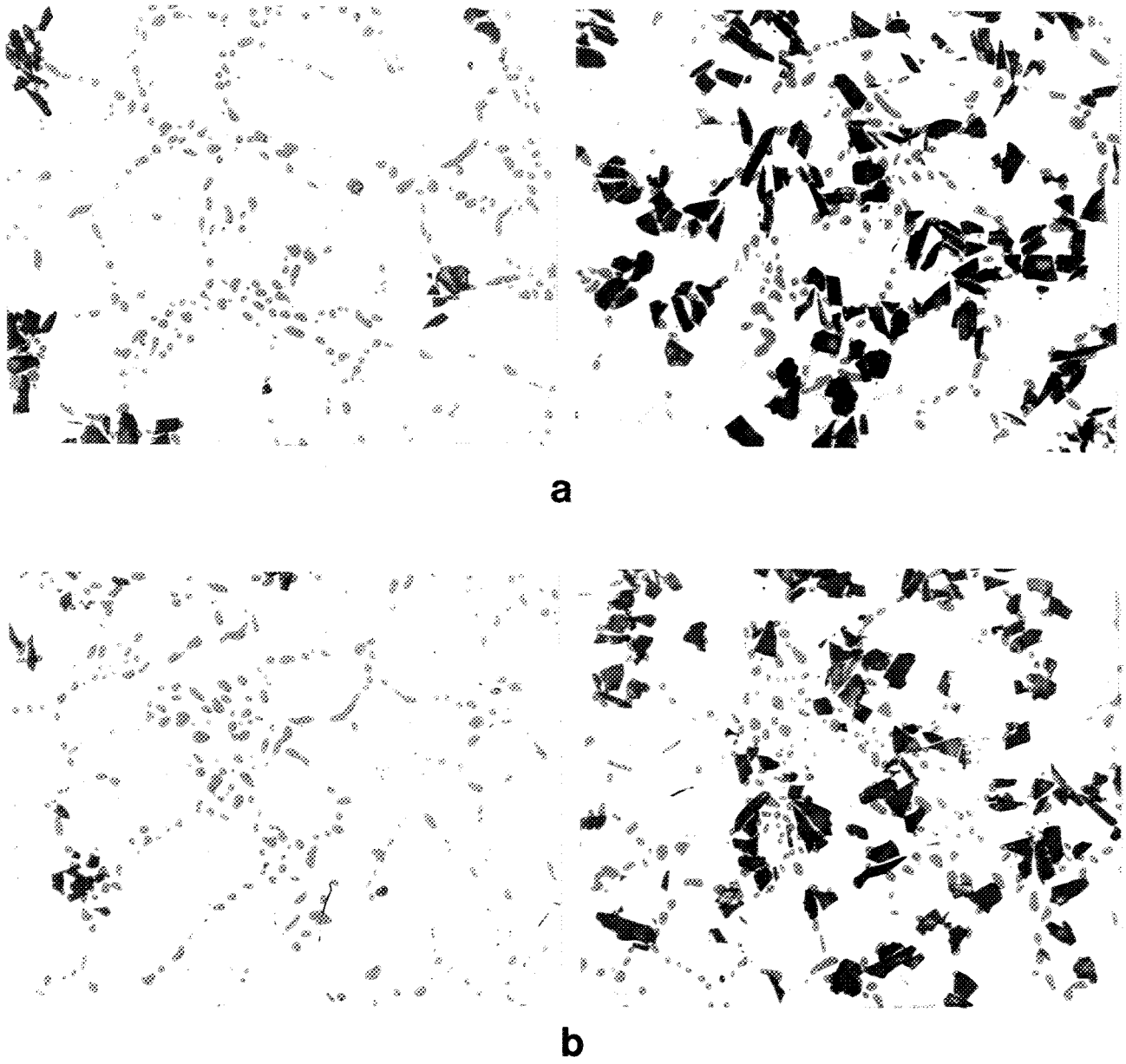

Figure IV.11. **Microstructures of 12 hr solution heat treated F3S.10S composite permanent mold test bar samples taken from both SiC_p-free and SiC_p-containing areas: (a) Sr concentration: 110 ppm, (b) Sr concentration: 75 ppm (750 X).**

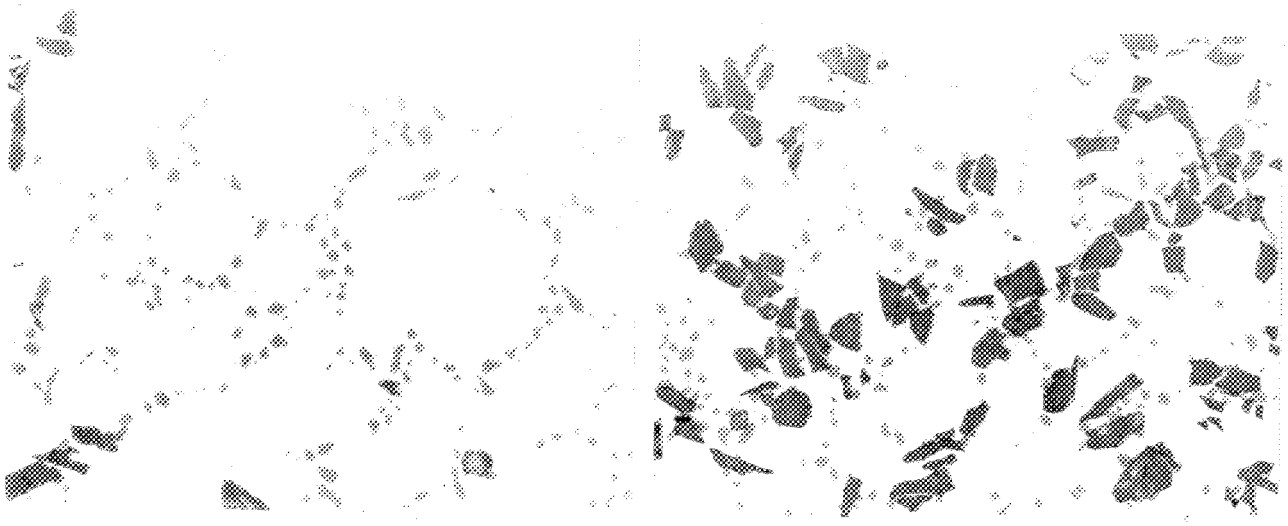

a

b

Figure IV.12. **Microstructures of 24 hr solution heat treated F3A.10S composite permanent mold test bar samples taken from both SiC_p-free and SiC_p-containing areas: (a) Sr concentration: 140 ppm, (b) Sr concentration: 100 ppm (750 X).**

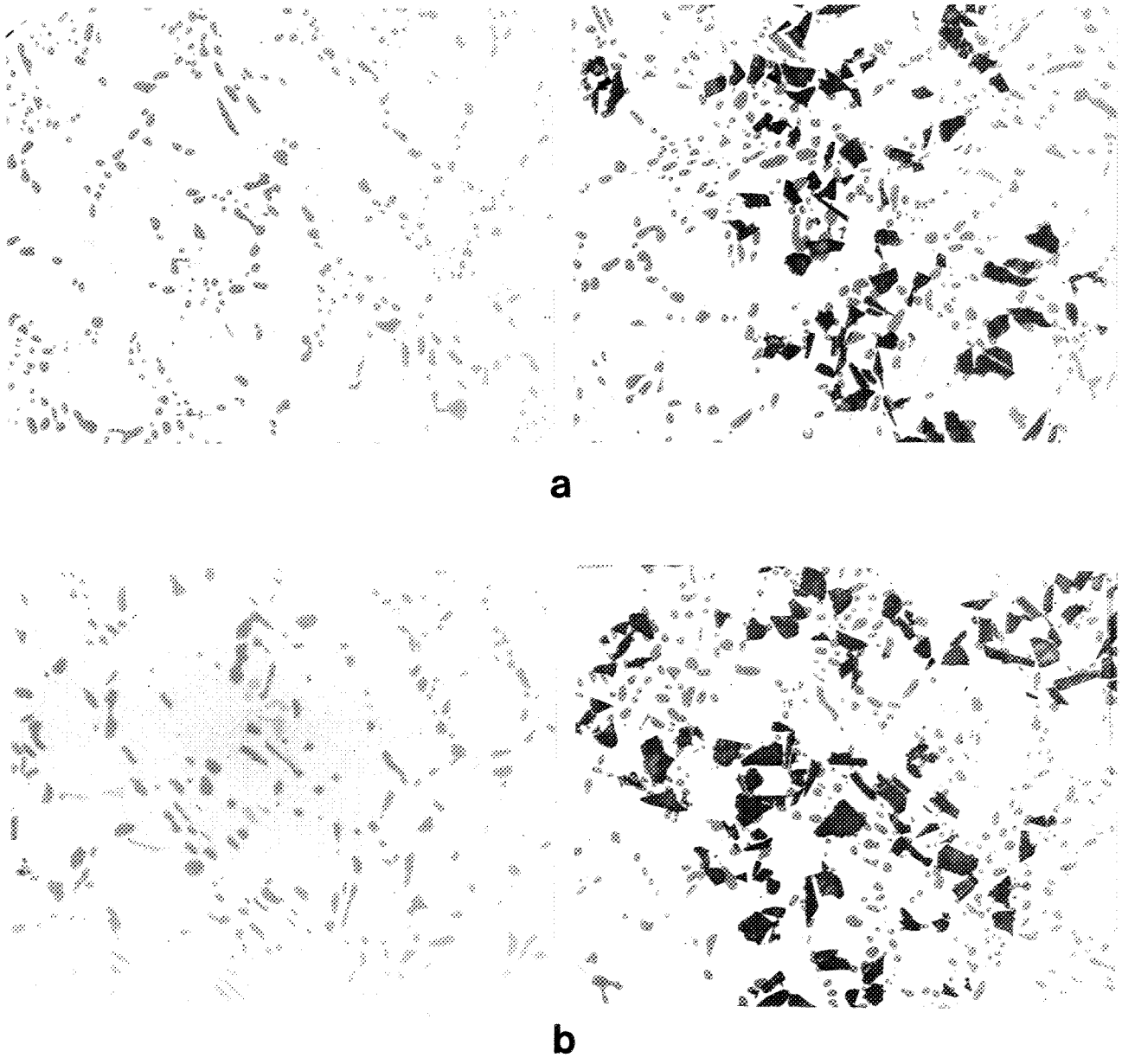

Figure IV.13. **Microstructures of 24 hr solution heat treated F3S.10S composite permanent mold test bar samples taken from both SiC_p-free and SiC_p-containing areas: (a) Sr concentration: 110 ppm, (b) Sr concentration: 75 ppm (750 X).**

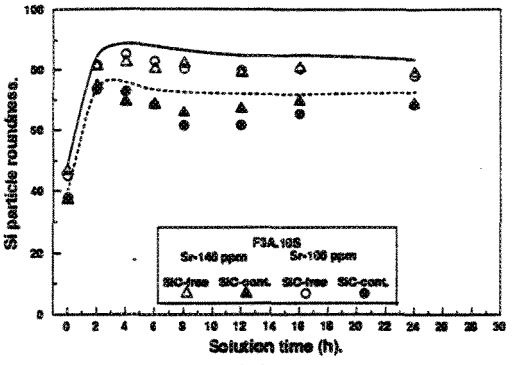
Si particle roundness.
Solution time (h).
F3A.10S
Sr-140 ppm
Sr-100 ppm
SiC-free SiC-cont. SiC-free SiC-cont.

(a)

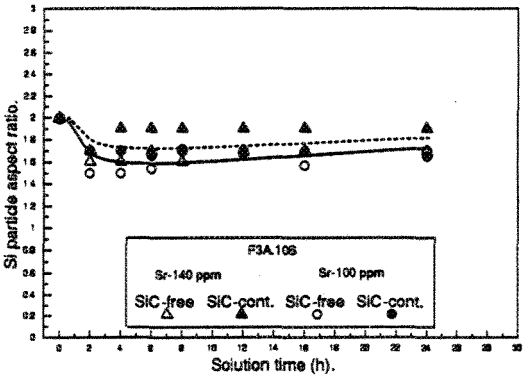
Si particle aspect ratio.
Solution time (h).
F3A.10S
Sr-140 ppm
Sr-100 ppm
SiC-free SiC-cont. SiC-free SiC-cont.

(b)

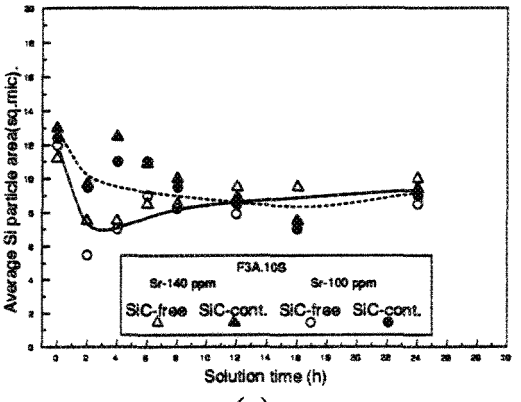
Average Si particle area(sq.mic).
Solution time (h)
F3A.10S
Sr-140 ppm
Sr-100 ppm
SiC-free SiC-cont. SiC-free SiC-cont.

(c)

(i) F3A.10S

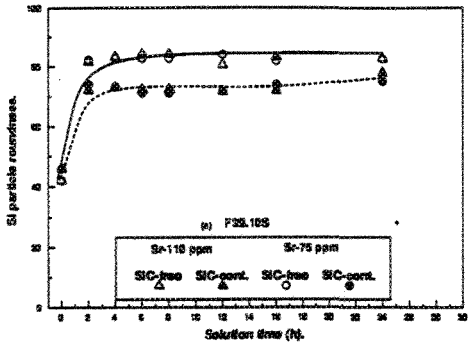

(a_1)

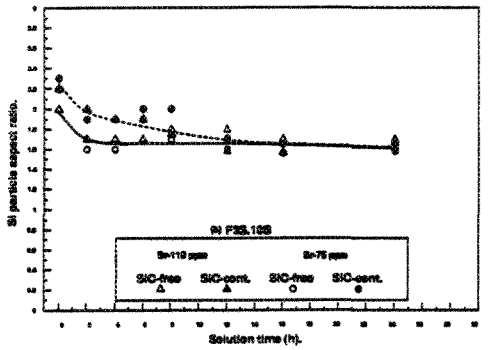

(b_1)

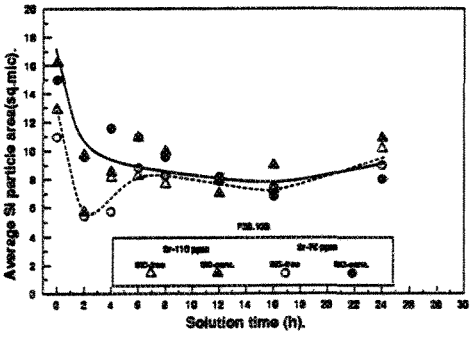

(c_1)

(ii) F3S.10S

Figure.IV.14. **Relation between solution time and Si particle morphology: (a & a_1) roundness, (b & b_1) aspect ratio, (c & c_1) area size, for two different Sr levels (140 and 110 ppm) in (i) F3A.10S, (ii) F3S.10S composites.**

IV.4. EFFECT OF AGING TREATMENT ON THE AVERAGE MECHANICAL PROPERTIES

(a) For F3A.10S

The effect of preaging (natural aging) on the average mechanical properties of F3A.10S is shown in Fig. IV.15.(and listed in Table IV.7 in the Appendix). From this figure, the optimum combination of strength and ductility were obtained after 12 hr aging only, this may be explained as a result of the higher dislocation density formed in the in the matrix during cooling from solution treatment temperature (540°C), due to the mismatch of the thermal expansion coefficient between Al and SiC_p (10:1); the higher dislocation density in the matrix of the composite is believed to aid the nucleation of the Mg_2Si precipitates and results in accelerated aging kinetics compared to the unreinforced alloy [105]. Increasing the aging time up to 24 hr does not result in any significant change in the average mechanical properties.

The influence of direct aging on the average mechanical properties of F3A.10S is shown in Fig.IV.16 (and listed in Table IV.8 in the Appendix). From this figure, F3A.10S alloy exhibits lower mechanical properties after 5 hr aging at 160°C. The average values of these properties were 42 ksi, 47 ksi and 1.0% for YS, UTS and EL%, respectively. Increasing the aging time up to 24 hr leads to higher YS and UTS values (47 ksi and 49 ksi) combined with lower fracture ductility, around 0.4%. Fig. IV.17 shows the relationship between UTS and EL% in the as-cast, T4 and T61 conditions for F3A.10S composite. The lower mechanical properties observed in the

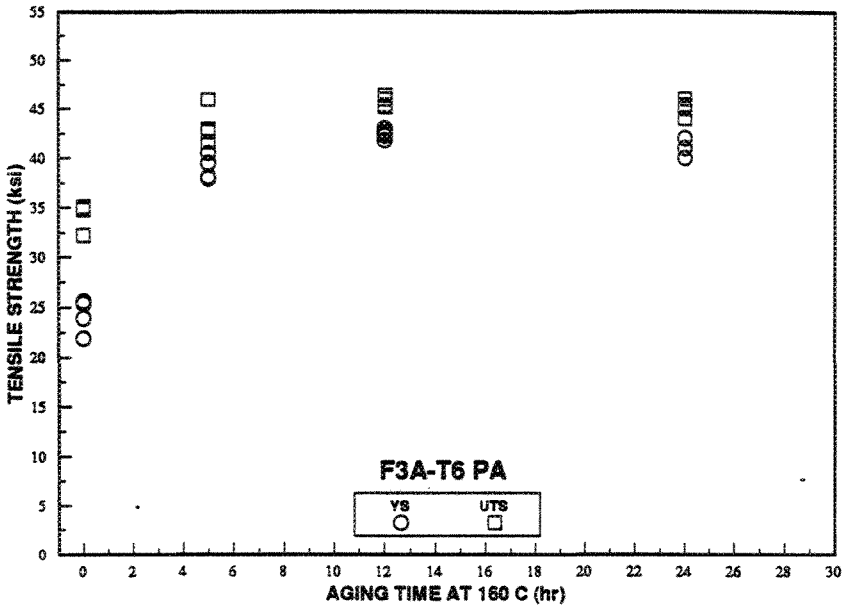

(a)

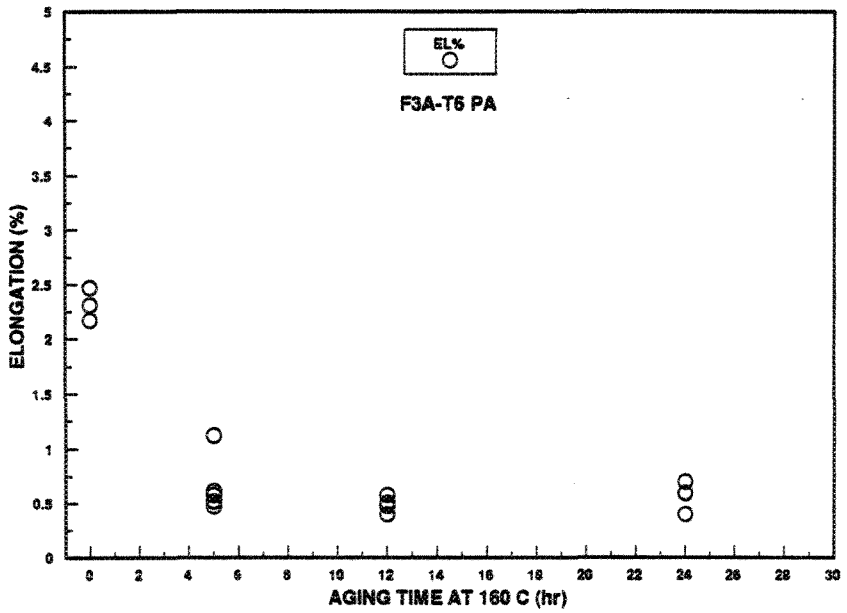

(b)

Figure IV.15. Effect of natural aging at 25°C for 24 hr prior to artificial aging at 155°C on (a) tensile strength (ksi), (b) elongation (%) of F3A.10S composite.

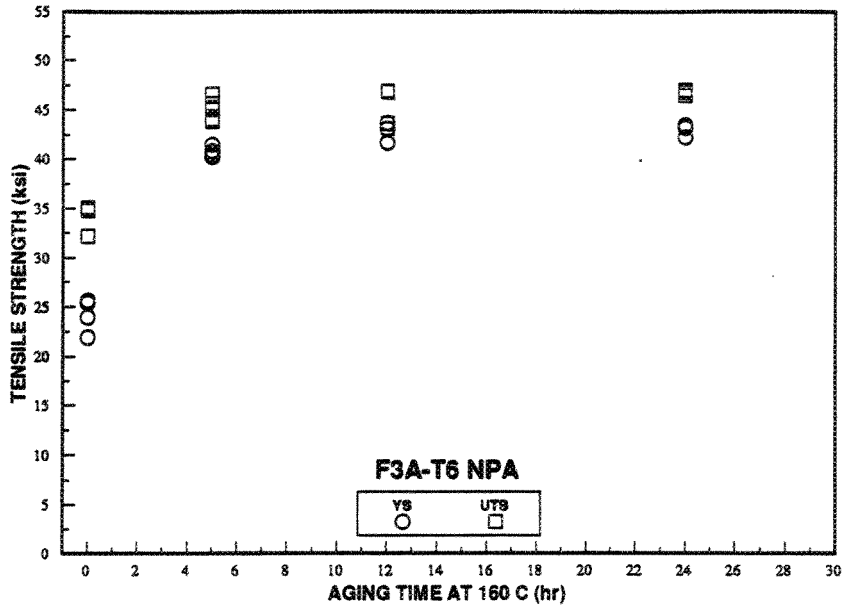

(a)

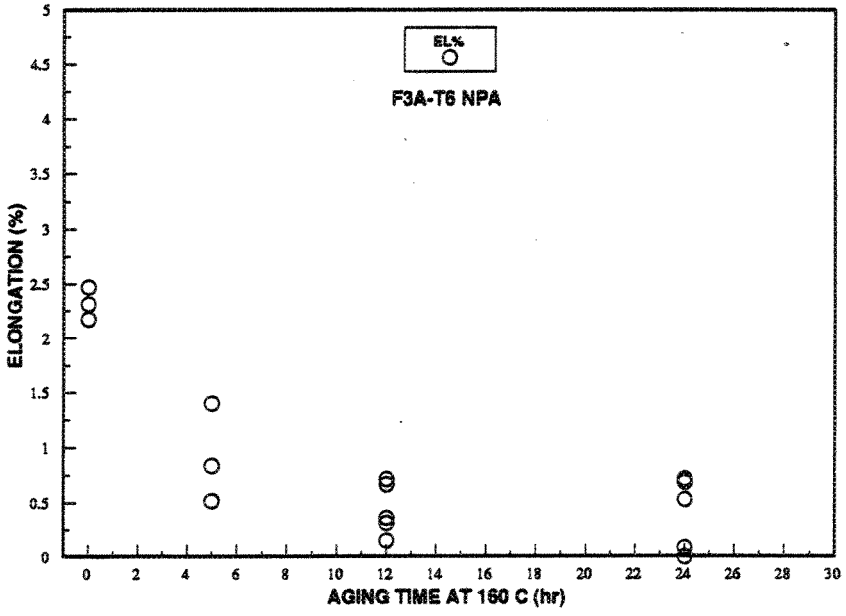

(b)

Figure IV.16. **Effect of aging at 160°C on (a) tensile strength (ksi), (b) elongation (%) of F3A.10S composite.**

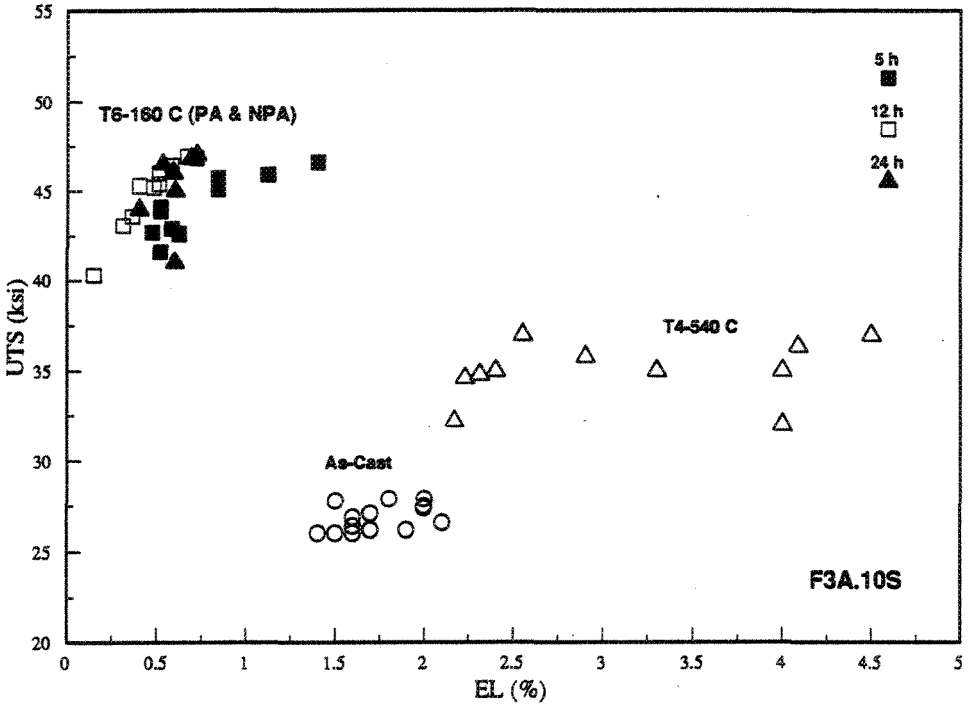

Figure IV.17. **Relation between UTS (ksi) and Elongation (%) in the as-cast, T4 and T61 conditions for F3A.10S composite.**

case of preaged test bars has been attributed to the presence of $AlTi_3$ needles (as shown in Fig. IV.18.) which are introduced into the melt through grain refiner addition which may delay the precipitation kinetics of Mg_2Si phase during aging.

(b) For F3S.10S

The influence of preaging on the average YS, UTS, EL% of F3S.10S is shown in Fig. IV.19, and listed in Table IV.9, in the Appendix. From this figure it can be seen that subjecting all the test bars to 5 hr aging at 155°C leads to a good combination of strength and ductility, the average mechanical properties being 42 ksi, 46.5 ksi and 0.7%. Increasing the aging time up to 24 hr at 155°C leads to higher tensile strength and a lower fracture ductility value i.e. 47 ksi, 49.5 ksi and 0.3% for YS, UTS and EL%, respectively.

On subjecting F3S.10S test bars to direct aging, the mechanical properties exhibit a good combination of strength and ductility after only 5 hr aging, reaching 43 ksi, 47 ksi and 1.0%. Increasing the aging time up to 24 hr at 155°C leads to higher tensile strength and lower fracture ductility values, 47 ksi, 50 ksi and 0.3%, for YS, UTS and EL%, respectively as shown in Fig.IV.20. (and listed in Table IV.10, in the Appendix). From the mechanical properties it seems both YS and UTS exhibit similar results for all test bars subjected to preaging. This may be explained as a result of the increased Si level (10 wt%) within the Al matrix which has been reported to rapidly decrease both the elongation and charpy impact values. Fig.IV.21 shows the

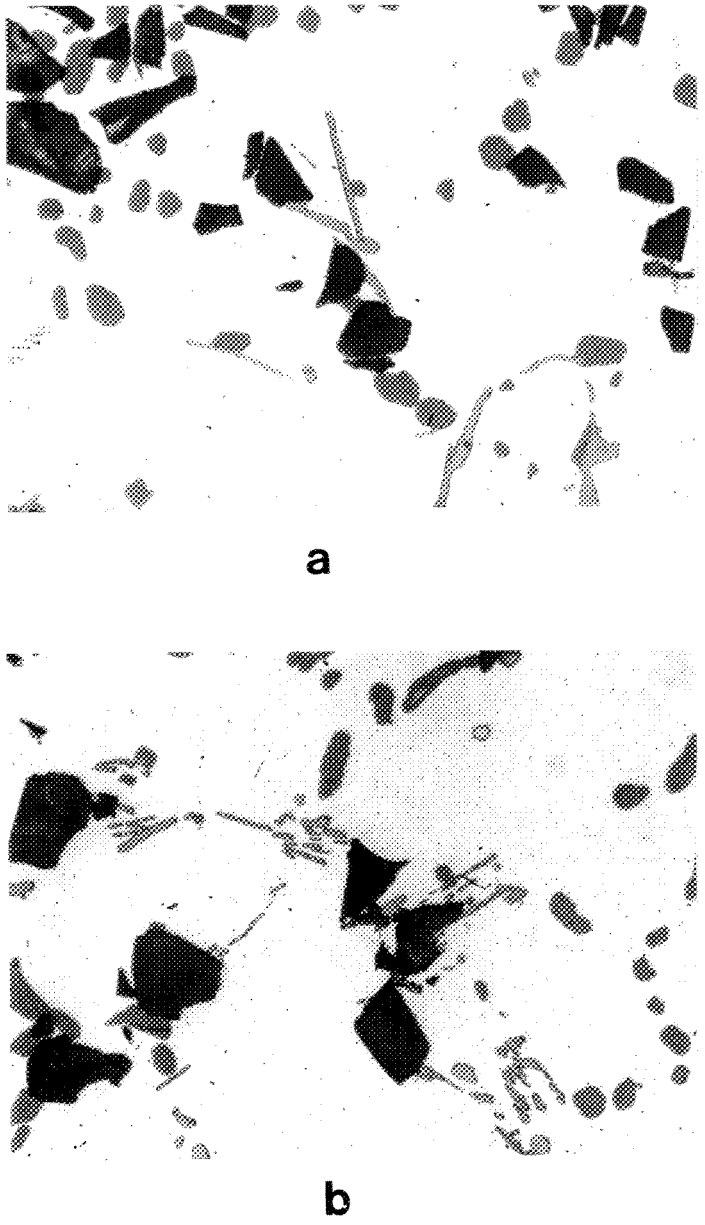

Figure IV.18. Optical micrographs showing the presence of $AlTi_3$ after T61 heat treatment in F3A.10S composite.

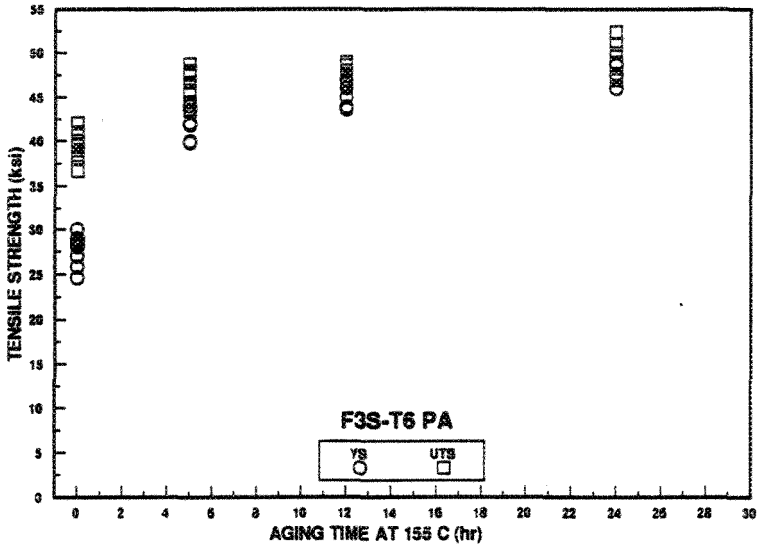

(a)

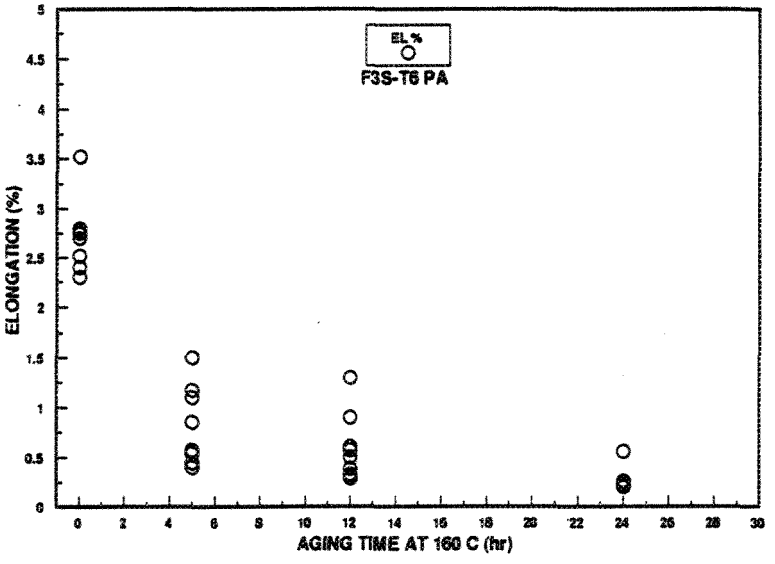

(b)

Figure IV.19. **Effect of natural aging at 25°C prior to artificial aging at 155°C on: (a) tensile strength (ksi), (b) elongation (%) of F3S.10S composite.**

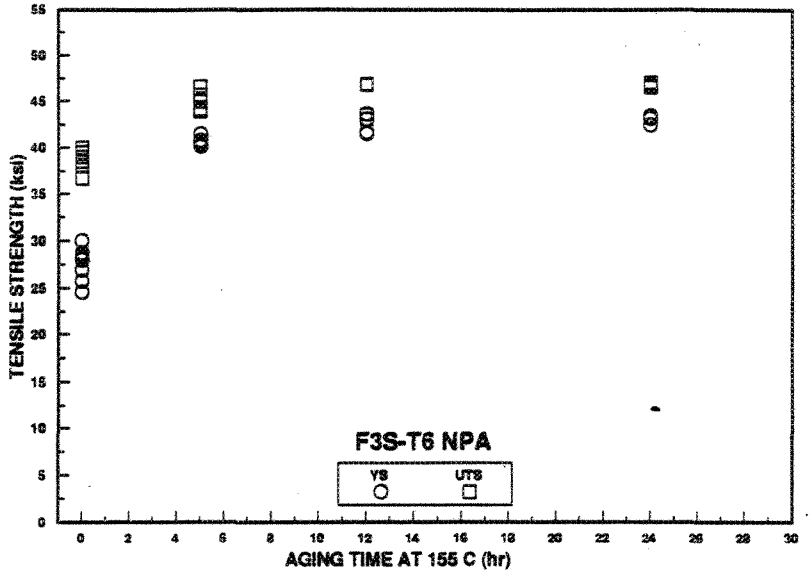

(a)

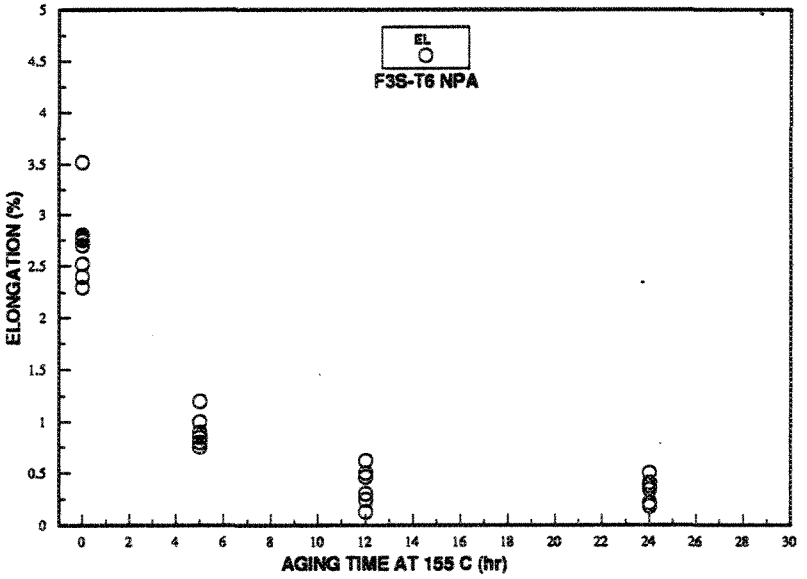

(b)

Figure IV.20. **Effect of aging at 155°C on (a) tensile strength (ksi), (b) elongation (%) of F3S.10S composite.**

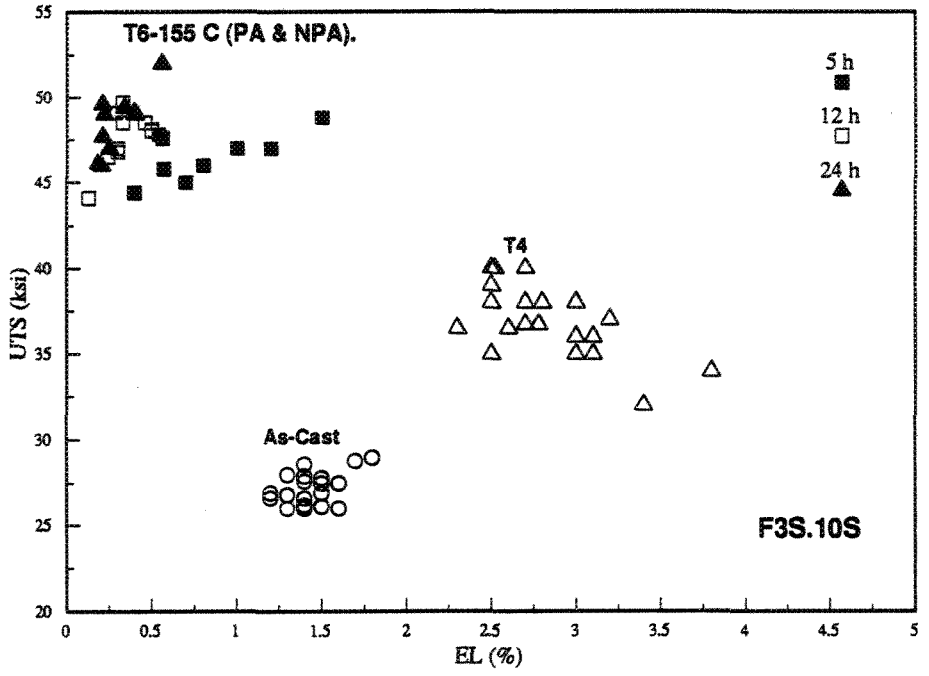

Figure IV.21. **Relation between UTS (ksi) and Elongation (%) in the as-cast, T4 and T6 conditions for F3S.10S composite.**

relationship between UTS and EL% in the as-cast, T4 and T61 conditions for F3S.10S composite.

IV.5. QUALITY INDEX Q

Quality index Q can be used either for assessing the alloy quality or for investigating the influence of a given parameter such as composition, production process and cooling or heat treatment. The quality index, a parameter that combines the ultimate tensile strength and elongation is expressed as [105,106]:

$$Q(ksi) = UTS(ksi) + 21.9\log(EL\%) \qquad (11)$$

The plots of elongation vs quality index (Q=UTS (ksi)+21.9 log(EL%), Fig. IV.22, show a linear relationship. From the least squares method, these relations may be written for F3S.10S composites as follows:

$$EL = 1.06 - 0.66X \qquad (12)$$

$$Q = 52.2 - 19.8X \qquad (13)$$

From the previous equations the quality index was calculated for the as-cast, solution heat treated and T6 tempered test bars of the two composites. The quality index (Q) increases with solution time due to the continuous dissolution of Mg_2Si and the spheroidization of the Si particles. Fig. IV.23 shows the relationship between the solution time and quality index for both composites.

For the composites no specific relationship between quality index (Q) and solution time (t) is obtained, unlike the $Q \alpha t^{1/3}$ relationship obtained for the unreinforced (A356) alloy. The quality index exhibits higher values in the case of F3S.10S than those obtained in the case of F3A.10S, due to the higher UTS values.

After aging heat treatment, elongation, however, exhibits an opposite trend; the Q values still remain close to the UTS values and are only slightly affected by the decrease in elongation which is typical of hard/brittle materials. Fig. IV.24 shows the relationship between aging time and quality index for (a) F3A.10S, (b) F3S.10S composites.

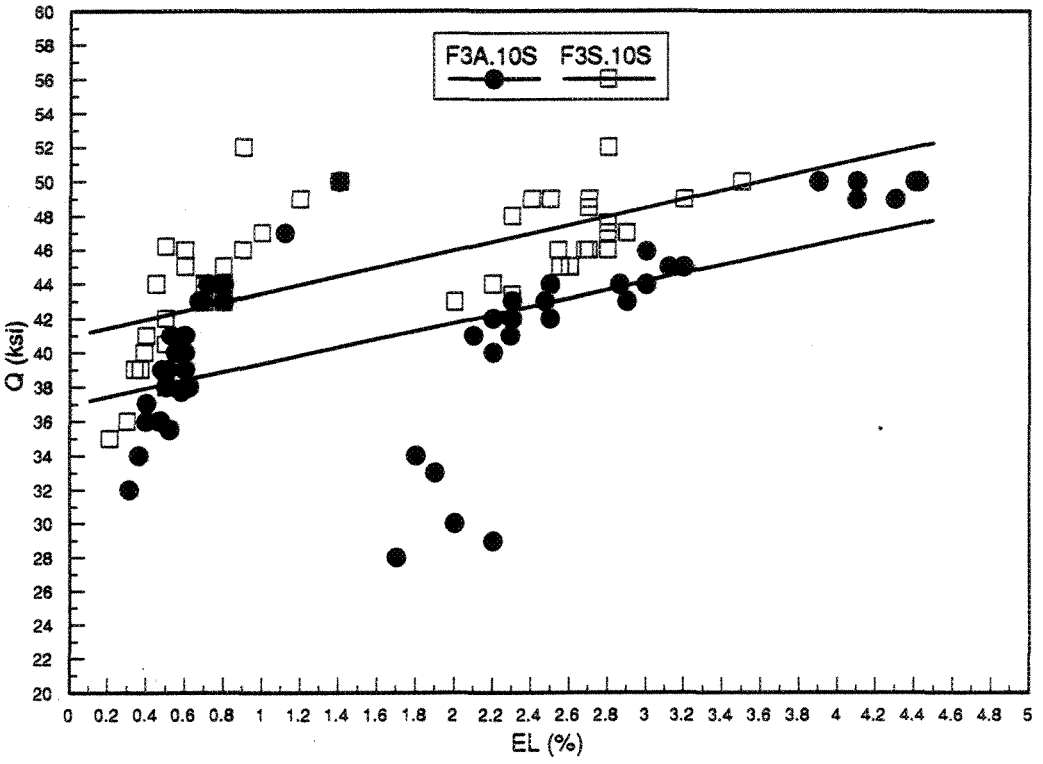

Figure IV.22. **Plot of Elongation vs Quality Index for F3A.10S and F3S.10S composites.**

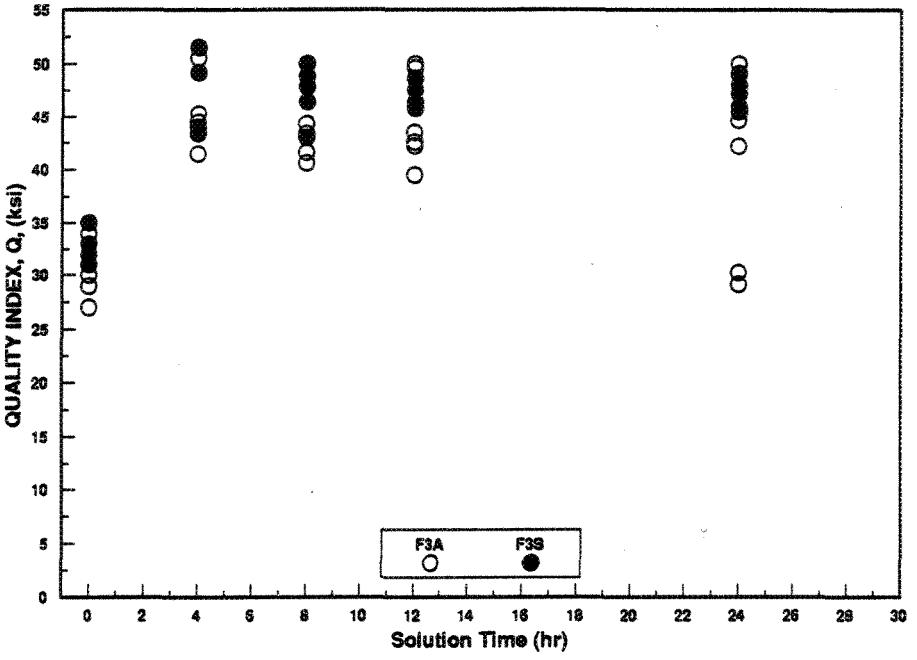

Figure.IV.23. **Relation between solution time and quality index (Q) for F3A.10S and F3S.10S composites.**

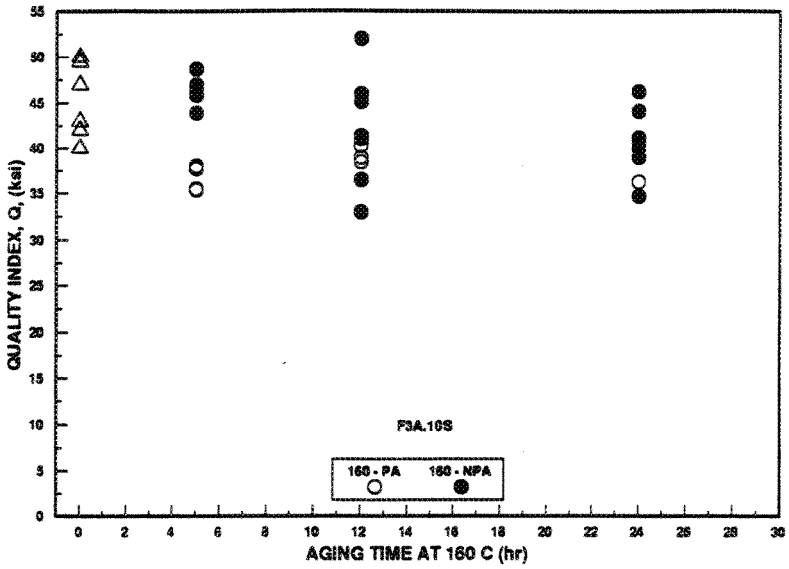

(a)

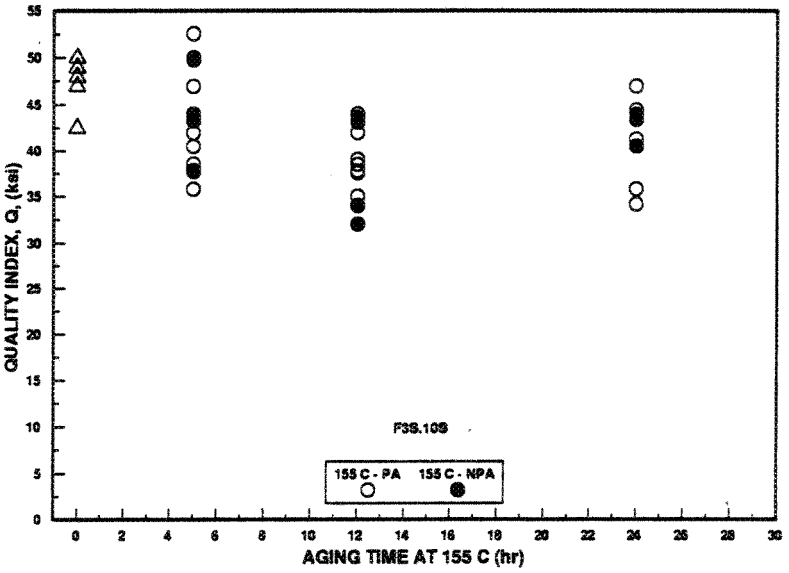

(b)

Figure IV.24 Relation between aging time and quality index (Q) for: (a) F3A.10S at 160°C, (b) F3S.10S at 155°C aging temperatures (PA: Preaging, NPA: No Preaging).

IV.6. FRACTURE MECHANISMS IN THE HEAT TREATED COMPOSITES

Lloyd et al. [92] summarized three possible types of fracture behaviour in particulate composites. If the particle/matrix interface is weak, the crack will propagate through the interface, but if the interface is strong, together with a strong matrix, the particles will loaded to their fracture stress and crack. In the case that the matrix is weak relative to the interfacial and particle strengths, the fracture will occur in the matrix by normal void nucleation and growth.

In real composites, with various shapes, sizes and distributions of the Si and SiC particles, a complex fracture process can result. Although the composite used in the present study exhibited limited ductility on a macroscopic scale, with fracture essentially normal to the loading axis, SEM examination revealed features reminiscent of ductile mechanism. A few SiC particulates are present in the fracture surfaces of T4 treated specimens, Fig. IV.25.

After aging at 155-160°C, the fracture surface exhibits brittle fracture, indicating a transgranular fracture corresponding to a relatively low ductile feature. The extent of SiC cracking appeared to be greater after 5 hr aging time at 155-160 °C, indicating a strong SiC/Al bond i.e. a strong interface together with a strong matrix. Test bars aged for 12 hr at this temperature reveals the propagation of a coarse microvoid, formed in the matrix. Aging for 24 hr at this temperature represents more or less the peak-aged condition, severe damage of the SiC particles is the main characteristic feature of the fracture mode. In this case, a zig-zag type of crack is seen

to propagate from the particle into the matrix, believed to have formed in the aluminum matrix and passing through the particle/matrix interface; this type of crack occurs if the interface is weak, as is evident from a comparison of Fig. IV.26 (a), (b) and (c) and Fig. IV.27 (a_1), (b_1) and (c_1).

The fracture of SiC_p can be examined in more detail by longitudinally sectioning the samples to obtain information from the interior of the sample rather than at the surface. A relatively large number of broken SiC_p were observed in the case of T6 and T61 tempered samples, around 200-320 fractured particles were measured, and this number reduced to 150-250 in the case of T4 tempered samples, as shown in Fig. IV.28, which shows the maximum particle fracture and voiding in specimens corresponding to (a) 5 hr artificial aging, (b) 12 hr artificial aging, and (c) 24 hr artificial aging at 160°C for F3A.10S composites.

The main difference between the T4 and T6 or T61 tempers was the number of broken SiC particulates, which was higher in the latter. It should be noted that elongation in these composites varied between 2.5-4.0% (T4-temper) and 1.2-0.6% (T6-temper), reflecting on the fact that the ductility is significantly influenced by the volume fraction and the number of broken particles, as shown in Fig. IV.29.

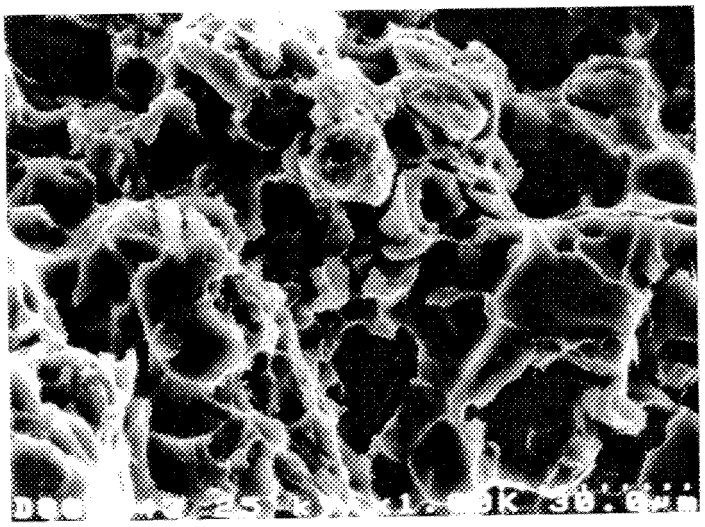

a

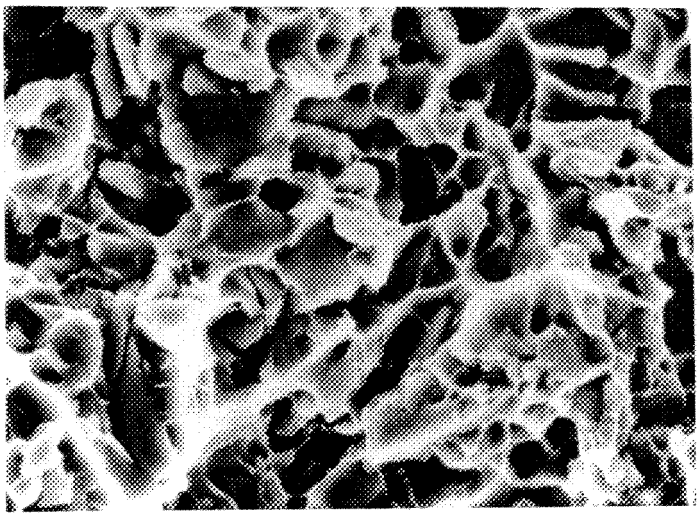

b

Figure IV.25. Fractographs showing the fracture mode of solution heat treated composites: (a) 8 hr for F3A.10S, (b) 12 hr for F3S.10S (1000 X).

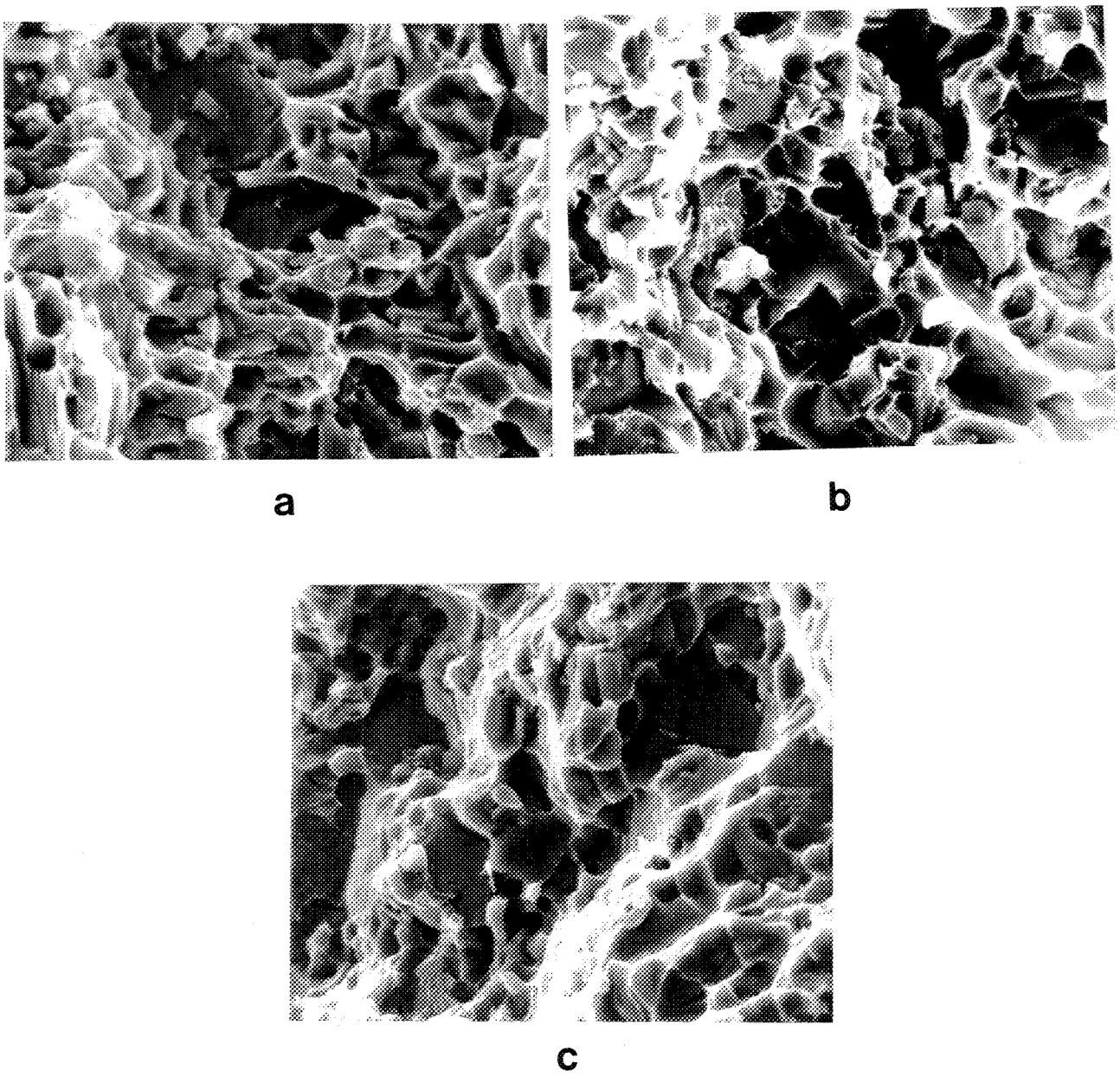

Figure IV.26. Fractographs showing the fracture mode of F3A.10S: (a) 5 hr aging at 160°C, (b) 12 hr aging at 160°C, (c) 24 hr aging at 160°C (1000 X).

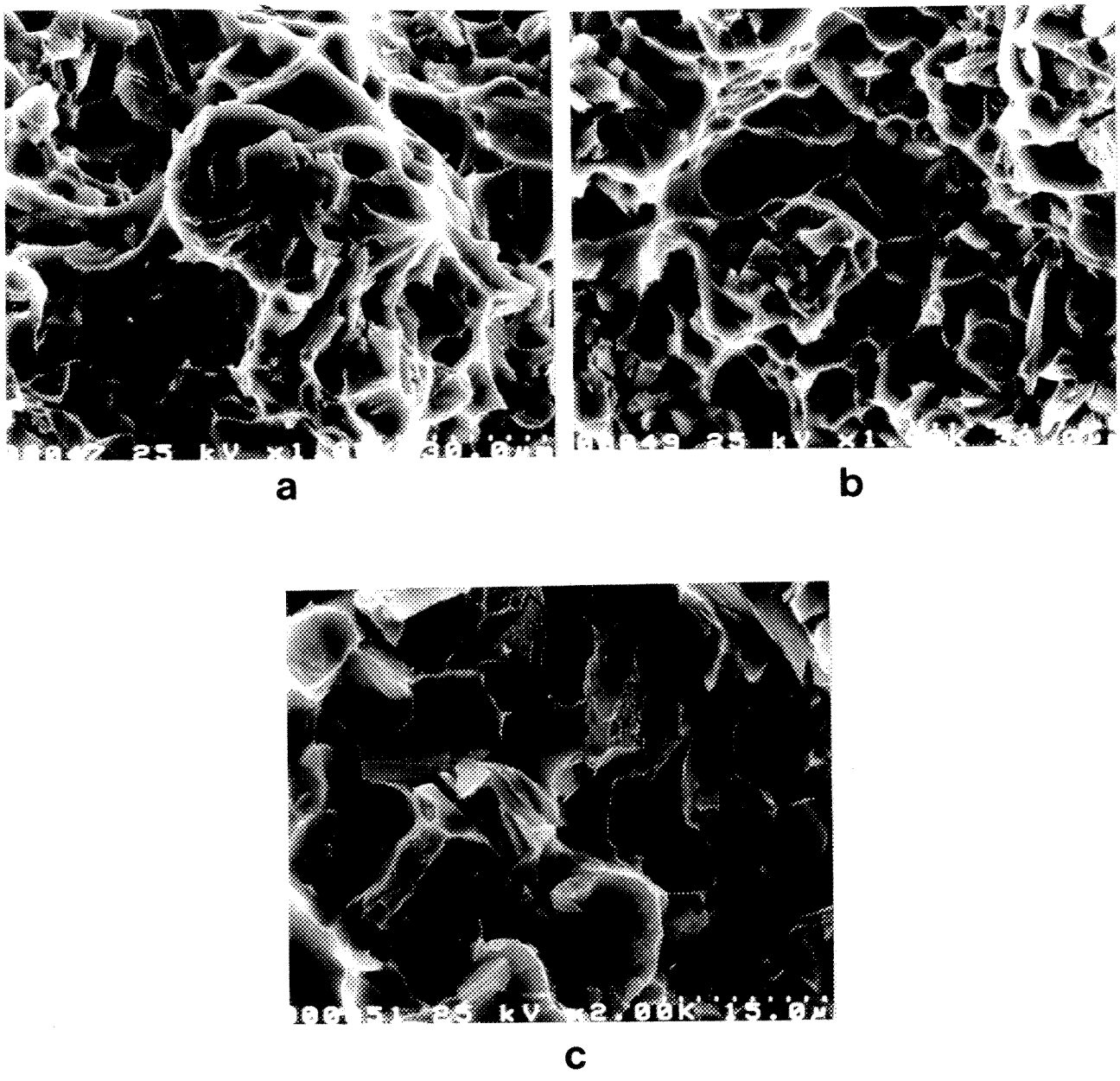

Figure IV.27. Fractographs showing the fracture mode of F3S.10S: (a) 5 hr aging at 160°C, (b) 12 hr aging at 160°C, (c) 24 hr aging at 160°C (1000 X).

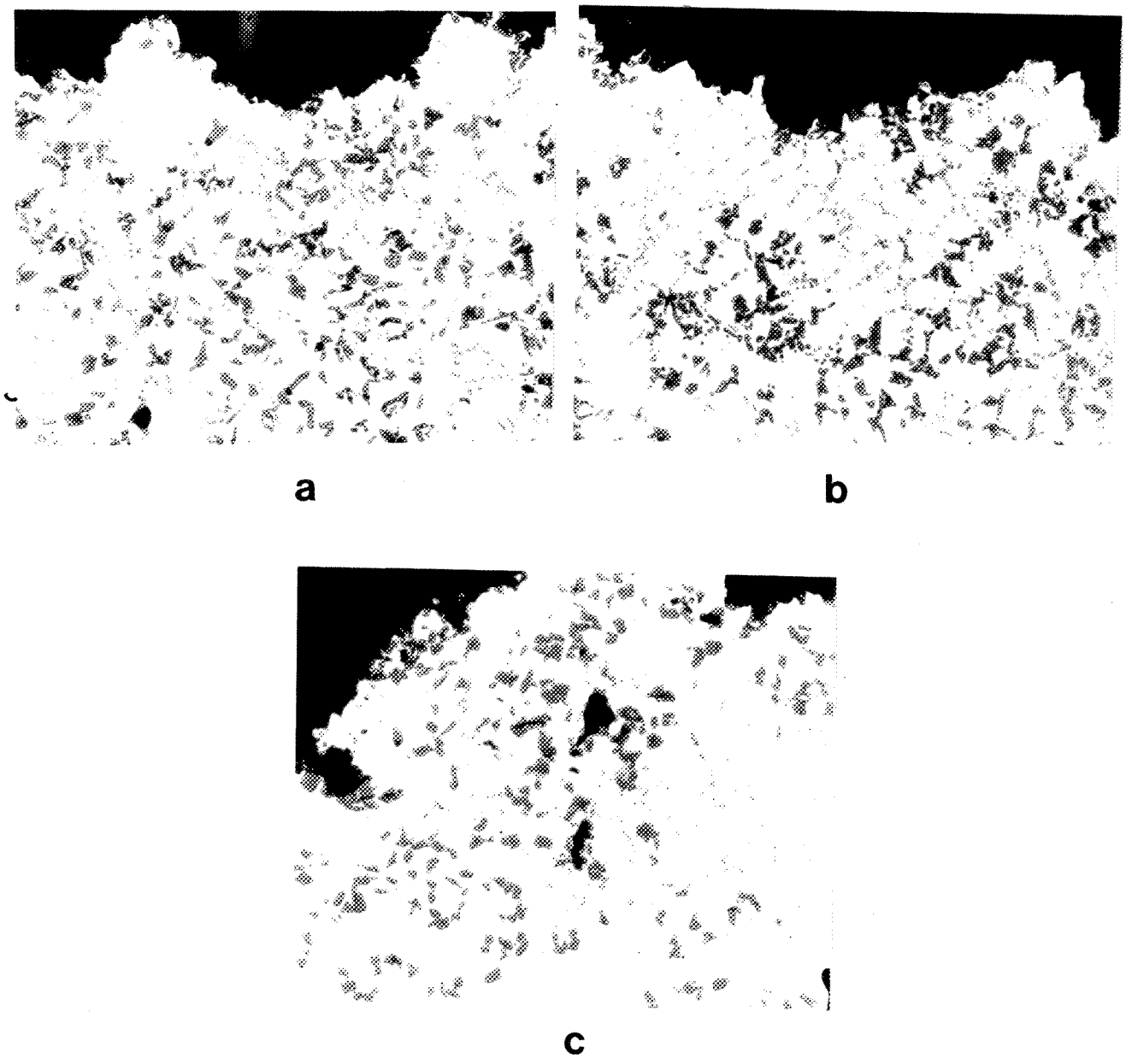

Figure IV.28. Maximum particle fracture and voiding in specimens corresponding to (a) 5 hr artificial aging at 160°C, (b) 12 hr artificial aging at 160°C, (c) 24 hr artificial aging at 160°C for F3A.10S composite (200 X).

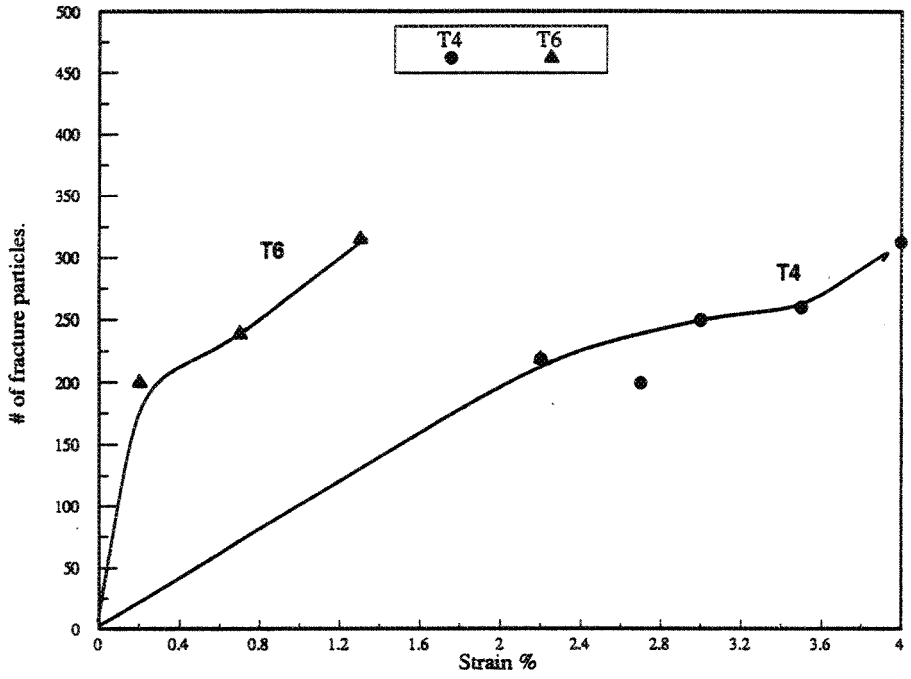

Figure IV.29. **Relation between strain (%) and number of fractured particles in T4 and T6 tempered F3A.10S composite.**

CHAPTER V
CONCLUSIONS

V.I. CONCLUSIONS

From the results obtained in the present study on the effect of melt and casting variables, solidification/cooling rate and heat treatment on the microstructure and mechanical properties of the two Al-Si-Mg/SiC_p composites F3A.10S and F3S.10S, the following conclusions may be drawn:

(1) The as-cast properties of SiC_p reinforced Al-Si-Mg metal matrix composites are basically controlled by the solidification rate.

(2) The presence of a higher silicon level in F3S.10S composite (10 wt% vs 7.5 wt% in the F3A.10S alloy) improves the composite fluidity and hence increases the mold temperature range from 350-450°C (for the F3A.10S composite) to 300-450°C (for the F3S.10S composite).

(3) Higher solidification rates promote homogeneous distribution of SiC particles with fewer denuded zones.

(4) SiC particles act as nucleation sites for gas porosity. The coarsening of both gas and shrinkage pores is restricted by the surrounding SiC particles, leading to a well distributed and finer porosity, compared to that formed in A356, where the porosity is mainly central shrinkage type, linked with gas porosity.

(5) In the case of F3A.10S composite, due to its low Si content, holding times longer than 1 hr at ~740 °C lead to the formation of small fragments of Al_4C_3 at the edges of or between the SiC particles. This reaction can be suppressed by increasing the Si content to 10 wt% (i.e. F3S.10S composite).

(6) Tensile properties for the as-cast composites, as measured by YS, UTS and EL% are stable for both F3A.10S and F3S.10S for mold temperatures in the range 300-450°C. The presence of SiC_p results in a 4 ksi increase in both YS and UTS as compared to the base alloy A356.

(7) The Sr concentration decreases with increasing stirring time, from 140 to 100 ppm for F3S.10S and from 110 to 75 ppm for F3A.10S, after 3 hr stirring time.

(8) Short (20, 40 and 60 min) or long (60, 120 and 180 min) stirring intervals do not result in any significant change in the volume fraction of SiC_p, which lies in the range 9-12% for both composites.

(9) Solution heat treatment at 540°C for various times (4, 8, 12 and 24 hr) results in improvement in the average tensile properties (YS, UTS and EL%) compared to the as-cast values. Prolonged solution time up to 24 hr does not bring any significant changes to these properties, the optimum combination of strength and ductility being achieved after only 4 hr.

(10) The eutectic Si morphology characteristics (roundness, aspect ratio and area size) for both composites vary in the SiC_p-free and SiC_p-containing regions d ue to the difference in physical properties and the chemical composition for each alloy.

(11) The presence of SiC_p plays a role in refining the Si particle morphology.

(12) After heat treatment, both F3A.10S and F3S.10S composites reveal similar tensile properties, thus the presence of 3 wt% more Si in the case of F3S.10S alloy is enough to reduce the heat treatment cycle time from 60 to only 13 hr.

(13) The YS and UTS levels obtained from composites are about 10 and 4-8 ksi higher, respectively, than those obtained for A356 alloy treated similarly. However, the ductility is reduced from ~6.0% in the case of A356 to ~1.0% for the composites.

(14) Elimination of natural aging and a lower artificial aging time (around 5 hr) gives the best combination of ductility and strength for both composites.

(15) The presence of the SiC particles within the Al-Si-Mg matrix enhances the aging kinetics of both composites. This enhancement is attributed to the higher cooling rate, the chemical composition and the aging temper applied to the casting.

(16) The fracture surfaces are characterized by a dimple morphology and cleavage of the SiC particles. The latter becomes more evident in the T6 or T61 tempered condition. The extent of SiC cracking reaches its maximum after 24 hr aging at 155-160 °C for both composites.

RECOMMENDATIONS

The results of this work on the mechanical properties of permanent mold test bars of F3A.10S and F3S.10S composites show that both composites exhibit lower ductility values (~1.0%) compared to the unreinforced alloy. These values may be improved to ~2.0-3.0% after T6 or T61 temper and by achieving a higher cooling rate, in the range 50-100°C/s^{-1}, which ensures a uniform distribution of SiC_p within the solidified casting and so higher ductility values. Also, elimination of any oxides and/or inclusions during remelting and casting of the two composites can lead to higher ductility values than those obtained.

Further work should include transmission electron microscopy to characterize the precipitate formation in both F3A.10S and F3S.10S alloys during aging and to compare the amount of precipitates obtained in each alloy.

Compression tests, fracture toughness tests and hardness tests of both composites are required to gain a better understanding of the mechanical properties.

REFERENCES

(1) W.R. Loué and W.H. Kool, Proc. Conf. " Cast Reinforced Metal Matrix Composites", S.G. Fishman and A.K. Dhingra (eds.) ASM International, Metals Park, OH, (1988), p. 327.

(2) M.M. Schwartz, "Composite Materials Handbook", McGraw-Hill Book Company, New York, 1984.

(3) Y. Flom and R.J. Arsenault, J. of Metals, 31 (1986) p. 31.

(4) D.J. Lloyd and B. Chamberlain, Proc. Conf. "Cast Reinforced Metal Matrix Composites", S.G. Fishman and A.K. Dhingra (eds.), ASM International, Metals Park, OH, (1988), p.263.

(5) J.E. Schoutens, "Introduction to Metal Matrix Composite Matreials,MMC1AC Tutorial Series, No. 272, (1982).

(6) S. Das, S.V. Prasard, T.K. Dan and P.K. Rohatgi, Proc. Conf. "Cast Reinforced Metal Matrix Composites", S.G. Fishman and A.K. Dhingra (eds.), ASM International, Metals Park, OH, (1988), p. 243.

(7) R. Minorutaya and R.J. Arsenault, "Metal Matrix Composites: Thermomechanical Behaviour", 1988, p. 2.

(8) J.W. Weeton, D.M. Peters and K.L. Thomas, "Engineers Guide to Composite Materials", American Society for Metals, Metals Park, OH, (1987).

(9) K.K. Chawla, " Composite Materials ", Springer-Verlag, New York, (1987).

(10) H. Lagacé and D.J. Lloyd, Canadian Metallurgical Quarterly, 28(2) (1989),

pp. 145-152.

(11) T.W. Clyne, M.G. Bader, G.R. Cappieman and P.A. Hubert, J. Mater. Sci., 20, (1985), p. 85.

(12) M. Tsukuda, M. Harada, T. Suzuki and S. Koike, J.Jpn. Inst. Light Metals, 28 (1978), PP. 109-115.

(13) W.A. Bailey, Foundry, (May 1964), pp.54-60.

(14) F. Paray and J.E. Gruzleski, Cast Metals, 5 (1993), pp. 187-198.

(15) B. Closset, R.A.L. Drew and J.E. Gruzleski, AFS Trans., 94 (1986), pp.9-16.

(16) B.L. Tuttle, A. Keslinke, D. Twarog and E. Daniels, AFS Trans., 97 (1989) pp. 889-902.

(17) K.G. Kreider and K.M.P. Prewo, in "Composite Materials", Vol.4. (ed. L.J. Broutman and R.H. Krock), Academic Press, New York, pp. 400-480.

(18) Y. Abe, S. Horikiri, K. Fujimura and E. Ichiki, Proc. Fourth Int. Conf. on Composite Materials, ICCM IV, (eds. T. Hayashi et al.), Tokyo, Japanese Society for Composite Materials, (1982), pp. 1427-1484.

(19) "Carbon Fiber Directory", D. Pamington (ed.), Pammac Directories, Slough, Berks., (1983).

(20) J. Tanaka, H. Ichikawa, T. Hayase, K. Okamura and T. Matsuzawa, Proc. Fourth Int. Conf. on Composite Materials, ICCM IV, (eds. T. Hayashi et al.), Tokyo, Japanese Society for Composite Materials, (1982), pp. 1407-1413.

(21) E. Fitzer and G. Jacobsen, Proc. Fourth Int. Conf. on Composite Materials, ICCM IV, (eds. T.Hayashi et al.), Tokyo, Japanese Society for Composite

Materials, (1982), pp. 1315-1322.

(22) J. Dinwoodie, E. Moore, C.A.J. Langman and W.R. Symes, Proc. Fifth Int. Conf. on Composite Materials, ICCM V, (eds. W.C. Harrigton et al.), AIME, New York, (1985), pp.671-685.

(23) S.V. Nair, J.K. Tien and R.C. Bates, Int. Met. Rev., 30 (1985), pp.275-290.

(24) J. White, I.R. Hughes, T.C. Wills and R.M. Jordan, Fourth Int. Al-Li Conference, (ed. G.Champier et al.), Sociéte Française de Metallurgie, Paris, (1987), pp. 347-353.

(25) E.A. Feest, A.M. Ball, A.R. Begg and D.A. Biggs, "Metal Matrix Composites Development in Japan", Harwell, Oxon., Ukaea (1986).

(26) M.H. Jacobs, Phil. Mag., 26 (1977), pp. 1-13.

(27) D.J. Lloyd, Compos. Sci.& Technol., 35 (1989), pp. 159-179.

(28) N. Wang, Z. Wang and G.C. Weatherly, Metall. Trans. A, 23A (1992), pp. 1423-1430.

(29) A.D. McLeod, Proc. ASM Int. Conf. on Fabrication of Particulates Reinforced Metal Matrix Composites, Montreal, PQ, Canada, September 16-19, 1990, pp. 25-29.

(30) F.H. Samuel, H. Liu and A.M. Samuel, Metall. Trans. A, 24A (1993), pp.1631-1645.

(31) K.M. Prewo and K.G. Kreider., Metall. Trans.A, 3A (1972), pp.2201-2211.

(32) A.G. Metcalfe, "Composites Materials", (eds. L.J. Broutman and R.H. Krack), Vol.4: Metallic Matrix Composites, (ed. K.G.Kreider), Academic Press, New York.

(33) P.R. Smith, F.H. Froes and J.T. Cammett, in "Mechanical Behaviour of Metal-Matrix Composites", (eds. J.E. Hack and M.F. Amateau), TMS of AIME, (1983), pp. 143-168.

(34) T. Donomoto, K. Funatani, N. Miura and N. Miyake, ASE Tech. paper 830252, 1983, Society for Automobile Engineering.

(35) A.P. Diwanji, I.W. Hall., Proc. ICCM-6/ECCM-2, (eds. F.L. Matthews et al.), Vol.2, Elsevier, London, (1987), pp. 2.265-2.274.

(36) H. Fukunaga, H. Goda, Y. Fujita, Ibid, pp. 2.362-2.371.

(37) H. Matsubara, Y. Nishida, M. Yamada, I. Shirayanagi and T. Imai, J. Mater. Sci. Letts., 6 (1987), pp. 1313-1315.

(38) J.A. Cornie, A. Mortensen and M.C. Flemings, Proc. ICCM-6/ECCM-2, (eds. F.L.Matthews et al.), Vol.2, Elsevier, London, (1987), pp. 2.297-2.319.

(39) Y. Abe, S. Horikiri, K. Fujimura and E. Ichiki, Proc. ICCM-4, Progress in Science and Engineering of Composites, (ed. T. Hayashi et al.), Japanese Society for Composite Materials, Vol.2, (1982), pp. 1427-1434.

(40) F. Girot, J.M. Quenisset, R. Naslain, B. Coutand and T. Macke, Proc. ICCM-6/ECCM-2, (eds. F.L. Matthews et al.), Vol.2, Elsevier, London, (1987), pp. 2.330-2.339.

(41) H.J. Rack, T.R. Baruch and J.L. Cook, Proc. ICCM-4, Progress in Science and Engineering of Composites, (eds. T. Hayashi et al.), Japanese Society for Composite Materials, Vol.2, (1982), pp. 1257-1258.

(42) T. Imai, Y. Yamada, M. Shirayanagi and H.J. Matsubara, J. Mater. Sci. Letts.,

6 (1987), pp. 1257-1258.

(43) J. Westfall, U.S. Patent Appl. SN 560035, (1985).

(44) NASA-Lewis Cont. Pub. 10003, Aeropropulsion 87, Session 1: Aeropropulsion Materials Research, NASA-Lewis Research Center, 17-19 November, 1987.

(45) M.W. Mahoney, A.K. Ghosh, C.C. Bampton, Proc. ICCM-6/ECCM-2, (eds. F.L.Matthews et al.), Elsevier, London, Vol.2, (1987), pp. 2488-2492.

(46) T.W. Clyne and M.G. Bader, Proc. ICCM-5, (eds. W.C.Harrigan, Jr. et al.), TMS of AIME, (1985), pp. 755-791.

(47) T. Morimoto and M. Taya, Proc. ICF-7, Pergamon Press, New York, in Press.

(48) F.M. Hosking, F.F. Partillo, R. Wunderlin and R.J. Mehrabian, J. Mater. Sci., 17 (1982), pp. 479-498.

(49) D.J. Lloyd, J. Mater. Sci., 19 (1984), pp. 2488-2492.

(50) P.K. Rohatgi, R. Asthana and S. Das, Int. Met. Rev., 31 (1986), pp. 115-139.

(51) F.A. Badia and P.K. Rohatgi, AFS Trans., 77 (1969), p. 402.

(52) R.T. Deonath and P.K. Rohatgi, J. Mater. Sci., 15 (1980), p. 1241.

(53) P.K. Rohatgi, B.C. Pai and S.C. Panda, J. Mater. Sci., 14 (1979), p. 227.

(54) A.A. Das and S. Chatterjee, Metall. Mater. Technol., 13 (1981), p. 137.

(55) J. Sugishita, S. Fujiyoshi and T. Imura, Wear, 81 (1982), p. 209.

(56) D.M. Karpinos, P.N. Askarov and O.V. Abromov, Poroshk. Metall., No.(3), (1982), p. 64.

(57) "Solidification Characteristics of Aluminum Alloys, Vol.2: Foundry Alloys",

(eds. L. Backerud, G. Chai and J.Tamminen), AFS/Skan Aluminium, Sweden (1990).

(58) "Aluminum: Properties and Physical Metallurgy", (ed. John Hatch), 1983.

(59) J.P. Clark and M.C. Flemings, "Moderne werkstoffe und ihre wirtschaftliche bedeutung", Specktrum der Wissenschaft Sonderheft Neue Werkstoffe, 1986.

(60) A. Labib, H. Liu and F.H. Samuel, AFS Trans., 100 (1992), pp. 1033-1041.

(61) A.M. Borchert, "Solidification Rate Effect in Metal-Matrix Composites", A Thesis Sumbmitted for the Master of Science in Material Science, University of California, San Diego, (1991).

(62) J.P. Cottu, J.J. Coudrec, B. Viguier and L. Bernard, J. Mater. Sci., 27 (1992), pp. 3061-3074.

(63) S.D. Dumolt, D.E. Laughlin and J.C. Williams, Scripta Metall., 18 (1984), p. 1347.

(64) L.F. Mondolfo, " Aluminum Alloys: Structure and Properties", Butterworth's and Co. Ltd., London, (1976).

(65) M.T. Tsukuda, M. Harada, T. Suzuki and S. Koike, J. Jpn. Inst. Light Metals, 28(3) (1978), pp. 109-115.

(66) W.A. Bailey, Foundry, (May 1964), pp. 54-60.

(67) B.N. Pramila Bai and S.K. Biswas, Acta Metall. Mater., 39(5) (1991), pp. 833-840.

(68) A. Couture, AFS Int. Cast Metals J., 6 (1981), pp. 9-17.

(69) "Duralcan Composite Casting Guidelines", Duralcan USA, San Diego, 1990, VIII-I.

(70) D.J. Lloyd, Compos. Sci. & Technol., 35 (1989), p. 159.

(71) P.K. Rohatgi, F.M. Yarandi and Y. Liu, (eds. S.G.Fishman and A.K.Dhingra). Proc.Conf. on Cast Reinforced Metal Matrix Composites, American Society for Metals, Metals Park, OH, (1988), p. 249.

(72) D.R. Ulhmann, B. Chalmers and K.A. Jackson, J. Appl. Phys., 35 (1964), p.2986.

(73) G.F. Bolling and J. Cisse, J. Cryst. Growth, 10 (1971), p. 56.

(74) A.M. Zubkov, V.G. Lubonv and V.V. Nikonova, Soviet. Phys. Crystallogr., 18 (1973), p. 273.

(75) M.K. Surappa and P.K. Rohatgi, Metall. Trans. B, 12B (1981), p. 327.

(76) J. Potschke and V. Rogge, J. Cryst. Growth, 94 (1989), pp. 726-738.

(77) D.M. Stefanescu, B.K. Dhindaw, S.A. Kacar, and A. Moitra, Metall. Trans. A, 19A (1988), pp. 2847-2855.

(78) D.M. Stefanescu and F. Rana, "A Model of Particle Distribution in Cast Metal Matrix Composites", (1990), pp.95-102.

(79) J. Potschke and V. Rogge, J. Cryst. Growth, 94 (1989), pp. 726-738.

(80) D. Apelian, S. Shivkumar and G. Sigworth, AFS Trans., 97 (1989), pp. 727-742.

(81) Metals Handbook, Vol.2, Tenth edition, American Society for Metals, Meatls Park, OH, (1988), pp. 39-40.

(82) T.J. Shin, D.N. Lee and J.Korean, Inst. Met., 23(10) (1985), pp. 1116-1122.

(83) D.E. Hammond, AFS Trans., 97 (1989), pp. 887-888.

(95) M. Skibo, P.L. Morris and D.J. Lloyd, in "Cast Reinforced Metal Matrix Composites", (eds. S.G. Fishman and A.K. Dhingra, ASM International, (1988), pp. 257-261.

(96) R. Carity, AFS Trans., 97 (1989), pp. 743-746.

(97) D.L. McDanels, Metall. Trans. A, 16A (1985), pp. 1105-1115.

(98) D.J. Lloyd, E. Dewing, Proc. Int. Symp. on Advanced Structural Materials, (ed. D.S. Wilkinson), Pergamon Press, New York, (1988), p. 71.

(99) K. Radhakrishna, S. Seshan and M.R. Seshadri, AFS Trans., 88 (1990), p. 69.

(100) M. Manoharan and J.J. Lewandowski, Scr. Metall., 23 (1989), p. 1801.

(101) B. Closset and J.E. Gruzleski, Fonderie-Fondeur d'Aujourd'Hui, no. 16 (1982), pp. 41-46.

(102) R. Dasgupta, C.G. Brown and S. Marek, AFS Trans., 96 (1988), pp.297-310.

(103) L. Hogan, S.Z.Lu and A. Hellawell, Metall. Trans. A, 18A (1987), pp. 1721-1739.

(104) J.R. Denton and J.A. Spittle, Mat. Sci. & Technol., 1 (1985), pp. 305-311.

(105) M. Vogelsang, R.J. Arsenault and R.N. Fisher, Metall. Trans. A, 17A (1986), p. 379.

(106) C.W. Meyers, AFS Trans., 93 (1985), pp. 741-750.

APPENDIX

Chapter III

Table III.1 Typical Physical Properties of A356 and F3A.10S [69].

PROPERTY		A356	F3A.10S
Density (lb/in^3)		0.0970	0.0986
Electrical Conductivity (% IACS)	72 °F	37.5	27.6
Thermal Conductivity (BTU/IB.°F)	72 °F 300 °F 400 °F 500 °F	87.0 - - - -	100.5 106.9 109.2 115.6
Specific Heat (BTU/IB.°F)	77 °F 212 °F 302 °F 392 °F 482 °F 572 °F	- - - - - -	- - - - - -
Average Coefficient of Thermal Expansion (10^{-6}/°F):	102-212 °F 120-570 °F 120-930 °F	11.9 - -	9.9 - -

Chapter III

Table III.2 Effect of Low Stirring Time Interval (20 min) and Mold Temperature on the Tensile Properties of F3A.10S Composite in the As-Cast Condition.

Mold Temp °C	20 min			40 min			60 min		
	YS ksi	UTS ksi	EL %	YS ksi	UTS ksi	EL %	YS ksi	UTS ksi	EL %
300 °C	16.0 17.0	26.0 26.3	1.8 1.7	17.0 17.2	26.3 27.5	1.7 1.6	17.3 17.4	27.1 27.5	1.8 1.9
Ave.	**16.5±.7**	**26.2±.6**	**1.8±.1**	**17.1±.2**	**27±.8**	**1.6±.1**	**17.4±.1**	**27.3±.2**	**1.8±.1**
350 °C	16.0 17.0	24.5 26.5	1.6 1.7	18.0 16.0	26.4 23.2	1.6 1.3	15.5 17.6	22.8 24.8	1.5 1.1
Ave.	**16.5±.7**	**25.5±.9**	**1.6±.1**	**17±.9**	**25±1.8**	**1.3±.3**	**17±.8**	**24±1.1**	**1.3±.2**
450 °C	19.2 17.4	26.1 26.3	1.5 2.2	16.5 18.1	27.8 28.0	2.8 1.7	18.5 18.6	28.9 26.8	1.7 2.1
Ave.	**18±.9**	**26±.2**	**1.9±.5**	**17±.9**	**28±.9**	**2.3±.8**	**18±.8**	**28±1.5**	**1.9±.3**

Table III.3 Effect of High Stirring Time Interval (60 min) and Mold Temperature on the Tensile Properties of F3A.10S Composite in the As-Cast Condition.

Mold Temp °C	60 min			120 min			180 min		
	YS ksi	UTS ksi	EL %	YS ksi	UTS ksi	EL %	YS ksi	UTS ksi	EL %
350 °C	17.6 18.4	26.7 27.4	1.7 1.8	17.2 17.1	26 25	1.8 1.4	18.1 18.2	25 26	1.2 1.5
Ave.	**18±.4**	**27±.5**	**1.8±.1**	**17±.1**	**26±.9**	**1.6±.4**	**18±.2**	**25±.9**	**1.4±.2**
450 °C	19 18	27 28	2.0 2.1	18.2 18.1	26 27	2.4 1.9	16 20	27 29	1.9 2.3
Ave.	**18±.9**	**27±.9**	**2.0±.1**	**18±.2**	**27±.2**	**2±.2**	**18±2**	**28±1**	**2.0±.2**

Chapter III

Table III.4. Effect of Low Stirring Time Interval (20 min) and Mold Temperature on the Tensile Properties of F3S.10S Composite in the As-Cast Condition.

Mold Temp. °C	20 min.			40 min.			60 min.		
	YS ksi	UTS ksi	EL %	YS ksi	UTS ksi	EL %	YS ksi	UTS ksi	EL %
300 °C	18.8	30.0	2.0	18.6	29.0	2.1	17.6	26.6	1.4
	18.6	29.0	1.7	18.7	30.2	1.7	18.7	28.4	1.5
	17.3	28.0	1.8	18.7	28.8	1.7	17.7	27.4	1.6
	18.4	28.0	1.8	17.7	27.1	1.4			
Ave.	**18±.7**	**28±1.3**	**1.8±.1**	**18±.6**	**29±1.7**	**1.7±.9**	**18±.6**	**27±1.1**	**1.5±.1**
350 °C	18.8	29.4	1.6	18.9	28.3	1.2	18.1	28.1	1.6
	20.4	27.8	1.2	19.1	30.6	2.2	18.5	27.4	1.8
	19.0	26.5	1.0	20.0	28.7	1.4	19.0	29.2	1.1
				19.0	26.9	0.8	20.4	27.2	0.7
Ave.	**19±1**	**28±1.1**	**1.3±.4**	**19±.6**	**29±1.7**	**1.4±.6**	**19±1.0**	**28±.7**	**1.3±.5**
400 °C	19.0	28.0	1.5	18.0	26.0	1.1	17.7	26.4	1.2
	17.9	27.1	1.3	18.0	25.9	1.6	18.1	26.0	1.1
Ave.	**18±1**	**28±.9**	**1.4±.2**	**18±0**	**26±.1**	**1.4±.3**	**18±.4**	**26±.4**	**1.2±.1**
450 °C	17.3	26.2	1.2	18.7	26.5	1.1	17.7	27.0	1.5
	17.8	26.0	0.9	18.5	27.2	1.4	18.2	25.2	0.8
Ave.	**17±.9**	**26±.2**	**1.1±.2**	**19±.6**	**27±.5**	**1.3±.1**	**18±.4**	**26±1.3**	**1.2±.5**

Chapter III

Table III.5 Effect of High Stirring Time Interval (60 min) and Mold Temperature on the Tensile Properties of F3S.10S Composite in the As-Cast Condition.

Mold Temp. °C	60 min.			120 min.			180 min.		
	YS ksi	UTS ksi	EL %	YS ksi	UTS ksi	EL %	YS ksi	UTS ksi	EL %
300 °C	18.7	28.4	1.5	16.5	26.0	1.4	17.2	26.0	1.3
	17.7	27.4	1.6	17.4	26.2	1.6	18.2	27.5	1.5
	17.6	26.6	1.4						
Ave.	**18±.7**	**27±1**	**1.5±.1**	**17±.6**	**26±.2**	**1.5±.1**	**18±.8**	**27±1**	**1.4±.1**
350 °C	18.1	28.1	1.6	17.5	26.5	1.3	19.0	27.5	1.1
	18.5	27.4	1.4	17.6	26.0	1.1	19.2	28.4	1.1
	18.9	30.3	3.0	18.7	24.2	0.9	17.8	25.2	1.2
				19.1	28.0	1.6	18.0	25.3	1.2
Ave.	**19±.7**	**29±1.6**	**2±.9**	**18±.8**	**26±1.6**	**1.2±.3**	**19±.9**	**27±1.7**	**1.2±.1**
450 °C	17.7	27.0	1.5	17.0	26.3	1.6	18.4	25.3	0.9
	18.2	24.1	0.8	17.1	26.0	2.0	17.5	25.3	0.9
	18.4	26.4	1.6	18.3	25.3	1.4	17.1	26.0	2.0
	18.3	27.4	2.2						
Ave.	**18±.4**	**26±1.5**	**1.5±.6**	**17±1**	**26±1**	**1.7±.3**	**18±.7**	**26±.7**	**1.3±.7**

Chapter IV

Table IV.1 Tensile Properties of Permanent Mold Test Bars of A356 in the T4 Condition [80].

Solution time hr	YS (ksi)	UTS (ksi)	EL (%)
1	29.9	35.4	3.6
2	29.6	36.9	5.4
5	27.5	37.5	6.5
10	30.7	41.6	5.1
15	27.5	41.1	6.9
20	27.0	39.9	7.1

Chapter IV

Table IV.2-4. Tensile Properties of Permanent Mold Test Bars of A356 in the T6 Condition at Various Temperatures (140, 160 and 180 °C) for Different Aging Times (5, 12 and 24 hr) [80].

Table IV.2 140°C

Aging times	YS (ksi)	UTS (ksi)	EL (%)
5	20.0	36.0	14.0
12	25.0	40.0	10.0
24	27.0	43.0	8.0

Table IV.3 160°C

Aging time hr	YS (ksi)	UTS (ksi)	EL (%)
5	23.0	38.0	12.0
12	30.0	40.0	7.0
24	32.0	41.0	6.0

Table IV.4 180°C

Aging time hr	YS (ksi)	UTS (ksi)	EL (%)
5	35.0	44.0	9.0
12	37.0	43.0	6.0
24	28.0	40.0	4.0

Table IV.5 Effect of Solution Time at 540°C on The Tensile Properties of F3A.10S Composite.

Solution Time(hr.)	YS (ksi)	UTS (ksi)	EL (%)	Q (ksi)
4	22.2 22.8 23.0 23.6 23.2	34.6 34.7 36.6 33.7 36.0	3.12 2.86 4.42 2.29 4.08	45.3 44.5 50.5 41.5 49.2
Average	23 ± 0.5	35 ± 1.2	3.4 ± 0.9	46.2 ± 3.6
8	22.8 22.6 24.4 23.3	34.0 33.5 33.8 33.9	3.0 2.9 2.1 2.3	44.3 43.4 40.6 41.6
Average	23.3 ± 0.8	34 ± 0.3	2.6 ± 0.5	42.5 ± 1.7
12	23.4 21.9 25.4 23.9 25.6 24.0 23.6 24.1	36.4 32.2 34.8 35.0 35.0 37.0 35.8 34.6	4.1 2.2 2.3 2.5 2.5 4.0 2.9 2.2	49.6 39.5 42.6 43.5 43.5 50.0 45.9 42.2
Average	24.0 ± 1.2	35.0 ± 1.4	2.8 ± 0.6	50.0 ± 6.0
24	18.9 19.7 23.0 22.3 22.4 23.0	26.1 26.5 35.9 35.2 33.8 33.4	1.5 1.3 4.4 4.3 3.2 2.5	30.3 29.2 50.0 49.0 44.7 42.2
Average	21.6 ± 1.6	32.0 ± 4.0	2.9 ± 1.3	41.0 ± 7.7

Chapter IV

Table IV.6. Effect of Solution Time at 538°C on the Tensile Properties of F3S.10S Composite.

Solution Time(hr.)	YS (ksi)	UTS (ksi)	EL (%)	Q (ksi)
4	23.6 23.5 29.0 28.0	35.5 36.6 42.0 41.0	2.3 2.2 2.8 2.4	43.4 44.0 51.5 49.2
Average	26.0 ± 2.9	38.8 ± 3.1	2.4 ± 0.2	47.0 ± 4.0
8	25.6 27.0 28.0 26.0 25.0	36.5 40.0 38.0 38.0 36.7	2.0 2.5 2.8 3.5 2.8	43.0 48.8 47.8 50.0 46.4
Average	26.3 ± 0.7	38.0 ± 1.4	2.7 ± 0.5	47.0 ± 2.7
12	24.5 26.5 28.0 28.5	36.5 37.0 39.0 38.0	2.7 2.7 2.7 2.8	45.8 46.4 48.5 47.6
Average	26.9 ± 1.8	37.6 ± 1.1	2.7 ± 0.03	47.2 ± 1.7
24	27.6 25.6 30.0 28.0 24.7 25.6 25.8	38.0 37.0 40.0 39.5 36.5 36.6 37.1	3.2 2.9 2.3 2.7 2.7 2.6 2.5	49.1 47.2 48.0 49.0 46.0 45.5 46.0
Average	26.7 ± 1.8	37.8 ± 1.5	3.1 ± 0.5	47.2 ± 1.7

Table IV.7 Effect of Natural Aging at 25°C for 24 hr prior to Artificial Aging at 160°C on the Tensile Properties of F3A.10S Composite. Samples were Solution Treated at 540°C for 12 hr-PA.

Aging time (hr)	YS (ksi)	UTS (ksi)	EL (%)	Q (ksi)
5	40.5	45.9	1.12	46.9
	39.5	42.9	0.58	37.7
	37.9	41.6	0.52	35.4
	39.4	42.7	0.47	35.5
	38.1	42.6	0.62	38.0
Average	39.1 ± 1.1	43.0 ± 1.6	0.66 ± 0.07	38.7 ± 5.0
12	42.4	46.0	0.55	40.3
	41.8	45.4	0.51	39.0
	42.7	45.3	0.40	36.6
	43.0	46.4	0.58	41.2
	42.7	45.5	0.48	38.5
Average	42.5 ± 0.5	45.7 ± 0.5	0.5 ± 0.06	39.0 ± 1.7
24	40.0	45.0	0.59	40.0
	41.0	46.0	0.60	41.2
	40.0	45.0	0.40	36.3
	41.0	44.0	0.60	39.0
Average	40.5 ± 0.8	45.0 ± 0.8	0.55 ± 0.1	39.1 ± 2.0

Chapter IV

Table IV.8 Effect of Aging Time at 160°C on the Tensile Properties of F3A.10S Composite. Samples were Solution Treated at 540°C for 12 hr-NPA.

Aging time (hr)	YS (ksi)	UTS (ksi)	EL (%)	Q (ksi)
5	44.0	47.6	0.56	42.0
	41.8	44.5	0.40	35.8
	43.5	47.8	0.54	38.6
	41.8	45.8	0.57	40.5
	43.6	48.8	1.50	52.6
	40.0	46.7	1.10	47.6
	41.0	45.5	0.85	44.0
	40.6	43.4	0.45	35.8
	42.2	48.5	1.17	50.0
Average	42.0 ± 1.4	46.5 ± 1.2	0.8 ± 0.4	43.0 ± 6.0
12	46.0	48.5	0.50	42.0
	47.6	49.7	0.33	39.1
	46.6	48.5	0.35	38.5
	47.2	49.1	0.30	37.6
	45.4	46.8	0.30	35.0
	43.6	46.5	0.40	37.8
	43.9	48.6	0.61	44.0
	43.5	47.5	0.57	42.0
Average	45.5 ± 1.6	48.0 ± 1.1	0.4 ± 0.1	39.5 ± 3.0
24	46.1	47.0	0.26	34.2
	48.9	52.4	0.56	47.0
	48.6	49.0	0.25	35.8
	47.0	51.0	0.50	44.4
	47.0	50.0	0.40	41.3
	45.0	47.6	0.21	32.7
Average	47.0 ± 1.5	49.5 ± 2.1	0.36 ± 0.1	39.2 ± 6.0

Table IV.9. Effect of Natural Aging at 25°C for 24 hr prior to Artifical Aging at 155°C on the Tensile Properties of F3S.10S Composite. Samples were Solution Treated at 538°C for 8 hr-PA.

Aging time (hr)	YS (ksi)	UTS (ksi)	EL (%)	Q (ksi)
5	42.0 41.0 44.0 42.5 44.0	47.0 46.0 47.0 47.5 48.0	1.0 0.8 1.2 0.9 0.8	47.0 43.9 48.7 46.3 45.8
Average	42.7 ± 1.5	47.1 ± 0.70	1.0 ± 1.8	46.0 ±1.8
12	45.3 44.8 45.9 45.2 45.4 42.3 46.6	48.5 48.0 46.5 47.0 49.6 52.2 50.7	0.5 0.5 0.2 0.3 0.6 1.0 0.6	41.1 41.4 33.0 36.5 45.1 52.0 46.0
Average	45.0 ± 1.3	49.0 ± 2.0	0.5 ± 0.2	42.0 ± 6.0
24	48.5 49.0 47.0 47.6 47.5 46.4 47.4 46.0	52.0 51.7 49.0 49.3 49.6 49.2 49.8 48.7	0.55 0.45 0.39 0.34 0.21 0.40 0.40 0.37	46.3 44.1 40.0 39.0 34.7 40.5 41.0 39.2
Average	47.4 ± 1.1	50.0 ± 1.1	0.4 ± 0.09	41.0 ± 3.5

Chapter IV

Table IV.10 Effect of Aging Time at 155°C on the Tensile Properties of F3S.10S Composite. Samples were Solution Treated at 538°C for 8 hr-NPA.

Aging time (hr)	YS (ksi)	UTS (ksi)	EL (%)	Q (ksi)
5	40.3 40.2 41.5 40.5 40.8	45.0 43.9 46.6 45.7 44.1	0.84 0.52 1.40 0.84 0.52	43.3 37.7 49.8 44.0 37.9
Average	40.7 ± 0.5	45.0 ± 1.1	0.82 ± 0.4	42.5 ± 5.0
12	43.7 43.1 41.6 41.7	46.9 46.8 43.1 43.6	0.67 0.72 0.31 0.36	43.1 43.6 32.9 34.0
Average	42.5 ± 1.0	45.0 ± 2.0	0.55 ± 0.20	38.0 ± 6.0
24	43.5 42.5 43.2	46.5 46.8 47.0	0.53 0.69 0.72	40.5 43.4 43.9
Average	43.0 ± 0.5	46.8 ± 0.3	0.65 ± 0.1	42.6 ± 2.0

PUBLICATIONS

PUBLICATIONS

1. **Influence of Grain Refinement, Cooling Rate and Heat Treatment on Castability, Microstructure and Mechanical Properties of Remelted Al-SiC Metal-Matrix Composites.**

   A. Labib, H. Liu, A.Sh. Rezk and F.H. Samuel.
   Presented at the 30th Annual CIM Conference of Metallurgists, Ottawa, Ontario, August 18-21, 1991.

2. **Effect of Remelting, Casting and Heat Treatment on Two Al-Si SiC-Particle Composites.**

   A. Labib, H. Liu and F.H. Samuel.
   AFS Transactions, vol. 100 (1992), pp. 1033-1041.

3. **Effect of Solidification Rate (0.1-100°C s^{-1}) on the Microstructure, Mechanical Properties and Fractography of Two Al-Si-10 Vol% SiC Particle Composite Castings.**

   A. Labib, H. Liu and F.H. Samuel.
   Materials Science and Engineering, vol. A160 (1993), pp. 81-90.

4. **Effect of Matrix Composition on the Microstructure and Tensile Properties of Two Al-Si-Mg/SiC/10p Heat-Treated Composites.**

   A. Labib, A.M. Samuel and F.H. Samuel.
   33rd Annual CIM Conference of Metallurgists, Toronto, Ontario, August 20-25, 1994; Prepared for submission.